Spring 5-31-1988

Investigation of forces in the course of the water jet--work piece interaction

Hung-Yuan Li
New Jersey Institute of Technology

Copyright Warning & Restrictions

The copyright law of the United States (Title 17, United States Code) governs the making of photocopies or other reproductions of copyrighted material.

Under certain conditions specified in the law, libraries and archives are authorized to furnish a photocopy or other reproduction. One of these specified conditions is that the photocopy or reproduction is not to be "used for any purpose other than private study, scholarship, or research." If a, user makes a request for, or later uses, a photocopy or reproduction for purposes in excess of "fair use" that user may be liable for copyright infringement,

This institution reserves the right to refuse to accept a copying order if, in its judgment, fulfillment of the order would involve violation of copyright law.

Please Note: The author retains the copyright while the New Jersey Institute of Technology reserves the right to distribute this thesis or dissertation

Printing note: If you do not wish to print this page, then select "Pages from: first page # to: last page #" on the print dialog screen

ABSTRACT

Title of Thesis : Investigation of Forces Developed In The Course of The Water Jet-Work Piece Interaction.

Hung-Yuan Li, Master of Science In Mechanical Engineering, 1988

Thesis Directed by : Dr. E. S. Geskin
Associate Proffessor
Mechanical Engineering Department

This study is concerned with the dynamic of the interaction between the water jet and the work-piece. The piezoelectric transducer was used to construct an experimental setup. The simultaneous use of the constructed setup and strain gage enables us to validate the experimental procedure. The forces in the impingment zone were measured at different operational conditions. Totally about 400 different combinations of these conditions were tested. It was found that the force is mainly determined by the diameter of the sapphire. The effects of the abrasive size , abrasive flow rate, the diameter of the carbide tube, and the stand-off distance were also determined. The acquired informations will be used to improve the understanding of the mechanism of the jet formation and optimize the condition of cutting.

INVESTIGATION OF FORCES DEVELOPED IN THE COURSE OF THE WATER JET--WORK PIECE INTERACTION

By
Hung-Yuan Li

Thesis submitted to to the Faculty of the Graduate School of the New Jersey Institute of Technology in partial fulfillment of the requirements for the degree of Master of Science in Mechanical Engineering
1988

APPROVAL SHEET

Title of Thesis : Investigation of forces Developed in the course of the water jet-work piece interaction.

Name of Candidate : Hung-Yuan Li

Master of Science in Mechanical Engineering

May, 1988

Thesis and Abstract Approved :

Dr. E. S. Geskin — Date

Associate Proffessor

Mechanical Engineering Department

VITA

Name: Hung-Yuan Li

Address: 140, Wilson Ave., Kearny, NJ 07032

Degree to be conferred and date: M.S.M.E. May 1988

Collegiate institutions:

Institution	Dates	Degree	Date of Degree
National Taipei Inst. of Tech.	9/73 - 6/77	B.S.M.E.	June, 1983
New Jersey Inst. of Tech.	1/87 - 5/88	M.S.M.E.	May, 1988

Position held:

Teaching Assistant, Dept. of Mechanical Engineering

N. J. I. T., Jan. 87 - Present

ACKNOWLEDGMENT

I take this opportunity to express my deepest gratitude to Dr. E.S. Geskin, Associate Professor, Mechanical Engineering Department of NJIT for his valuable guidance throughout the course of this work.

TABLE OF CONTENTS

LIST OF TABLES

LIST OF FIGURES

INTRODUCTION

High pressure water jets have been used as an industry tool for many years[1-10]. This cutting method shows great potential not only in cutting and drilling minerals, rocks, or concrete, but also in comparison with conventional cutting and drilling tools which are inherently limited by their lack of both strength and resistance to abrasion. This cutting technology has proved to possess many advantages such as low production cost, high cutting speed, and low material loss. However, the most important feature is its ability to reduce the total cost of part production[1-16].

The application of high pressure water jet cutting technology has two different directions. First one is the pure water jet cutting. The success of this technology has been traced back to the 1970's when the jet was used in cutting some soft materials (non-metal) with a pressurized pure water jet of 20-30 ksi. This application began by using a high pressure and low flow rates water jet in cleaning[8], mining[14-15], and cutting woods or paper products[4,5]. Working pressure of the water jet at a maximum of 50000 psi proved to be able to cut a variety of relatively soft material at a high cutting rate.

In the beginning of the 1980's, it was found that by

mixing the abrasive particles in the jet the cutting capability will be increased so that almost any type of materials could be cut[13]. The jet developed through the entraining of the solid particles became the abrasive water jet. During this process, The abrasive particles are flown into the down stream of a pure water jet which guides the particles into a carbide tube where mixing takes and forms the water jet stream. In the carbide tube the particles are accelerated, this means that the kinetic energy of the particles increases and creates the high cutting capability of the developed two-phase mixture[5,6,9].

A number of research works have been performed in order to find new applications of the jet cutting, to determine the jet properties, and to improve the jet performance[16-20]. Computer integrated manufacturing technology has extended the areas and applications of water jet cutting [10]. Under the new application, abrasive water jet cutting is more efficient, more accurate, and less material consuming than any other traditional cutting methods. New Jersey Institute of Technology started the research in water jet cutting technology in 1986 with a water jet cutting machine comprised of a 5-axis robotic water jet cutting cell manufactured by Ingersoll-Rand Inc..

The water jet cutting system is composed of two sub-

systems: (1) Water preparation system and (2) Robotics system. The robotic system is the control station and the water preparation system includes booster pump, filter, water softener, intensifier, and accumulator. The water preparation system combined with the nozzle assembly and abrasive feeder and the guiding robot constitutes a water jet cutting cell.

To ensure a continuous flow into the high pressure cylinder, the booster pump is used to push the water into the low pressure water circuit. The water has to be softened first to remove any dissolved solids which will damage the system during the pressurization process. A major part of the water preparation system is an intensifier. The intensifier is driven by oil and can develop a water pressure up to 60000 psi. The oil is compressed up to 3000 psi by the action of rotary pump. Then, the oil is used in the intensifier driver to make the double acting reciprocating move. The oil and water loop are separated so that the oil will not pollute the water. The acting time of the intensifier can be adjusted by a control valve.

The high pressure water from the intensifier is then discharged to an accumulator which is used to compensate the water compressibility and to stabilize the water pressure so that the water will be transmit to every portion of the

system uniformly. In the water preparation section, pressure safety gauges and safety control features are properly installed.

After the pressure preparation section, water is supplied the nozzle assembly where the internal energy of the water will be converted into the kinetic energy. In the nozzle assembly, the water first passes through a sapphire and is accelerated to the velocity 2000-3500 fps. The water jet is formed in this nozzle. The abrasive particles then enter the stream of the water jet in a carbide tube which is used as a mixing chamber. The abrasive inlet angle, the diameter of sapphire and carbide tube, and the diameter of the inlet path are all parameters of the nozzle assembly which determine the jet properties.

The abrasive particles are stored in a vertical hopper and supplied to the nozzle assembly by an abrasive feeder. The abrasive feeder is an electric vibration tray which regularize the the abrasive flow rate. By changing the voltage to the vibration device, the abrasive flow rate can be controlled. Beyond the vibrator conditions, the abrasive flow rate also depends on the size of the particles.

In this experiment, a 5-axis robot is used to control the movement of the nozzle and corresponding to the motion of

the jet.

OBJECTIVE

In this experiment, the intensive study of both abrasive and non-abrasive water jet cutting has been carried out. The mechanism for the interaction between the cutting substance and a work-piece is not understood. However, the forces developed in the impingment zone provided substantial information about the process of cutting. Effects of the process conditions on these forces enabled us to estimate the optimal range of process variables. Because of this, the magnitude of the forces developed in the course of the jet-work piece interaction provided the substantial information necessary for the design and control of water jet cutting. The investigation of the forces developed in the jet impingment zone was the objective of this study.

Presently there is no documented technique of measuring the forces created during the interaction between a high speed two phase jet and a solid. Because of this, our first task included the development and verification of the measurement procedure.

The next task involved the investigation of the effect of the distance between the work-piece and the nozzle(stand-off distance) on the force. Because the general pattern of the relationship between the stand-off distance and the force

is known, this study enabled us to verify the measurement procedure. It also provides new information about the hydrodynamic of the high speed two phase jet.

The following task involved the estimation of the effect posed by different process conditions on the forces; and specially, the effect of the nozzle wear on these forces studied.

The sequence of the tasks above enabled us to develop a new experimental procedure and to use this procedure for the evaluation of some basic characteristics of the water jet cutting technology.

To simplify our text, we will use the following terms :

Sapphire	=	Sapphire nozzle.
Carbide	=	Carbide tube.
Nozzle assembly	=	Diameter of sapphire and carbide tube used in the combination in this experiment.
Stand-off distance	=	The distance between nozzle and work-piece.
Pure water jet	=	Water jet without additional abrasive.

PRINCIPLES OF THE PIEZOELECTRICITY

In carrying out this experiment, we were faced with various difficulties. The creation of a continuous liquid jet of supersonic velocity (ranging in diameter of 1 mm) required a large delivery rate from the apparatus. It seemed almost impossible to probe the interior of a jet of such a small diameter since the introduction of any extraneous object as a measuring instrument will produce a large disturbance into it. Therefore, a measuring device, treated as an obstacle placed in front of the jet was developed to attain the momentum from the jet[20-22]. In this experiment, we use piezoelectric force transducer to measure the momentum distribution along the axis of the jet for the piezoelectric transducer can provide high frequency (a property of high pressure jet) and high measuring dynamics measurement with satisfied accuracy[21-36].

Piezoelectricity can be defined as the electric polarization produced upon the application of mechanical strain or deformation to piezoelectric materials. The polarization is proportional to the strain and the plus or minus sign with it. This is generally referred to as the name of the direct piezoelectric effect which was discovered in 1880 by brothers Curie when they placed a weight on the surface of a crystal and found that the charge appeared on

the surface with a magnitude proportional to the weight[23].

The converse piezoelectric effect, found in 1881 by French Physicist Lippmann and verified by Curie latter, applies an electric field to a crystal to generate mechanical stress and strain in this crystal[24].

This phenomena of crystal piezoelectricity can be explained by the behavior of a spring. When the force is applied to a spring, it deformed the spring and the deformation is measured to calculate the acting force. The usually linear relation between the force and the deformation is determined by a spring constant. The direct and converse piezoelectric effects can be explained by the relation between force and deformation in the spring. The higher is the stiffness of the crystal, the smaller is the disturbance caused by the measurement.

The direction of the current generated in a crystal is determined by " one-wayness " in the crystal internal structure. This means that the crystal has a structure bias which can determine whether a given region on the structure should follow a positive or negative charge on compression. In the converse effect, the same "one-wayness" determines the sign of the deformation when an electric field is applied to the crystal[23].

Generally, the crystal can be divided into 32 possible classes by the symmetry they exhibit. Of the 32 classes, there are 20 that poses "one-wayness". With all the rest there is nothing to determine the direction of the polarity on deformation; hence they do not have the properties of polarization at all[23].

In 1964, Cady derived two sets of equations for both the direct and converse piezoelectrical effects, which given as follow[23]:

$$P_x=e_{11}x_x+e_{12}y_y+e_{13}z_z+e_{14}y_z+e_{15}z_x+e_{16}x_y$$
$$P_y=e_{21}x_x+e_{22}y_y+e_{23}z_z+e_{24}y_z+e_{25}z_x+e_{26}x_y$$
$$P_z=e_{31}x_x+e_{32}y_y+e_{33}z_z+e_{34}y_z+e_{35}z_x+e_{36}x_y$$

$$P_x=d_{11}X_x+d_{12}Y_y+d_{13}Z_z+d_{14}Y_z+d_{15}Z_x+d_{16}X_y$$
$$P_y=d_{21}X_x+d_{22}Y_y+d_{23}Z_z+d_{24}Y_z+d_{25}Z_x+d_{26}X_y$$
$$P_z=d_{31}X_x+d_{32}Y_y+d_{33}Z_z+d_{34}Y_z+d_{35}Z_x+d_{36}X_y$$

$$X_x=e_{11}E_x+e_{21}E_y+e_{31}E_y$$
$$Y_y=e_{12}E_x+e_{22}E_y+e_{32}E_y$$
$$Z_z=e_{13}E_x+e_{23}E_y+e_{33}E_y$$
$$Y_z=e_{14}E_x+e_{24}E_y+e_{34}E_y$$
$$Z_x=e_{15}E_x+e_{25}E_y+e_{35}E_y$$
$$X_y=e_{16}E_x+e_{26}E_y+e_{36}E_y$$

Where E : electric field strength

X,Y,Z : stress related

x : strain related

P : electric polarization

e_{ij} : piezoelectric stress coefficient

d_{ij} : piezoelectric strain coefficient

i,j : notation of different constants

(For example, X_x,Y_y,and Z_z mean the X,Y,Z axis stress in x,y,z direction separately.)

In these equations, all coefficients are constant and determined by the kind of crystal.

The following two values of the piezoelectric coefficient are used in the Kistler force transducer at 20 C. and utilized in our experiment:

$$d_{11}=2.3*10^{-12} \quad C/N$$

$$d_{14}=0.67*10^{-12} \quad C/N$$

The piezoelectricity of a crystal is determined by the following: longitudinal, transverse and shear effect.

These three effects are distinguished according to the position of the quartz crystal axes in relation to the force

sustained.

With the longitudinal effect, the negative lattice points in the crystal lattice are displaced by the force imposed towards the positive one so that the equilibrium of the charges is disturbed; and measurable charge differences result on the surfaces of the crystal plates. The resulting charge from this effect depends solely on the applied force. The simplified longitudinal effect of crystal is depicted in Fig. 3.1.

When the force is applied in the direction, say F_z of one of the neutral crystal axes z, an electrical charge is set up on the surfaces of the axes polar to it, this is called the transverse effect. The charge magnitude depends on the geometry of the quartz which is contrast to the longitudinal effect. This is illustrated in Fig. 3.2. When shear stress is applied to the quartz, the surface of quartz will produce a current. This phenomenon is called shear effect. The shear effect depends on the geometry and size of the quartz element and the charge distribution similarly to the longitudinal effect(Fig. 3.3)[33,37].

Due to these effects, the current is generated and sent to the charge amplifier to convert into a voltage change which can be detected by a recording system.

EXPERIMENTAL APPARATUS AND PROCEDURE

The measuring system used in this study includes a work piece bolted to a piezoelectric force transducer, charge amplifier and read out devices. The jet emanating from the nozzle impinges on the work-piece and develops the force measured by the transducers . Proper setting of each component of this system can provide an adequate measuring range and an accurate result[38,39].

4.1 Experimental apparatus:

4.1.1 Piezoelectric force transducer:

The sketch of the transducer is given in Fig. 4.1. Two identical, three components force measurement platforms are used in this study. Each multi-component transducer is assembled by stacked quartz disks, loaded mechanically in a series with electrode interlayers[37].

The force to be measured acts on the work-piece so that each quartz disk produces the same amount charge in the same direction at the same time. In our study, two Kistler three-component force measurement platforms 9257A are used.

4.1.2 Work-piece:

A steel plate, 14"*4"*0.75" shown in Fig. 4.2, contained 20 0.0375 inch diameter holes which are used to connect the steel plate with the insulation wood plate and the transducers. The bottom surface of the work-piece is machined to prevent the possible vibration of the work-piece and the insulation wood.

4.1.3 Charge amplifier:

A charge amplifier is used as a classic electrometer to enable the charge alteration at the quartz transducers to be measured. Each component of the charge amplifier has its own sensitivity switch and measuring range scale switch determined by each measuring axis[33]. In this study, Kistler three components charge amplifier Model# 5007 is used.

4.1.4 Read out devices:

A Fluke Model# 8101A digital multi-meter and a Gould two-channel recorder are used. These two are connected in parallel to the charge amplifier. For future study, a digital oscilloscope connected to the computer to record the signal from the charge amplifier is recommended.

4.2 Experimental procedure:

This study is concerned with estimating the components of the force acting on a work-piece during the water jet and work-piece interaction. In order to determine these components, we set up two transducers, putting on a flat surface, to probe the force. The work-piece is post-machined to flat and fixed on the top surface of the transducers. Between the work-piece and the transducers, a thin wood plate is inserted as an insulation material to reduce the disturbed signal of the transducers caused by the thermal effect. Both the work-piece and the wood plate are fixed on the transducers by screws. By this, the thermal and vibration effects on the transducers can be reduced. The constructed set up is shown in Fig. 4.1(a).

The outputs of the transducers are connected to the charge amplifier where the signal will be converted into a voltage proportional to the force acting on the work-piece. Because the Z axis sensitivity is the same in both transducers, the position of the force acting on the work-piece is not as important as that it is within the measuring range of the work-piece. The allowed measurement of the work piece is shown in Fig.4.2. The relation of different positions and force are shown in Fig 4.3(a) and 4.3(b) The voltage from the charge amplifier then will be transmitted to

the read-out equipments which are connected in parallel to the amplifier. The form of the recorder print out is depicted in Fig.4.5

The results of the measurement by the use of the transducers are compared with the results of the measurement by a Lebow strain gage(Model # 3168) to check the accuracy of the determination of the forces. The comparison was carried under the jet flow through the sapphire at 10/1000 inch diameter and carbide 30/1000 diameter. The difference between the results of the two measurement methods ranged from 4% to 8%, depending on the stand-off distance and the jet pressure. The result of the comparison is shown in Fig. 4.4.

In the course of experiment, the combinations of the sapphire nozzles(4/1000 inch, 5/1000 inch, 7/1000 inch, 10/1000 inch, and 14/1000 inch) and carbide tubes (30/1000 inch, 43/1000 inch, and 63/1000 inch) were tested. The nozzle was kept vertical and normal to the target plate. The plate is fixed on the transducers by six axis-symmetric position screws. Two transducers are connected to the charge amplifier in parallel.

The control panel of the charge amplifier, is equipped with the several switches. Transducer sensitivity which is

used to control the charges produced by one specified mechanical force unit. Each measuring axis has its own sensitivity which is calibrated by the manufacturer. However, the sensitivity will be influenced by the temperature. So the calibration work is needed to sustain this. The charge is then transmitted to the charge amplifier and converted to voltage. This conversion factor is controlled by a range switch and maximum switch combined with the sensitivity switch. Proper setting of these switches can provide almost any measuring range. For example, a sensitivity 7.85 pc/N with a range switch 500 N/V and the maximum voltage it can produced 10 V will provide a measuring range +-500*10=+-5000 N and one volt represent 500 N. The time constant switch is on "long", representing the high frequency property of the jet.

This study included the following tasks:

1). The validation of the selected procedure.

2). Abrasive water jet force measurement.

3). Jet force variation as a function of nozzle wear.

In the first part, the forces created by the interaction between the water jet and the work-piece are

measured at different combinations of sapphires and carbide tubes at the stand-off distance of 2.54 mm, 12.7 mm, 25.4 mm, 50.8 mm. The function can be expressed as:

$$Force=f(d_1,d_2,z)$$

d_1 :sapphire diameter

d_2 :carbide tube diameter

z :stand-off distance

In the second part, the abrasive size and the abrasive flow rate have to be considered in addition to the sapphire size, carbide tube size, and stand-off distance. Four abrasive sizes (50 HP, 80 HP, 120 HP, and 220 HP) and two flow rate grid are under inspection. The function can be expressed as

$$Force=f(d_1, d_2,z,s,m)$$

d_1 :sapphire diameter

d_2 :carbide tube diameter

z :stand-off distance

s :abrasive size

m :abrasive flow rate

The third part will investigate the force variation caused by the abrasive consumption. The abrasive consumption represents the nozzle wear condition which affects the

force. The number of tests in this study are limited. However, sufficient information is still revealed.

Whenever the jet impings on a work-piece, the amplifier must first reset. Resetting discharges the voltage in the transducer. Therefore, the force which will act on the work-piece can be measured and displayed correctly by the adequate setting of the amplifier control switches.

In the course of the experiment, the following precautions have to be taken:

1). To measure the abrasive jet force, the switch for the abrasive has to be turned on after the jet passes through the carbide tube and turned off before jet exists to prevent the abrasive particles chokes in the mixing chamber

2). The nozzle must change acting position on the X-Y plane of the work-piece because the cavity produced by the jet increases the stand-off distance.

EXPERIMENTAL RESULTS

The results of the measurement of the pure water jet force due to the interaction between work-piece and jet are given in Table 5.1:

The values of the abrasive water jet force are shown in Tables 5.2-5.4. This experiment was carried out at the sapphire exit diameter of 0.007 in., 0.01 in., and 0.014 in. because the abrasive particles can choke the carbide tube. The force at the sapphire diameter of 0.004 in. and 0.005 in. can not be measured.

NON-ABRASIVE WATER JET FORCE AT DIFFERENT COMBINATIONS
(NEWTON)

		STAND-OFF DISTANCE (mm)				
SAPPHIRE EXIT AREA (mm2)	CARBIDE EXIT AREA (mm2)	2.54	12.7	25.4	50.8	76.2
0.008	0.456	1.6	1.82	1.97	1.72	1.83
	0.937	1.8	2	1.8	2.2	2.1
	2.011	2	2.3	2.6	2.6	2.4
0.013	0.456	4.2	4.36	4.36	4.2	4.1
	0.937	4.3	4.52	4.5	4.46	4.38
	2.011	4.8	4.8	4.8	4.85	4.9
0.025	0.456	11.3	12.6	11.2	10.9	10.2
	0.937	11.5	12.8	12.1	11.6	10.6
	2.011	12	13.4	12.5	12.1	11.1
0.051						
	0.456	20.8	20.9	20.5	20.2	19.4
	0.937	21.4	22.1	21.2	20.8	19.8
	2.011	21.9	23.4	21.6	21.5	20.7
0.099						
	0.456	37	37	38	37.4	37
	0.937	38	38.6	38.4	38.3	38.1
	2.011	39.1	40.5	39.4	39.1	38.7

TABLE 5.1

ABRASIVE WATER JET FORCE AT SAPPHIRE DIAMETER 0.007 in. AND OTHER COMBINATIONS
(NEWTON)

	ABRASIVE SIZE (HP)							
	50		80		120		220	
CARBIDE TUBE EXIT AREA 0.456 mm2								
STAND-OFF DIST(mm)	ABRASIVE FLOW RATE (g/min)							
	150	540.8	109	445	118.5	498.5	64	318.5
2.54	10.70	10.60	11.00	10.80	11.50	11.40	12.00	11.80
12.7	11.10	10.80	11.50	11.20	12.00	11.50	12.60	12.50
25.4	10.60	10.50	11.00	10.80	11.30	11.20	11.90	11.70
50.8	10.20	10.40	10.60	10.50	11.20	10.90	11.70	11.50
76.2	10.00	10.30	10.40	10.10	11.00	10.80	11.50	11.40
CARBIDE TUBE EXIT AREA 0.937 mm2								
2.54	10.40	9.70	11.30	10.90	12.10	11.50	13.50	11.80
12.7	10.80	10.30	11.90	11.30	12.50	11.60	13.80	12.70
25.4	10.60	10.00	11.70	10.80	12.40	11.50	13.60	13.50
50.8	10.30	9.50	11.50	10.50	11.90	11.40	12.70	12.30
76.2	10.00	9.20	11.20	10.40	11.80	11.20	11.90	11.60
CARBIDE TUBE EXIT AREA 2.011 mm2								
2.54	10.30	9.87	11.40	11.00	12.10	11.90	13.90	12.50
12.7	10.50	10.23	12.00	11.60	12.70	12.20	14.00	12.80
25.4	11.00	10.53	11.80	11.50	12.50	12.10	13.70	12.60
50.4	10.30	10.27	11.70	11.30	12.40	11.80	13.60	12.50
76.2	9.80	9.30	11.40	11.20	12.10	11.50	13.30	12.30

TABLE 5.2

ABRASIVE WATER JET FORCE AT SAPPHIRE DIAMETER 0.01 in. AND OTHER COMBINATIONS
(NEWTON)

	ABRASIVE SIZE (HP)							
	50		80		120		220	
CARBIDE TUBE EXIT AREA 0.456 mm2								
STAND-OFF DIST(mm)	ABRASIVE FLOW RATE (g/min)							
	150	540.8	109	445	118.5	498.5	64	318.5
2.54	21.2	22.26	21.22	22.13	22.32	24.2	23.84	27.32
12.7	21.33	22.71	21.6	22.71	22.85	24.9	25.1	28.67
25.4	21.46	21.86	22.2	22.4	23.1	25.54	27.93	29.1
50.8	20.4	20.94	20.85	21.42	22.43	24.31	26.53	27.72
76.2	19.66	20.05	20.3	20.63	21.89	23.71	26.21	24.25
CARBIDE TUBE EXIT AREA 0.937 mm2								
2.54	23.29	23.42	24.21	25.26	25.63	26.53	26.88	29.4
12.7	24.24	24.9	25.1	26.63	26.31	27.53	28.23	31.18
25.4	25.29	26.21	25.63	27.63	26.47	28.05	29.7	32.06
50.8	23.53	25.78	24.8	27.1	25.53	27.24	27.65	29.41
76.2	21.62	24.44	22.68	25.34	23.63	25.42	26.67	25.59
CARBIDE TUBE EXIT AREA 2.011 mm2								
2.54	24.76	26.98	27.35	29.14	28.43	30.59	28.65	31.76
12.7	25.55	28.3	28.82	30.74	29.69	32.94	30.41	34.12
25.4	26.21	29.2	29.41	31.81	29.98	33.82	30.95	35.59
50.4	25.41	28.28	27.94	30.2	28.23	32.35	28.82	32.94
76.2	23.21	24.90	25.82	26.2	26.59	27.94	27.32	27.65

TABLE 5.3

ABRASIVE WATER JET FORCE AT SAPPHIRE DIAMETER 0.014 in. AND OTHER COMBINATIONS
(NEWTON)

	ABRASIVE SIZE (HP)							
	50		80		120		220	
CARBIDE TUBE EXIT AREA 0.456 mm2								
STAND-OFF DIST(mm)	ABRASIVE FLOW RATE (g/min)							
	150	540.8	109	445	118.5	498.5	64	318.5
2.54	37.1	39.2	38.2	39.7	39.4	40.23	40.22	41.6
12.7	38.2	41.32	38.5	39.4	40.1	41.9	40.7	41.8
25.4	38.8	42.2	39.1	40.3	40.9	42.7	41.5	42.5
50.8	37.5	38.8	38.2	39.8	40.5	42.3	41.1	41.9
76.2	36.9	37.9	37.3	39.1	40.2	41.6	40.8	41.4
CARBIDE TUBE EXIT AREA 0.937 mm2								
2.54	38.3	41.2	41.3	42.7	42.1	44.2	43.7	46.2
12.7	39.2	42.2	42.2	43.1	42.4	44.7	44.4	46.6
25.4	40.7	44.1	42.8	44.6	42.8	45.1	45.1	45.7
50.8	38.9	40.4	42.	43.3	42.6	44.6	44.8	46.3
76.2	38.6	39.4	41.7	42.7	42.5	44.2	44.5	46.2
CARBIDE TUBE EXIT AREA 2.011 mm2								
2.54	41.7	42.8	44.2	45.2	45.4	48.2	47.5	49.7
12.7	40.5	44.3	45.2	46.4	45.7	48.6	47.9	50.2
25.4	39.7	45.4	46.2	47.9	46.8	49.3	48.3	50.8
50.4	39.5	42.2	45.9	47.2	46.3	48.6	47.8	50.1
76.2	39.3	41.4	45.6	46.9	45.8	48.3	47.2	49.2

TABLE 5.4

ANALYSIS OF EXPERIMENTAL RESULTS

The first task of our study is to develop measurement of the force for a high speed jet. After the device was set up, the validation of the results must be checked. In our study, the results are checked with a strain gauge, used in industry as a force measurement device for decades[40-42]. Strain gauge, Lebow Model #3168, used here was connected with a recorder which can provide a balanced Wheaston bridge function and print out the bridge voltage difference when a load is applied. The comparison of these two results gives 3% to 8% difference and the is shown in Fig. 4.4. With this the experiment can be carried out.

6.1 Investigation of non-abrasive water jet force.

This task was accomplished by the monitoring forces developed for similar jet conditions by the use of experimental devices and a strain gauge. The results of the measurement are shown in Fig.4.4. As this graph shown, the difference between these two results roughly ranged from 3% to 8%. Thus, the error of measurement does not exceed 8% and probably is equal to 4-5%. At this stage, the objective of the study is the qualitative evaluation of the effects developed in the course of cutting; therefore, the accuracy of 5% is considered sufficient.

6.1.1 Effect of sapphire exit area to the non-abrasive water jet force.

In this study, we compare the effect of two parameters: carbide tube exit area and stand-off distance.

The variation of the sapphire exit cross section area, as a function of the force at the different carbide tube exit area, is clearly shown in Fig. 6.2 to Fig. 6.4. As shown in the graphs, the force increases as the sapphire exit area increases and the relation is pratically linear. This phenomenon satisfies the principles of mass and momentum conservation. At the steady state, the force can be approximated by the equation:

$$F=K_1*m*V$$

where K_1: constant.

V : mean velocity of the water.

m : mass flow rate of the water.

The values of m and V are given as the following:

$$m=A*\rho*V$$

$$V=K_2*\sqrt{P}$$

where A : cross section of the sapphire.

ρ : density of the water.

K_2: constant.

P : water pressure before the nozzle.

Because in our experiment, P and V are constant, so the mass flow rate of the water is directly proportional to the sapphire exit area. Therefore, the force is also directly proportional to the sapphire exit area.

Fig. 6.2 shows the relationship between the force and the sapphire exit area at carbide exit area of 0.456 mm^2(30/1000 inch diameter). The second variable in this graph is stand-off distance. The maximum force is obtained at the stand-off distance of 12.7 mm. The force at this condition drops from 38 Nt. to 1.97 Nt. while the sapphire exit area changes from 0.099 mm^2 to 0.008 mm^2. As similar relationship at the carbide exit area of 0.937 mm^2(43/1000 inch diameter) and 2.011 mm^2 (63/1000 inch diameter) is shown in Fig. 6.3 and Fig. 6.4, which proving that the relationships are similar to each others. These results show that the sapphire exit area is a primary variable of the force function, since changing the carbide tube does not have much influence on the force.

The effect of the process variable on the force at the fixed stand-off distances of 2.54 mm, 12.7 mm, 25.4 mm, 50.8 mm, and 76.2 mm is shown in Fig. 6.5-6.9. These figures show that the largest amount of force occurs at the largest sapphire exit area and the largest exit area of the carbide. And, the smallest amount of force occurs at the smallest combination of the sapphire diameter and the carbide tube. In Fig. 6.7 , the maximum force is 39 Nt. and the minimum is 1.6 Nt. If the focus on the sapphire exit area 0.025 mm^2, the force difference is 1.9 Nt. with a carbide exit area of 2.011 mm^2 and 0.456 mm^2. In other sapphires, the differences are 0.4 Nt., 0.6 Nt., 0.7 Nt., and 2 Nt., corresponding to the sapphire exit areas of 0.008 mm^2, 0.013 mm^2, 0.025 mm^2, and 0.099 mm^2. These demonstrate that the non-abrasive jet forces change in significantly at a given range of change in the stand-off distance and carbide tube diameter.

6.1.2 Effect of the carbide tube exit area on the non-abrasive water jet force.

The parameters in this study are sapphire exit area and stand-off distance.

Fig. 6.10 to Fig. 6.14 were constructed at sapphire exit area of 0.008 mm^2, 0.013 mm^2, 0.025 mm^2, 0.051 mm^2, and 0.099 mm^2 separately. Here, we can clearly see that the

diameter of the carbide tube will not have much of an influence on the force as the sapphire exit area and the relations are pratically linear. For example, in Fig. 6.13 at the stand-off distance of 12.7 mm, the maximum force drops from 23.4 Nt. to 22.1 Nt. to 20.9 Nt. when the carbide tube changes from 2.011 mm^2 to 0.937 mm^2 and to 0.456 mm^2. This phenomenon is due to the interaction between the jet and the carbide tube internal surface. The smaller is the carbide tube diameter, the stronger interaction takes place. Consequently, more kinetic energy is lost. Because of this, the use of a sapphire instead of the nozzle assembly results in a larger force as it is shown in Fig. 6.1.

The second relationship discussed is the force vs. the carbide tube exit area when the stand-off distance is held as the parameter. The results are shown in Fig.6.15-6.19. In these graphs, the effect of the sapphire exit area on the force is clearly depicted and proves the conclusion in the previous section that the sapphire exit area is the main variable of the force function. Also in the graph, the linearity of the force vs. the carbide exit area is clearly depicted.

6.1.3 The optimum stand-off distance.

Important information is revealed when the effect of

the stand-off distance on the force is shown. The existence of the force extremity value was consistently observed in all our experiments.

Fig. 6.20-6.24 are show that the extreme point always occurs at the stand-off distance ranged of 12.7 mm to 25.4 mm. For example, in Fig. 6.23 at carbide tube exit area of 0.456 mm^2, the force is 20.8 Nt. at the 2.54 mm stand-off distance and increases to 20.9 Nt. at 12.7 mm, then drops to 20.5 Nt, 20.2 Nt., and 19.4 Nt. when the distance increases from 25.4 mm to 50.8 mm and to 76.2 mm.

The relationship between the force and the stand-off distance at a constant diameter of the carbide tube and variable diameter of the sapphire is shown in Fig. 6.25-6.27. These graphs show that the force at all combinations of the sapphire and carbide tube are almost the same even if the stand-off distance is changed. This phenomena is due to the relatively small energy dissipation at the observed length of the jet. In our next study, the extended length of the jet will be observed.

6.1.4 The effect of carbide tube on the water jet force.

The carbide tube is used as a mixing chamber for water and abrasive particles. In our study, we determined the

influence of the carbide tube exit area on the jet force. We compared the forces of the jet developed by a sapphire nozzle only (sapphire exit area 0.051mm^2) with the force developed by a nozzle assembly(sapphire exit area 0.051mm^2, carbide area 0.456 mm^2). The force from the nozzle assembly is smaller than the force from the sapphire. The comparison is shown in Fig. 6.1. The force of the jet drops from 26.3 Nt. to 21.6 Nt. which is nearly 20% difference when the sapphire is replaced by the nozzle assembly. The change is due to the interference between the jet and the internal surface of the carbide tube.

6.2 Investigation of abrasive water jet force.

This work involves the detailed analysis of the effect of process variables on the force developed in the impingment zone.

The variables involved and their values are given in Table[6.1].

Because of lack of the informations about the interaction between variables and non-linearity of the process, all possible combinations of variables were test.

Each series of experiments involved the change of three variables while two others were fixed. The results of these experiment are shown in Fig.6.28 to Fig.6.70.

The analysis of these figures enables us to estimate the effect of tested variables on the jet force in the impingment zone. The acquired informations is given in Tables 6.3-6.6.

6.2.1 Effect of stand-off distance.

The constructed diagrams enable us to compare the abrasive water jet force and the pure water jet force.

The result shown now the process extermality: maximum force is developed at the stand-off distance of 10-25 mm. The increase of the force with increase in the stand-off distance at a low value of the stand-off distance is due to strong turbulence at the space between nozzle and the work-piece. When the effect of the work-piece on exit from the nozzle is totally faded, the increase in the stand-off distance diminishes the force. The range of the force changes due to the change in the stand-off distance that does not exceed 3 Nt. The effect of other process conditions is shown in table 6.3.

6.2.2 Effect of abrasive flow rate.

With some exceptions which are due to experimental errors, increase of the abrasive flow rate will force the addition of small particles. The effect of the abrasive flow rate on the force is almost linear. However, in several of the experiments, this situation has been observed. With small size particles, the flow rate of the abrasive has a stronger effect on the force. The comparison of the effect of different process conditions are given in Table 6.4.

6.2.3 Effect of carbide exit area.

Increases in the carbide exit area results in the increase of the total jet force. Relationship between the force and exit area are monotonous and almost linear. Other process conditions are not greatly affected by this relationship. However, the sapphire cross section area of 0.025mm, the carbide does not influence on the force. The influence of other process conditions on the force are compared in table 6.5.

6.2.4 Effect of sapphire exit area.

The sapphire cross section area is a principal factor determining the force. As it follows from Fig.6.66-6.69 and

Table 6.6, the effect of other process conditions, except for the abrasive flow rate, is negligible compared to the sapphire cross section area.

6.3.3 The influence of carbide wearing condition on the force.

The abrasive particles passing through the carbide tube damage the inside surface of the tube and change the shape of the jet. Therefore, an investigation of the carbide tube wearing condition on the force was carried out. The total abrasive consumption was used to represent the duration of the use of the nozzle. The results are shown in Fig.6.71-6.74.

From these graphs of this study is followed that when the total consumption of abrasive increases the abrasive jet force decreases, but the pure water jet force increases.

CONCLUSION

The apparatus for measuring a high speed water jet force by means of piezoelectric transducers has been constructed. The comparison of the results of the measurement of the device constructed and conventional Lebow strain gage demonstrates the validity of the developed measuring procedures. The constructed setup was used to measure forces of the water jet at different operational conditions. Totally about 400 combinations of operational conditions have been tested. The performance demonstrate the effectness of the constructed devices. However, some improvements in the existing design is required. It is necessary to increase the accuracy and sensitivity of the recording system. Design of the work-piece is also suggested to modifies.

The performed experiment enables us to determine some important phenomena which occurred in the course of water jet cutting. It was found that developed force pratically is determined by the water flow rate at constant water stagnation pressure and became proportional to the exit sapphire area. Other variables inquisition. Diameter of the carbide tube, flow rate and size of abrasive particles, and stand-off distance have much less effect on the force developed in the impingment zone. It was found that the carbide tube reduces the force developed by the sapphire

about 20%. Effect of the stand-off distance on the force has an extreme character. Between the stand-off distance 12.7 mm to 25.4 mm, there is a maximum value of the force, The increase of force at low stand-off distance is due to the rebound effect. The decrease of the force at high stand-off distance is due to tubulent losses. The effect of the additional abrasive particles depends on the diameter of the sapphire. Adding abrasive particles in the jet causes the force decreases if the sapphire diameter is smaller than 0.18 mm and increases when the diameter is larger than 0.18 mm. The increase of the abrasive particle size increase the force and the force containing fine particles is minimum. At the experimental conditions, the additional abrasive monotonous increases the force. The form of the constructed graphs however shows abrasive flow rate is fading or even inversing. It is possible that at higher abrasive flow rate the maximum of the jet force will be observed.

The obtaining information enables us to make some recommendation directed to the improvement of the cutting technology. For example, it was found the range of the force in the impingment zone is from 2 to 50 Nt. These data is used to select the fixture holding work-piece in the course of cutting. Other recommendations about selection of operational conditions can also be made.

EXPERIMENTAL VARIABLES AND VALUES

VARIABLRE	NOTATION	VALUE	UNIT
STAND-OFF DISTANCE	z	2.54, 12.7, 25.4 50.8, 76.2	mm
SAPPHIRE EXIT AREA	N	0.025, 0.051, 0.08	mm^2
CARBIDE EXIT AREA	C	0.458, 0.837, 2.011	mm^2
ABRASIVE SIZE	S	50, 80, 120, 220	HP
ABRASIVE FLOW RATE	m	0, 5, 10*	**

* : 0 MEANS PURE WATER JET. 5, 10 ARE SCALES ON THE CONTROLLER
** : REAL FLOW RATE SHOWN IN TABLE 6.2.

TABLE 6.1

ABRASIVE FLOW RATE

(gram per minute)

SCALE	ABRASIVE SIZE (HP)			
	50	80	120	220
5	150	109	118.5	64
6	258.35	214.5	225.5	123.5
7	351.75	299.25	333	191.5
8	462.7	370	411.5	248.5
9	517.9	419.5	472	291
10	540.75	447	498.5	318.5

TABLE 6.2

EFFECT OF PROCESS CONDITIONS AT FIXED STAND-OFF DISTANCE

	EFFECT		
VARIABLE	STRONG	MIDDLE	WEAK
ABRASIVE SIZE		X	
SAPPHIRE EXIT AREA	X		
CARBIDE EXIT AREA			X
ABRASIVE FLOW RATE		X	

TABLE 6.3

EFFECT OF PROCESS CONDITIONS IN FIXED ABRASIVE FLOW RATE

	EFFECT		
VARIABLE	STRONG	MIDDLE	WEAK
ABRASIVE SIZE		X	
SAPPHIRE EXIT AREA	X		
CARBIDE EXIT AREA			X
STAND-OFF DISTANCE			X

TABLE 6.4

EFFECT OF PROCESS CONDITIONS IN FIXED CARBIDE EXIT AREA

	EFFECT		
VARIABLE	STRONG	MIDDLE	WEAK
ABRASIVE SIZE		X	
SAPPHIRE EXIT AREA	X		
ABRASIVE FLOW RATE		X	
STAND-OFF DISTANCE			X

TABLE 6.5

EFFECT OF PROCESS CONDITIONS IN FIXED SAPPHIRE EXIT AREA

	EFFECT		
VARIABLE	STRONG	MIDDLE	WEAK
ABRASIVE SIZE		X	
CARBIDE EXIT AREA	X		
ABRASIVE FLOW RATE			X
STAND-OFF DISTANCE		X	

TABLE 6.6

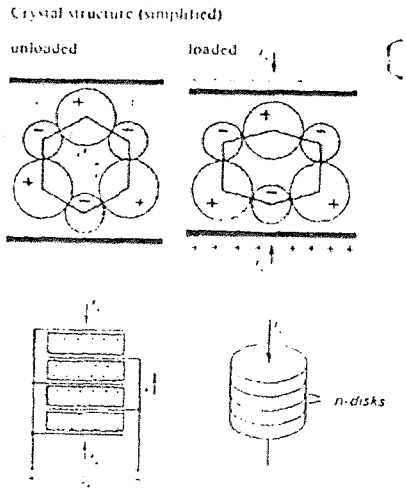

Fig. 3.1
Principle of the longitudinal piezoelectric effect (tpp) and schematic assembly of a transducer (bottom)

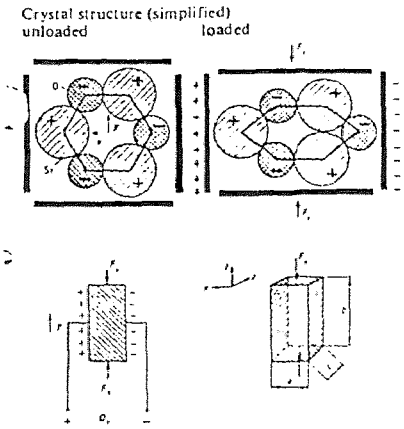

Fig. 3.2

Principle of the transverse piezoelectric effect(top) and its practical utilization(bottom).

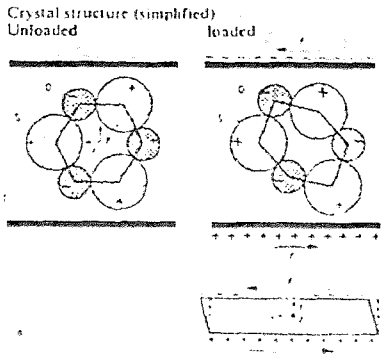

Fig. 3.3

Principle of the sheer effect (top) and mode of force application (bottom).

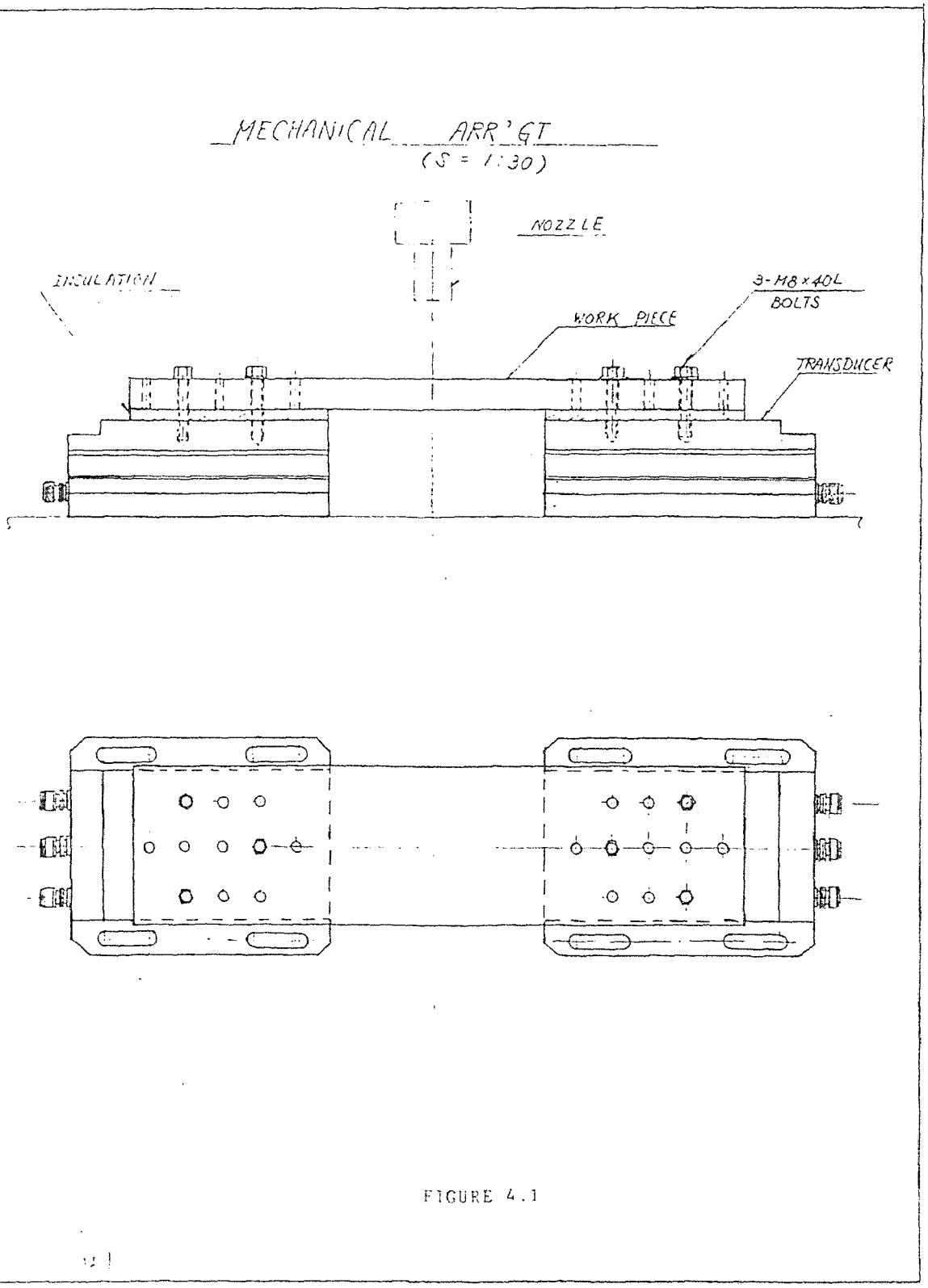
MECHANICAL ARR'GT
(S = 1:30)
NOZZLE
INSULATION
3-M8 x 40L
BOLTS
WORK PIECE
TRANSDUCER

FIGURE 4.1

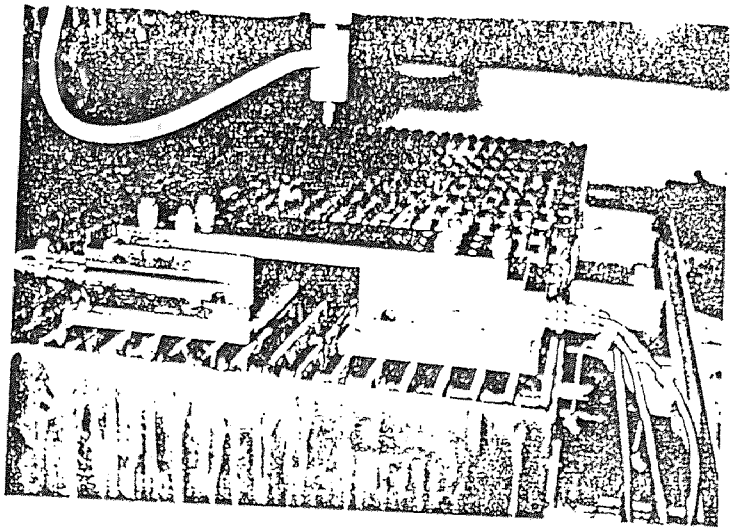

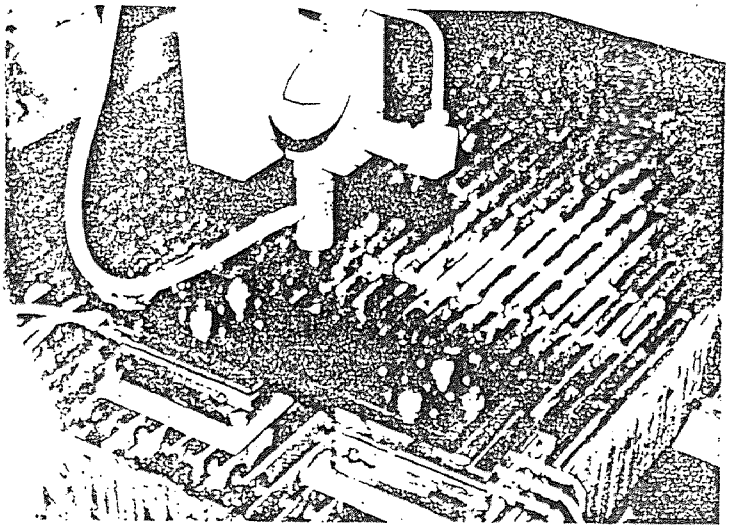

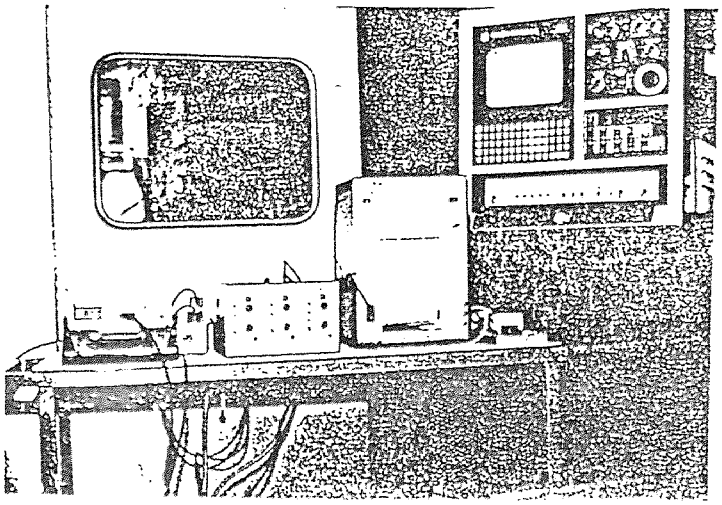

Figure 4.1(a) Measurement Devices Picture

DETAIL OF WORK PIECE
(S = 1:30)

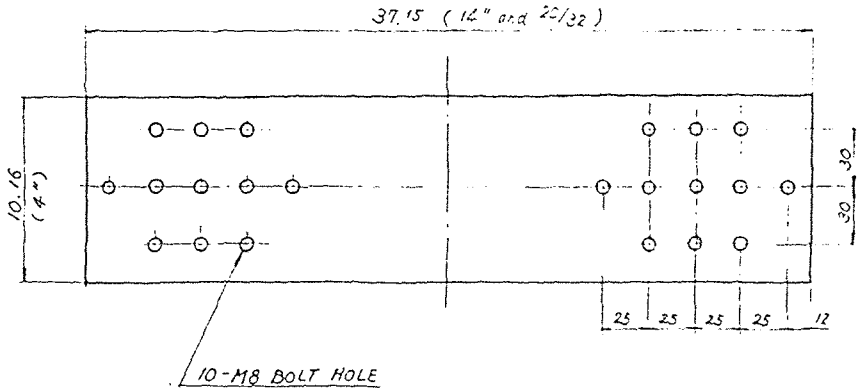

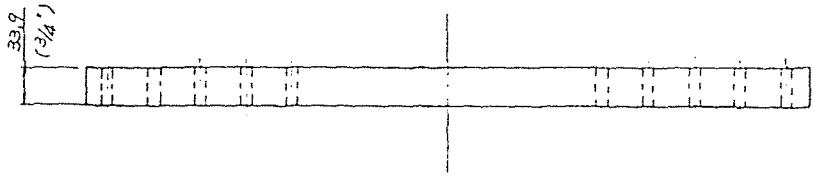

FIGURE 4.2

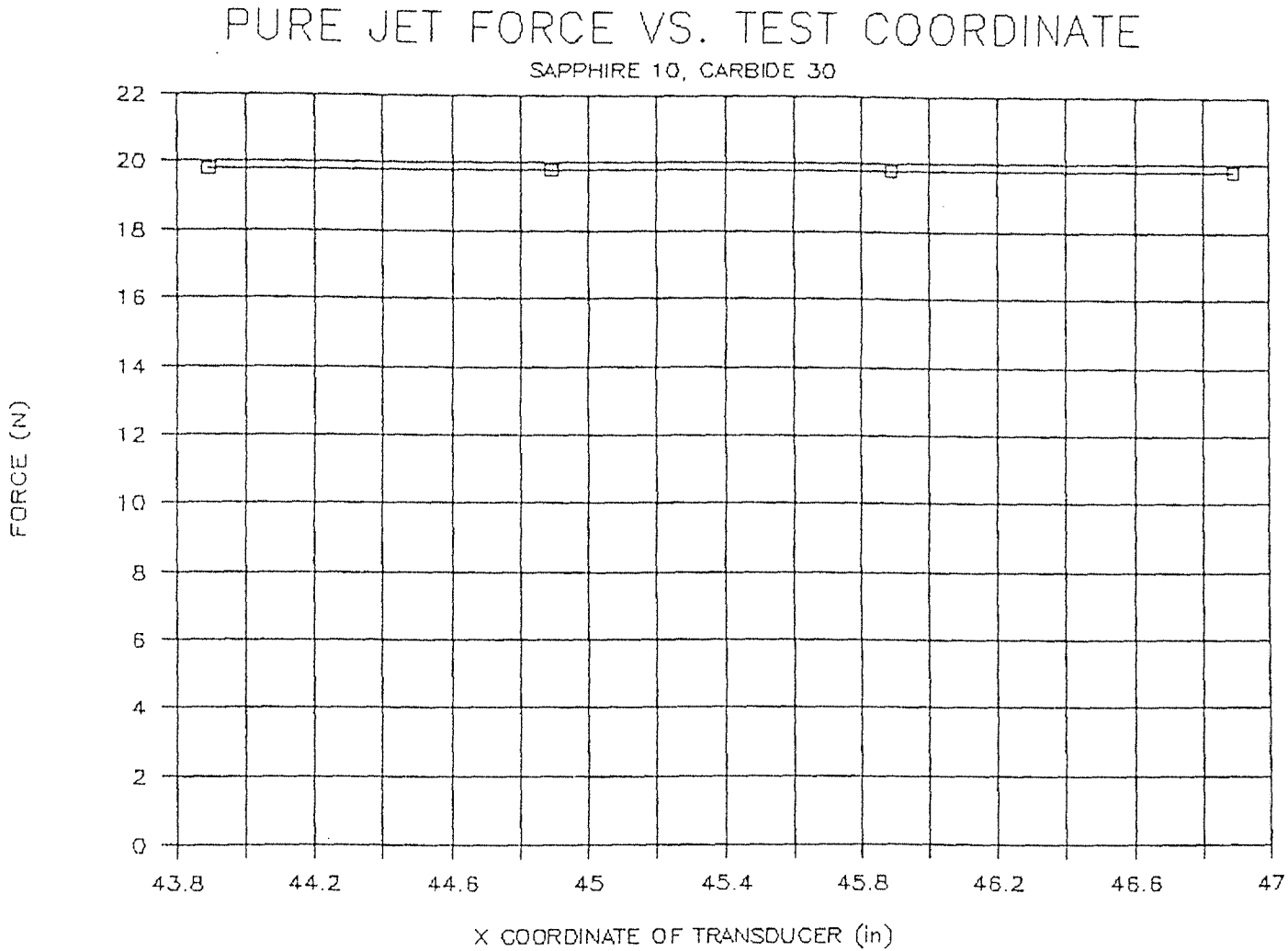
PURE JET FORCE VS. TEST COORDINATE
SAPPHIRE 10, CARBIDE 30
FORCE (N)
22
20
18
16
14
12
10
8
6
4
2
0
43.8
44.2
44.6
45
45.4
45.8
46.2
46.6
47
X COORDINATE OF TRANSDUCER (in)

FIGURE 4.3(a)

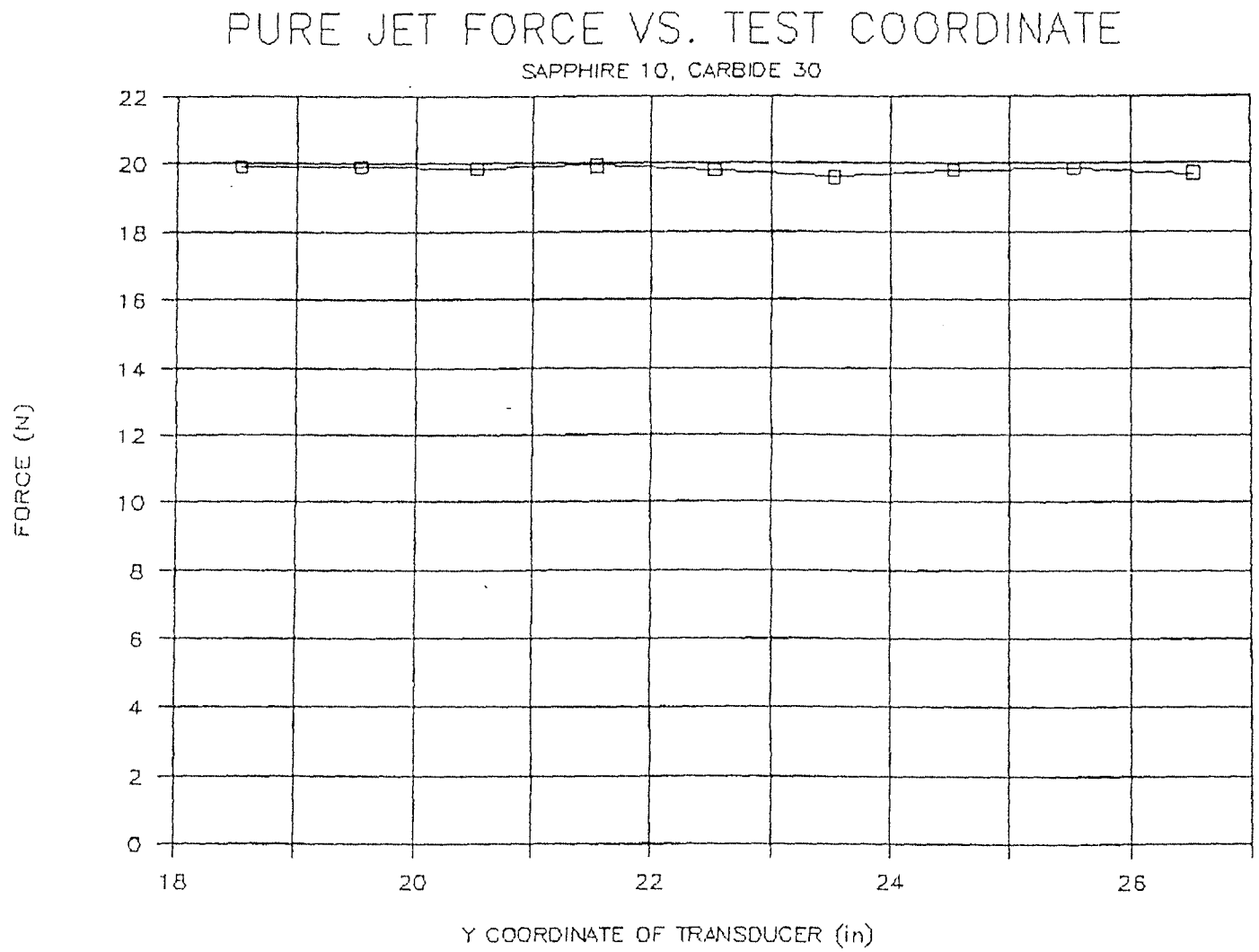
PURE JET FORCE VS. TEST COORDINATE
SAPPHIRE 10, CARBIDE 30
FORCE (N)
22
20
18
16
14
12
10
8
6
4
2
0
18
20
22
24
26
Y COORDINATE OF TRANSDUCER (in)

FIGURE 4.3(b)

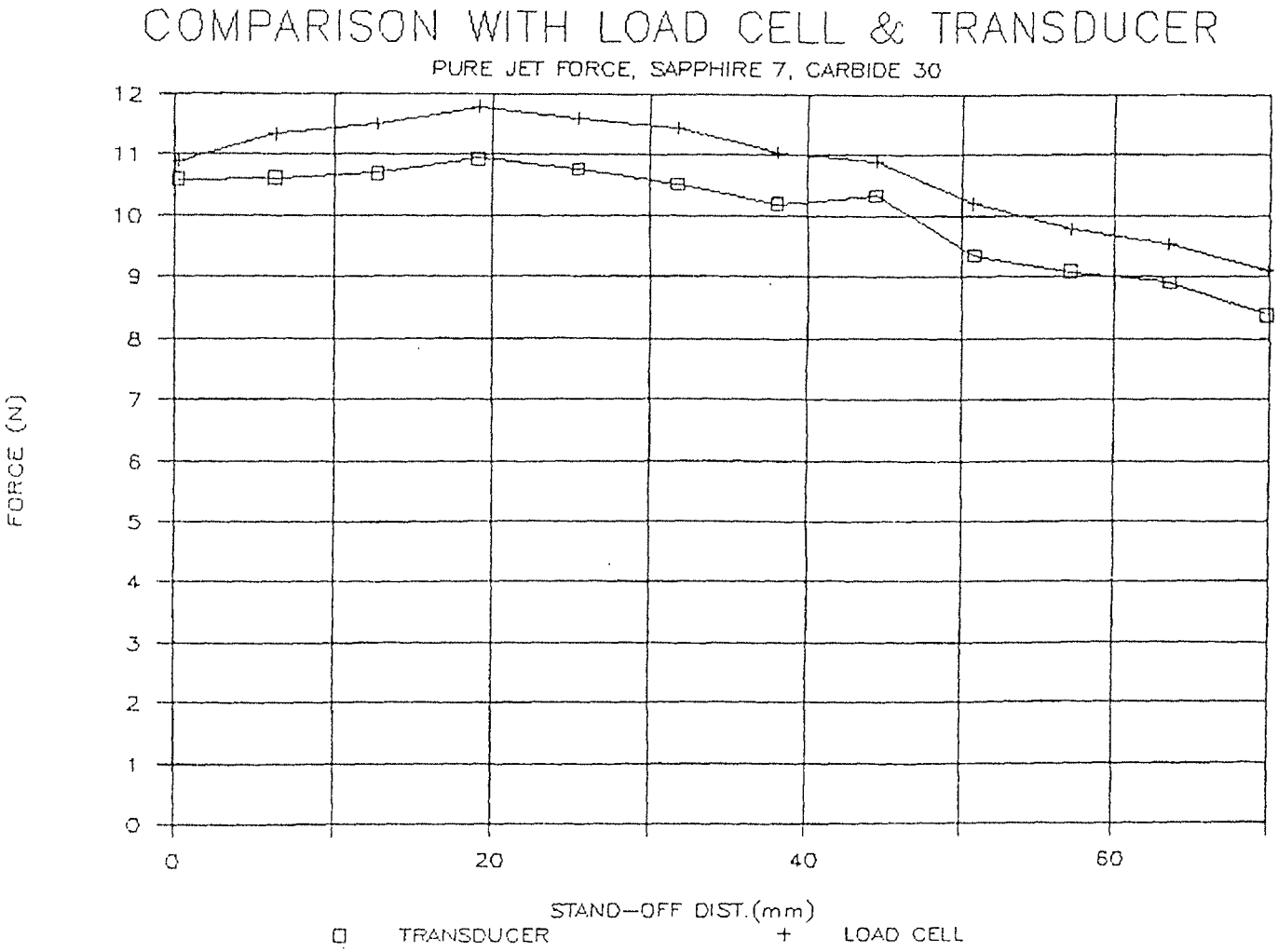
COMPARISON WITH LOAD CELL & TRANSDUCER
PURE JET FORCE, SAPPHIRE 7, CARBIDE 30
FORCE (N)
12
11
10
9
8
7
6
5
4
3
2
1
0
0
20
40
60
STAND-OFF DIST.(mm)
TRANSDUCER
LOAD CELL

FIGURE 4.4

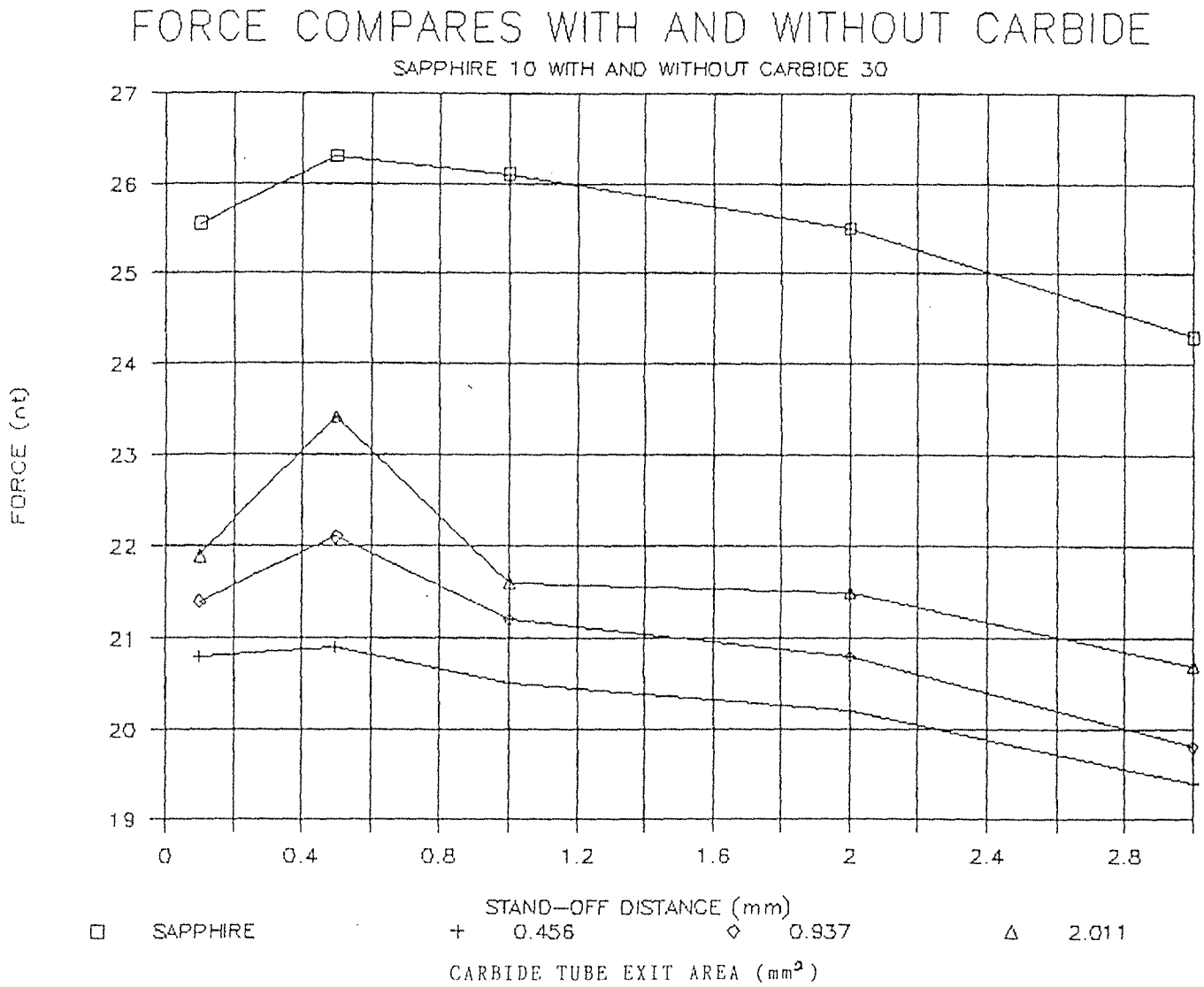
FORCE COMPARES WITH AND WITHOUT CARBIDE
SAPPHIRE 10 WITH AND WITHOUT CARBIDE 30
FORCE (nt)
27
26
25
24
23
22
21
20
19
0
0.4
0.8
1.2
1.6
2
2.4
2.8
STAND-OFF DISTANCE (mm)
□ SAPPHIRE
+ 0.456
◇ 0.937
△ 2.011
CARBIDE TUBE EXIT AREA (mm²)

FIGURE 6.1

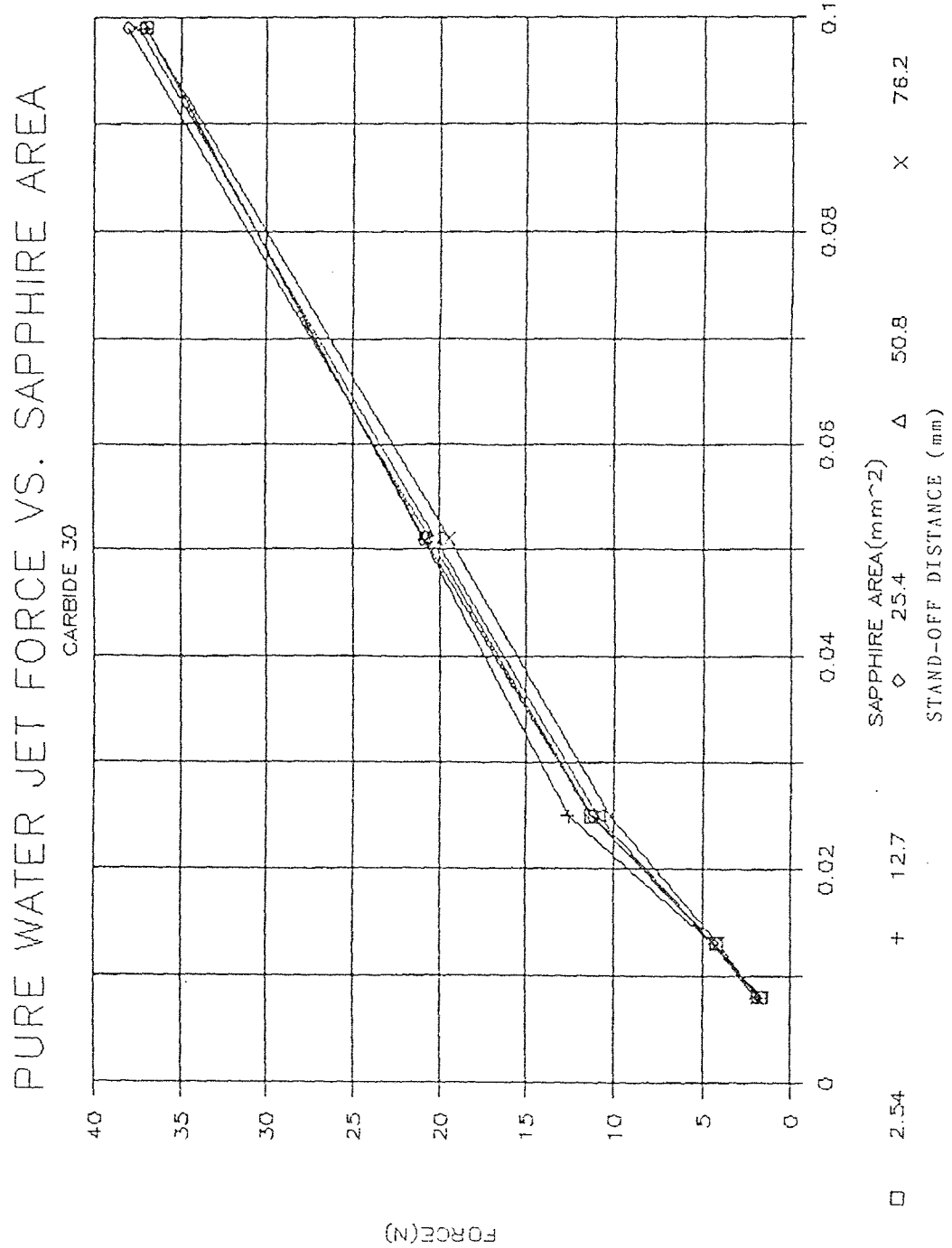
PURE WATER JET FORCE VS. SAPPHIRE AREA
CARBIDE 30
FORCE(N)
40
35
30
25
20
15
10
5
0
0
0.02
0.04
0.06
0.08
0.1
SAPPHIRE AREA(mm^2)
◇ 25.4
Δ 50.8
□ 2.54
+ 12.7
× 76.2
STAND-OFF DISTANCE (mm)

FIGURE 6.2

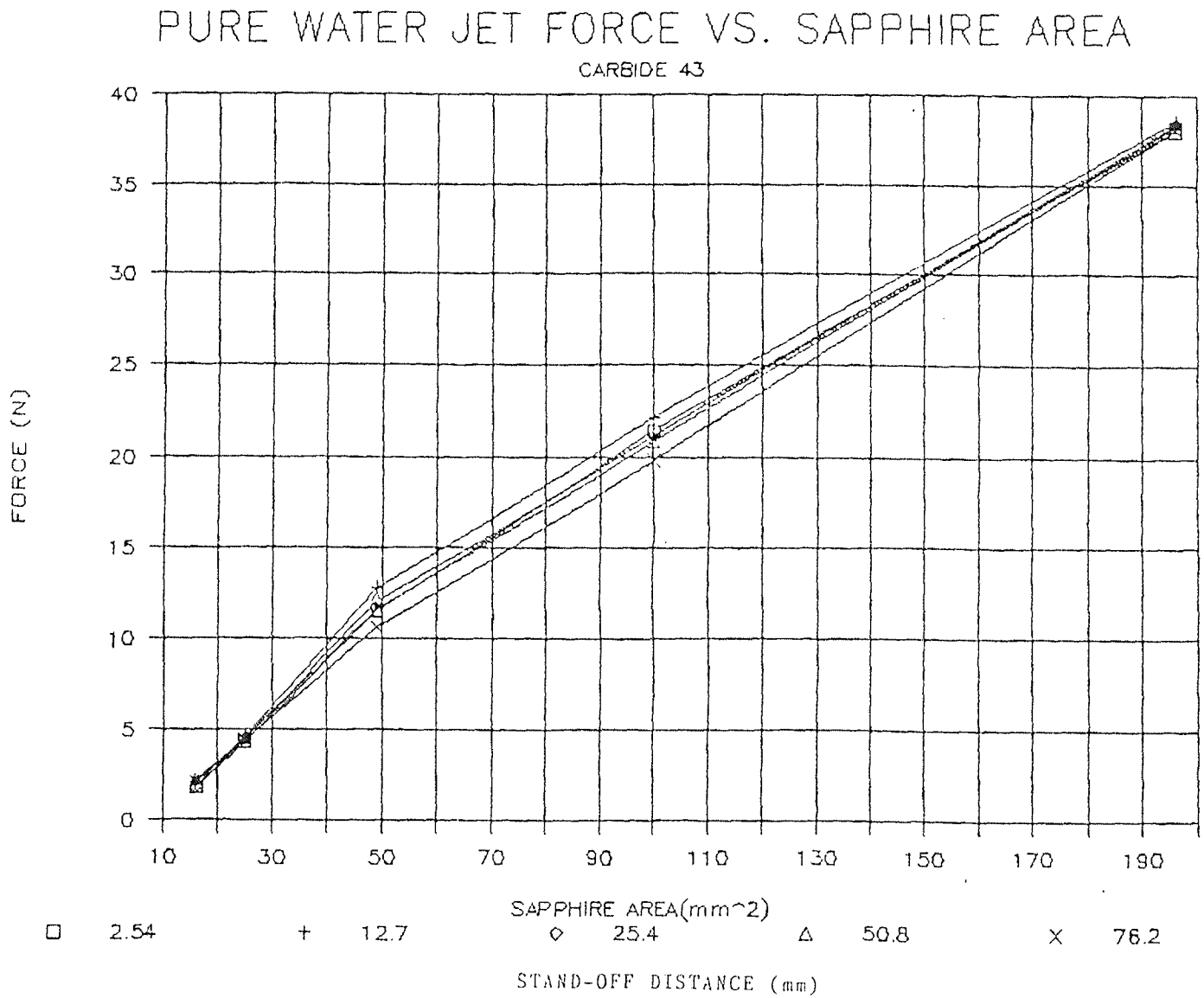
PURE WATER JET FORCE VS. SAPPHIRE AREA
CARBIDE 43
FORCE (N)
0
5
10
15
20
25
30
35
40
10
30
50
70
90
110
130
150
170
190
SAPPHIRE AREA(mm^2)
□ 2.54
+ 12.7
◇ 25.4
△ 50.8
X 76.2
STAND-OFF DISTANCE (mm)

FIGURE 6.3

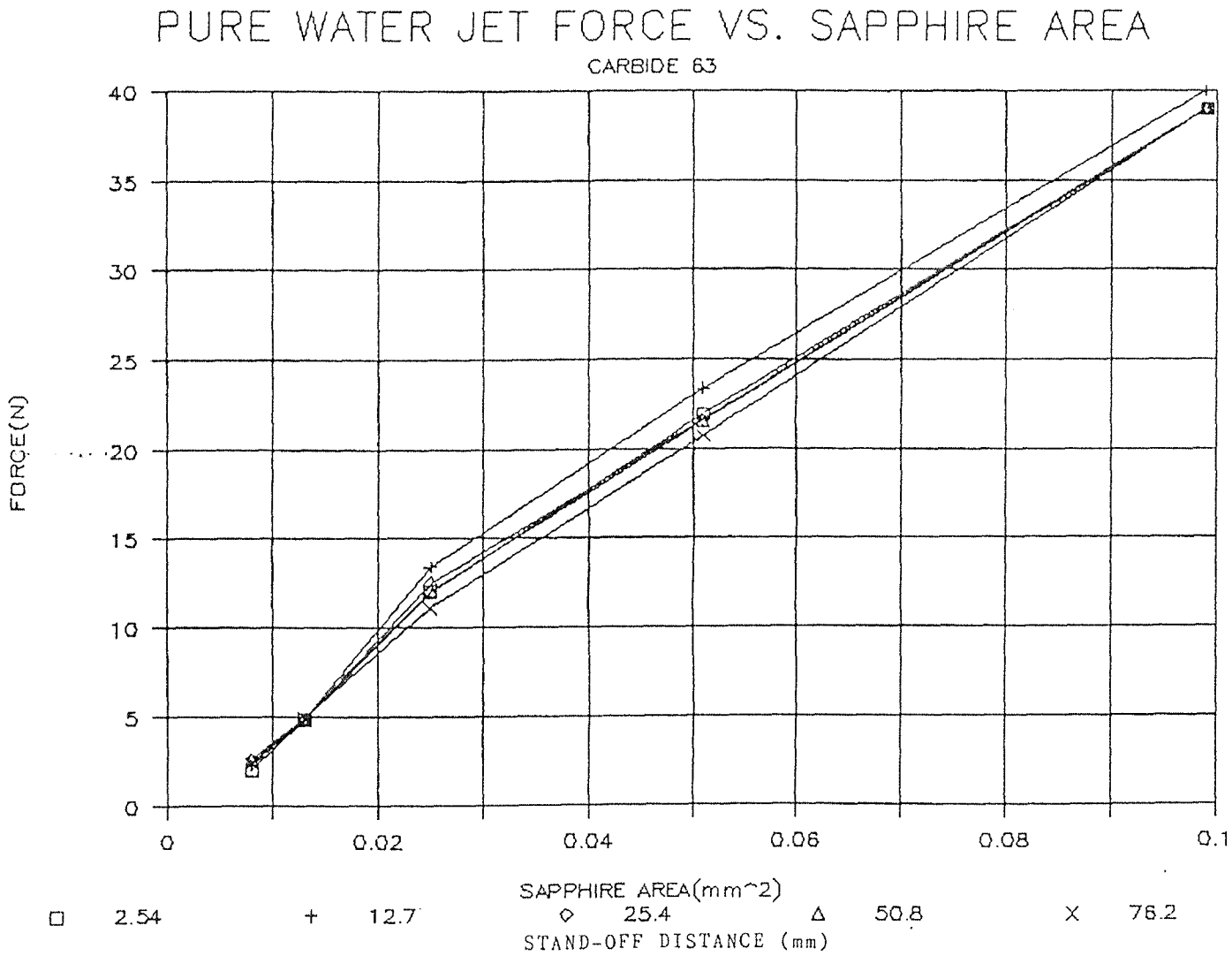
PURE WATER JET FORCE VS. SAPPHIRE AREA
CARBIDE 63
FORCE(N)
40
35
30
25
20
15
10
5
0
0
0.02
0.04
0.06
0.08
0.1
SAPPHIRE AREA(mm^2)
□ 2.54
+ 12.7
◇ 25.4
Δ 50.8
X 76.2
STAND-OFF DISTANCE (mm)

FIGURE 6.4

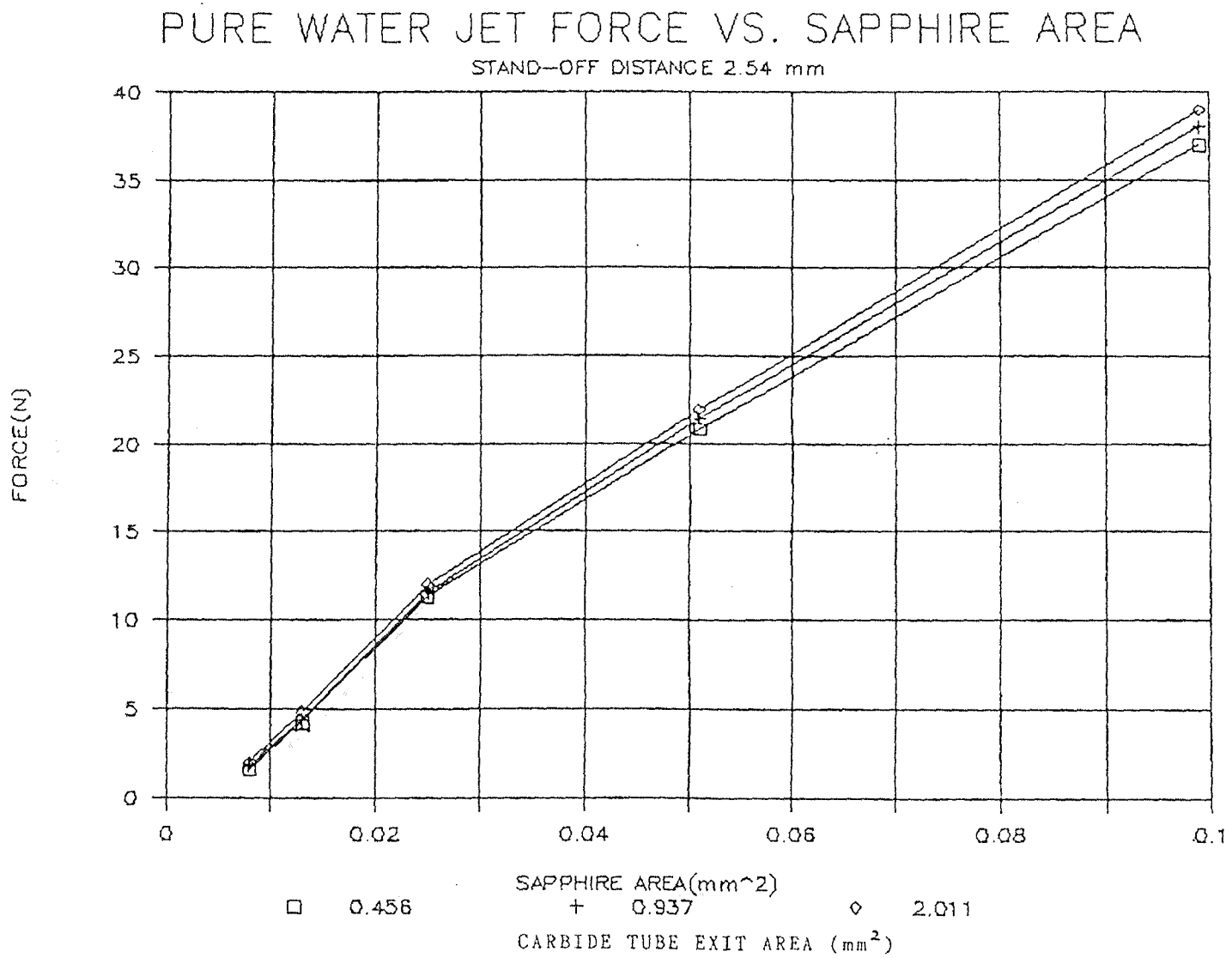
PURE WATER JET FORCE VS. SAPPHIRE AREA
STAND-OFF DISTANCE 2.54 mm
FORCE(N)
40
35
30
25
20
15
10
5
0
0
0.02
0.04
0.06
0.08
0.1
SAPPHIRE AREA(mm^2)
□ 0.456
+ 0.937
◇ 2.011
CARBIDE TUBE EXIT AREA (mm²)

FIGURE 6.5

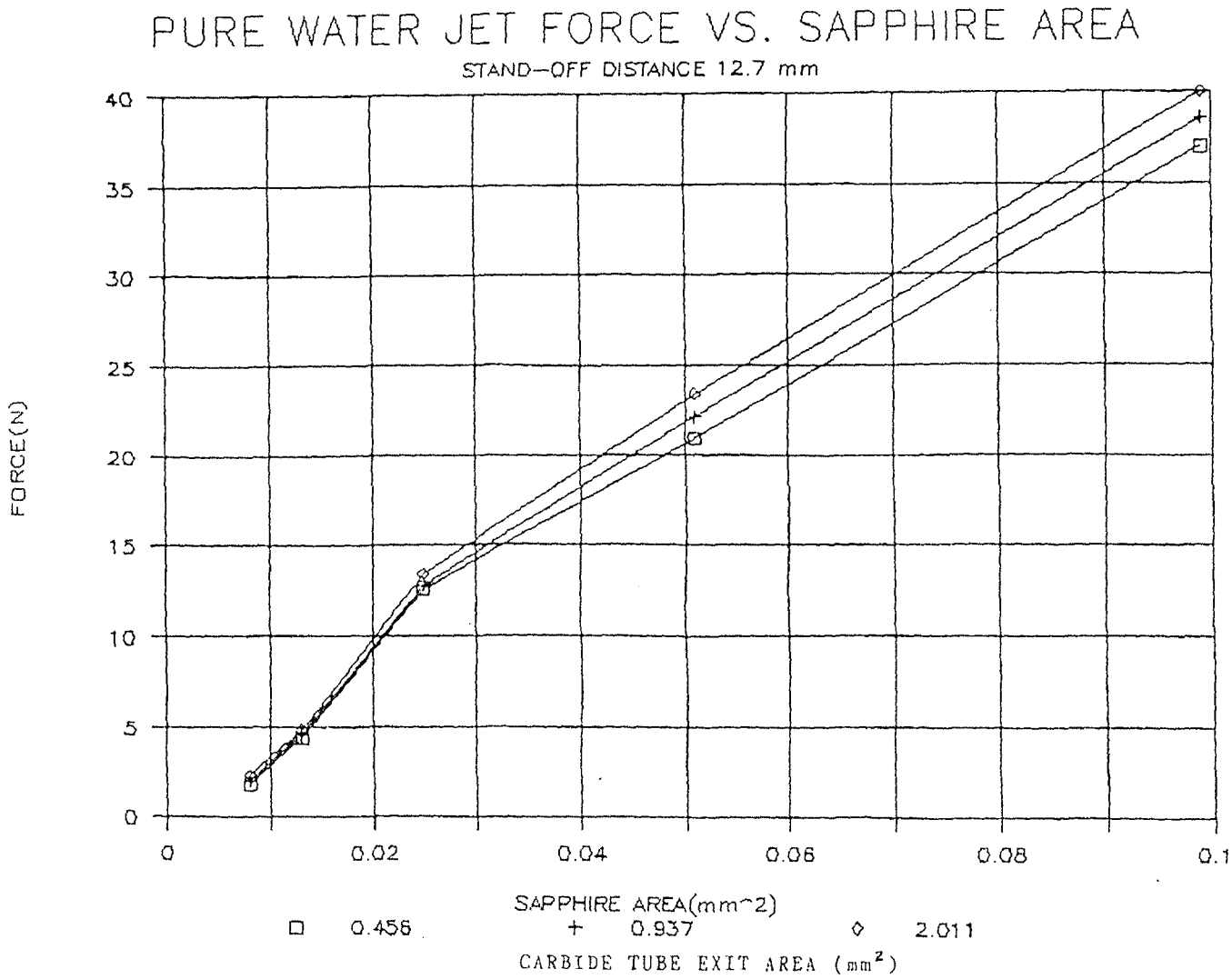
PURE WATER JET FORCE VS. SAPPHIRE AREA
STAND-OFF DISTANCE 12.7 mm
FORCE(N)
40
35
30
25
20
15
10
5
0
0
0.02
0.04
0.06
0.08
0.1
SAPPHIRE AREA(mm^2)
□ 0.456
+ 0.937
◇ 2.011
CARBIDE TUBE EXIT AREA (mm²)

FIGURE 6.6

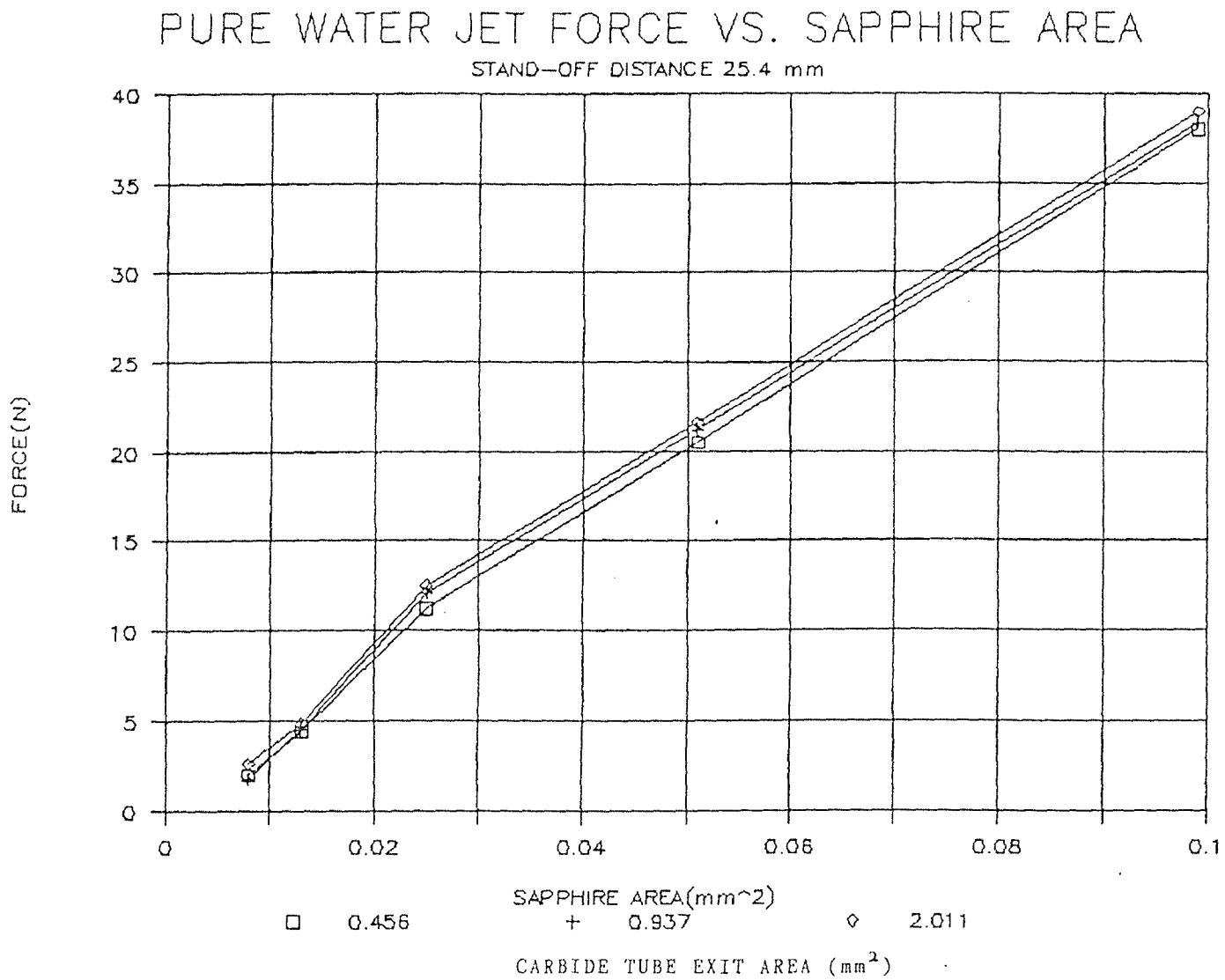
PURE WATER JET FORCE VS. SAPPHIRE AREA
STAND-OFF DISTANCE 25.4 mm
FORCE(N)
40
35
30
25
20
15
10
5
0
0
0.02
0.04
0.06
0.08
0.1
SAPPHIRE AREA(mm^2)
□ 0.456
+ 0.937
◇ 2.011
CARBIDE TUBE EXIT AREA (mm²)

FIGURE 6.7

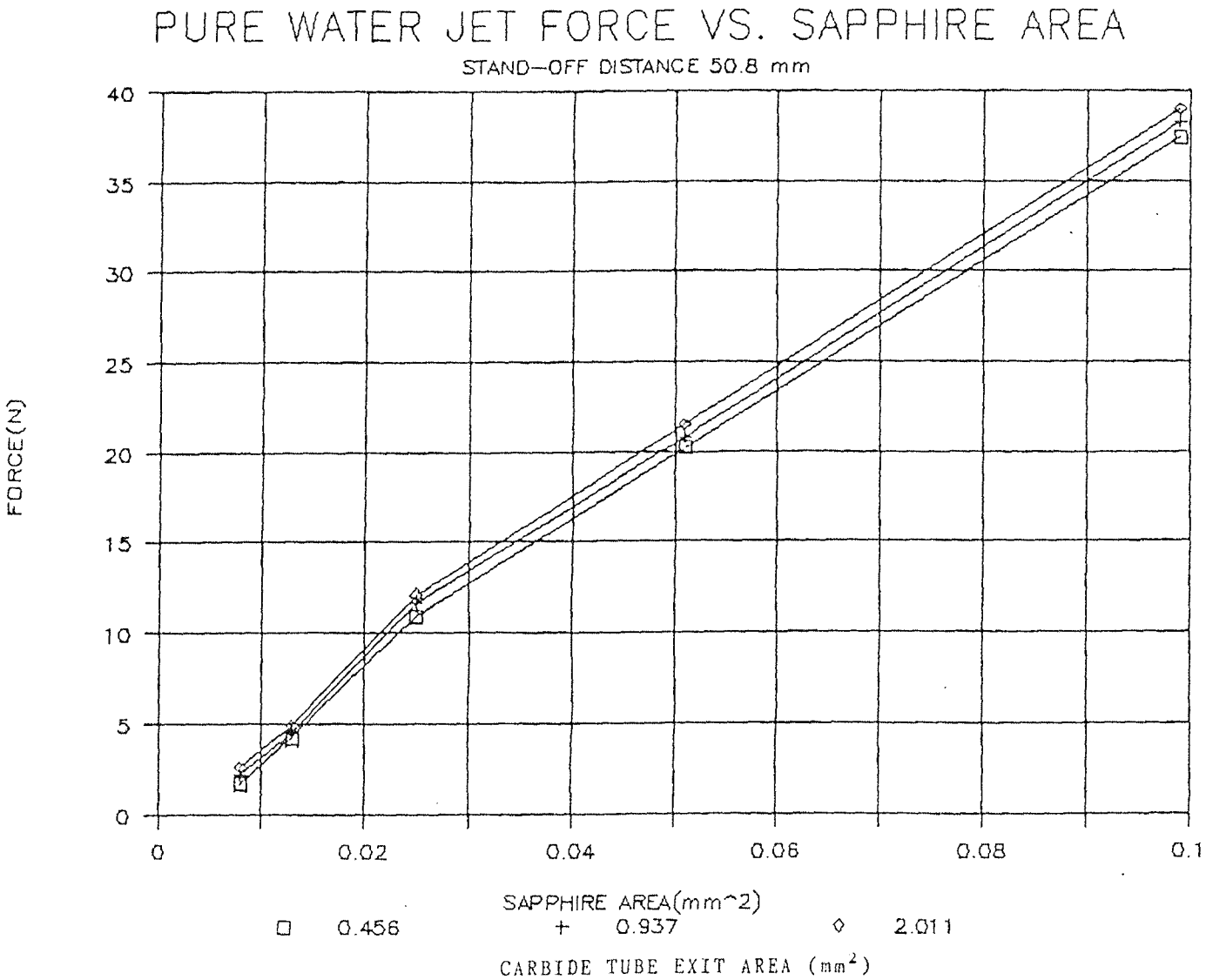
PURE WATER JET FORCE VS. SAPPHIRE AREA
STAND-OFF DISTANCE 50.8 mm
FORCE(N)
40
35
30
25
20
15
10
5
0
0
0.02
0.04
0.06
0.08
0.1
SAPPHIRE AREA(mm^2)
□ 0.456
+ 0.937
◇ 2.011
CARBIDE TUBE EXIT AREA (mm²)

FIGURE 6.8

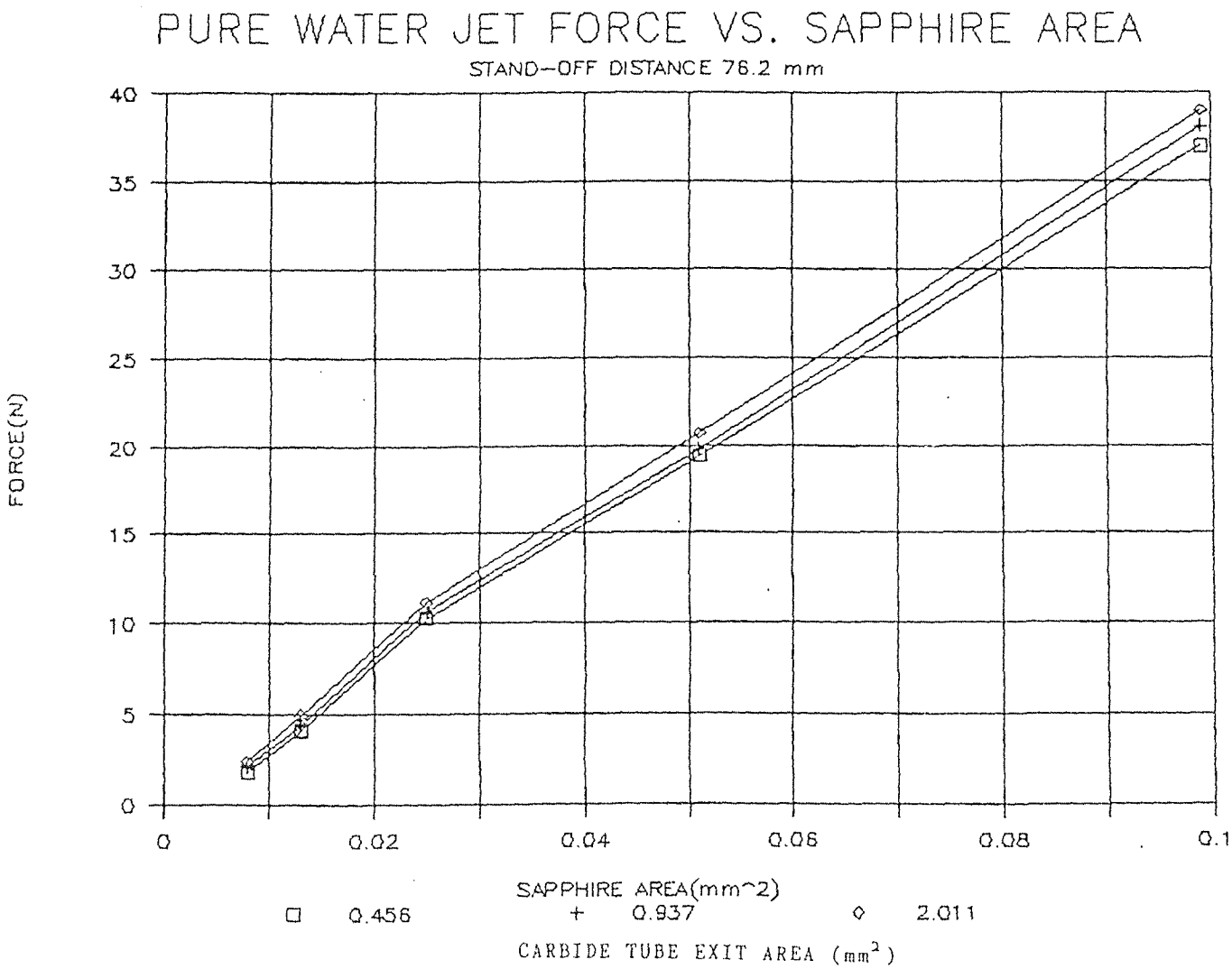
PURE WATER JET FORCE VS. SAPPHIRE AREA
STAND-OFF DISTANCE 76.2 mm
FORCE(N)
40
35
30
25
20
15
10
5
0
0
0.02
0.04
0.06
0.08
0.1
SAPPHIRE AREA(mm^2)
□ 0.456
+ 0.937
◇ 2.011
CARBIDE TUBE EXIT AREA (mm²)

FIGURE 6.9

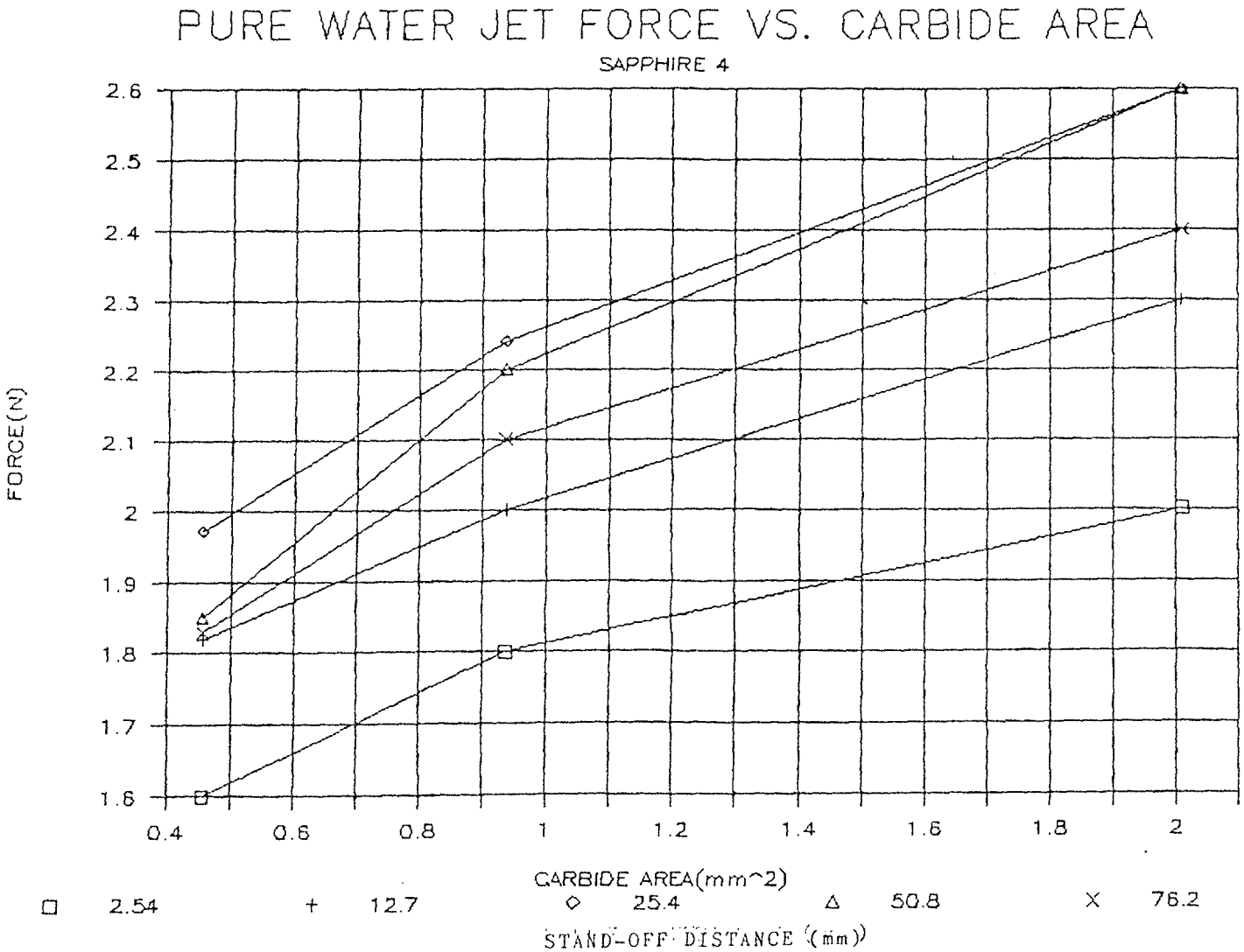
PURE WATER JET FORCE VS. CARBIDE AREA
SAPPHIRE 4
FORCE(N)
2.6
2.5
2.4
2.3
2.2
2.1
2
1.9
1.8
1.7
1.6
0.4
0.6
0.8
1
1.2
1.4
1.6
1.8
2
CARBIDE AREA(mm^2)
□ 2.54
+ 12.7
◇ 25.4
△ 50.8
X 76.2
STAND-OFF DISTANCE (mm)

FIGURE 6.10

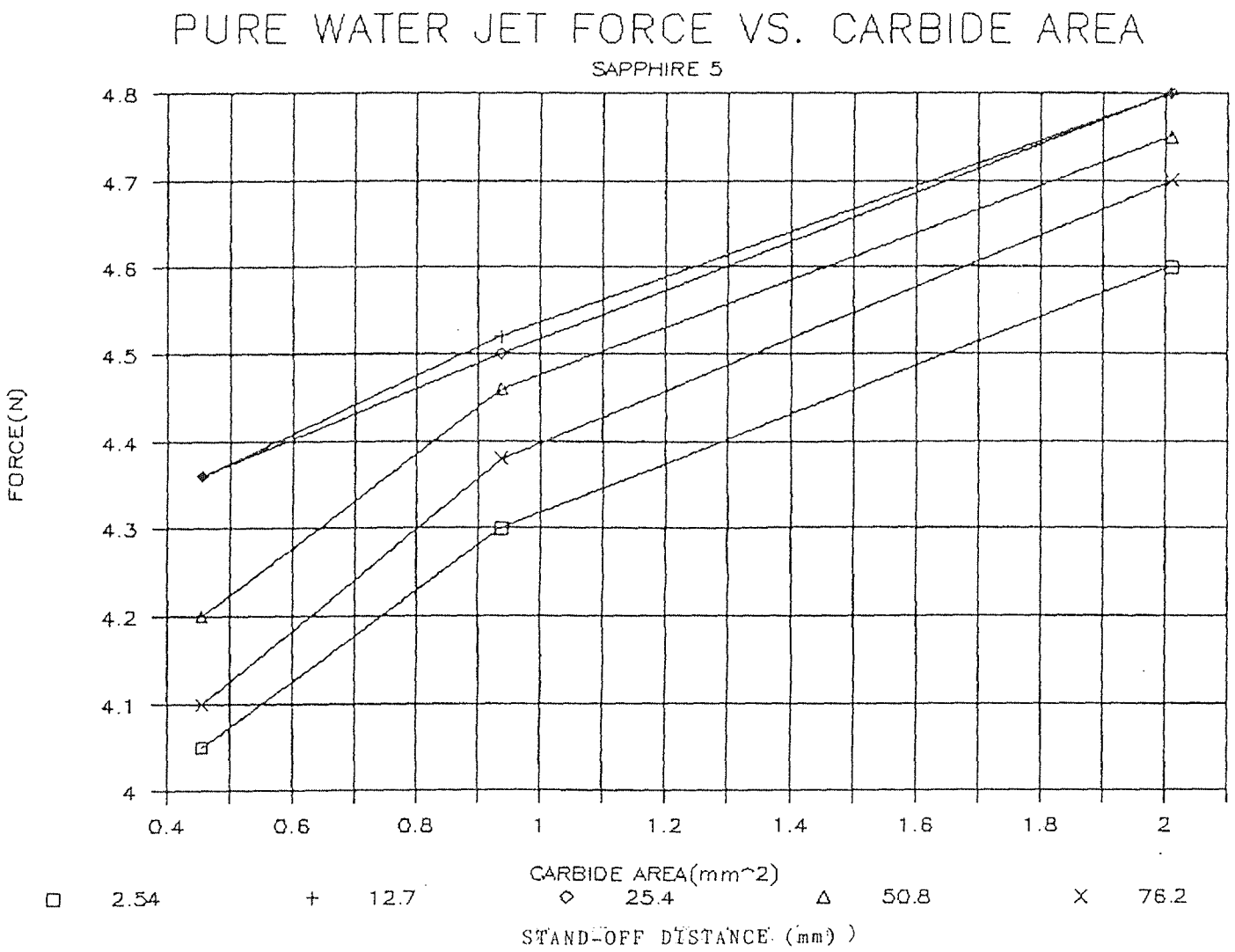
PURE WATER JET FORCE VS. CARBIDE AREA
SAPPHIRE 5
FORCE(N)
4.8
4.7
4.6
4.5
4.4
4.3
4.2
4.1
4
0.4
0.6
0.8
1
1.2
1.4
1.6
1.8
2
CARBIDE AREA(mm^2)
□ 2.54
+ 12.7
◇ 25.4
△ 50.8
X 76.2
STAND-OFF DISTANCE (mm))

FIGURE 6.11

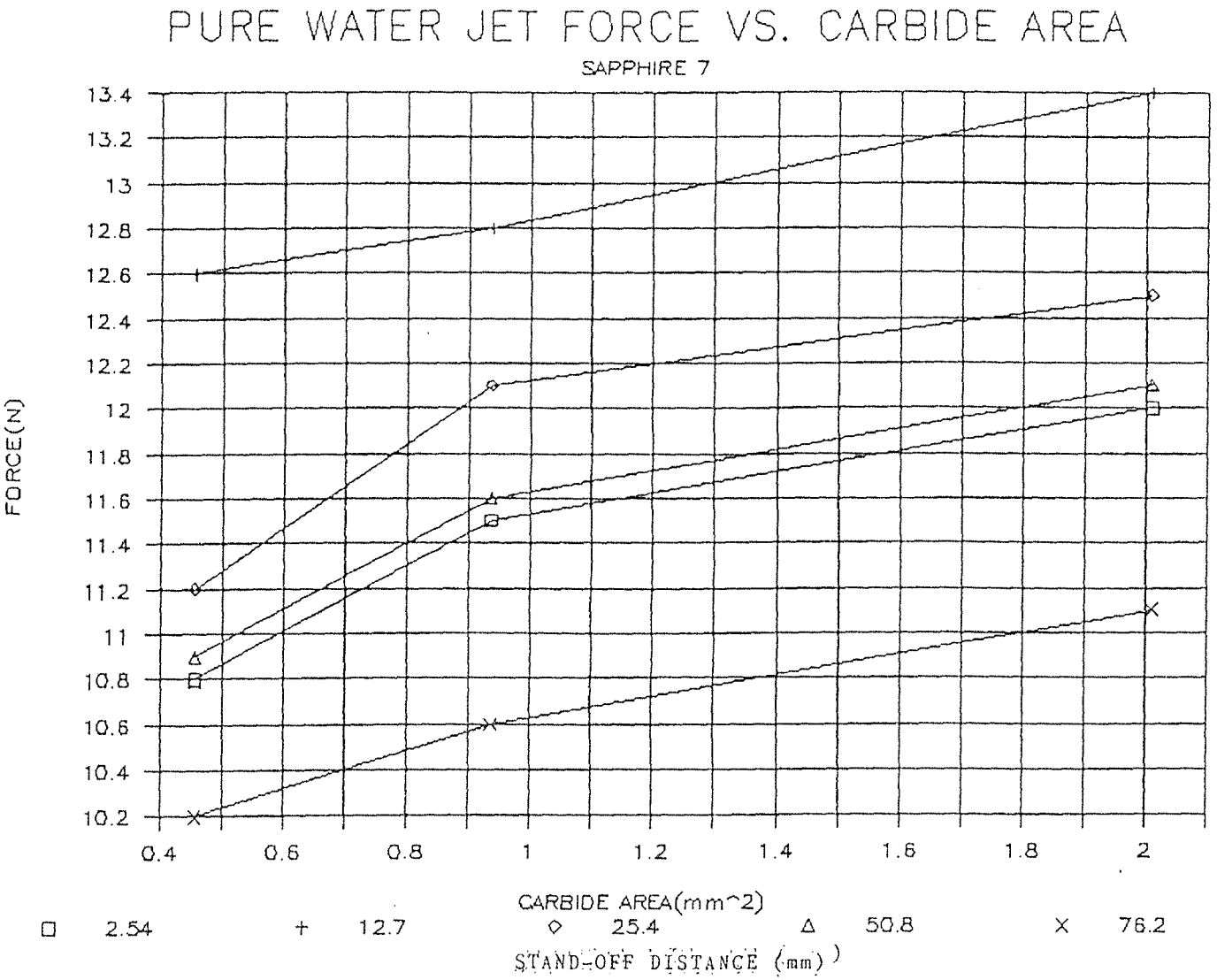
PURE WATER JET FORCE VS. CARBIDE AREA
SAPPHIRE 7
FORCE(N)
13.4
13.2
13
12.8
12.6
12.4
12.2
12
11.8
11.6
11.4
11.2
11
10.8
10.6
10.4
10.2
0.4
0.6
0.8
1
1.2
1.4
1.6
1.8
2
CARBIDE AREA(mm^2)
□ 2.54
+ 12.7
◇ 25.4
△ 50.8
× 76.2
STAND-OFF DISTANCE (mm)

FIGURE 6.12

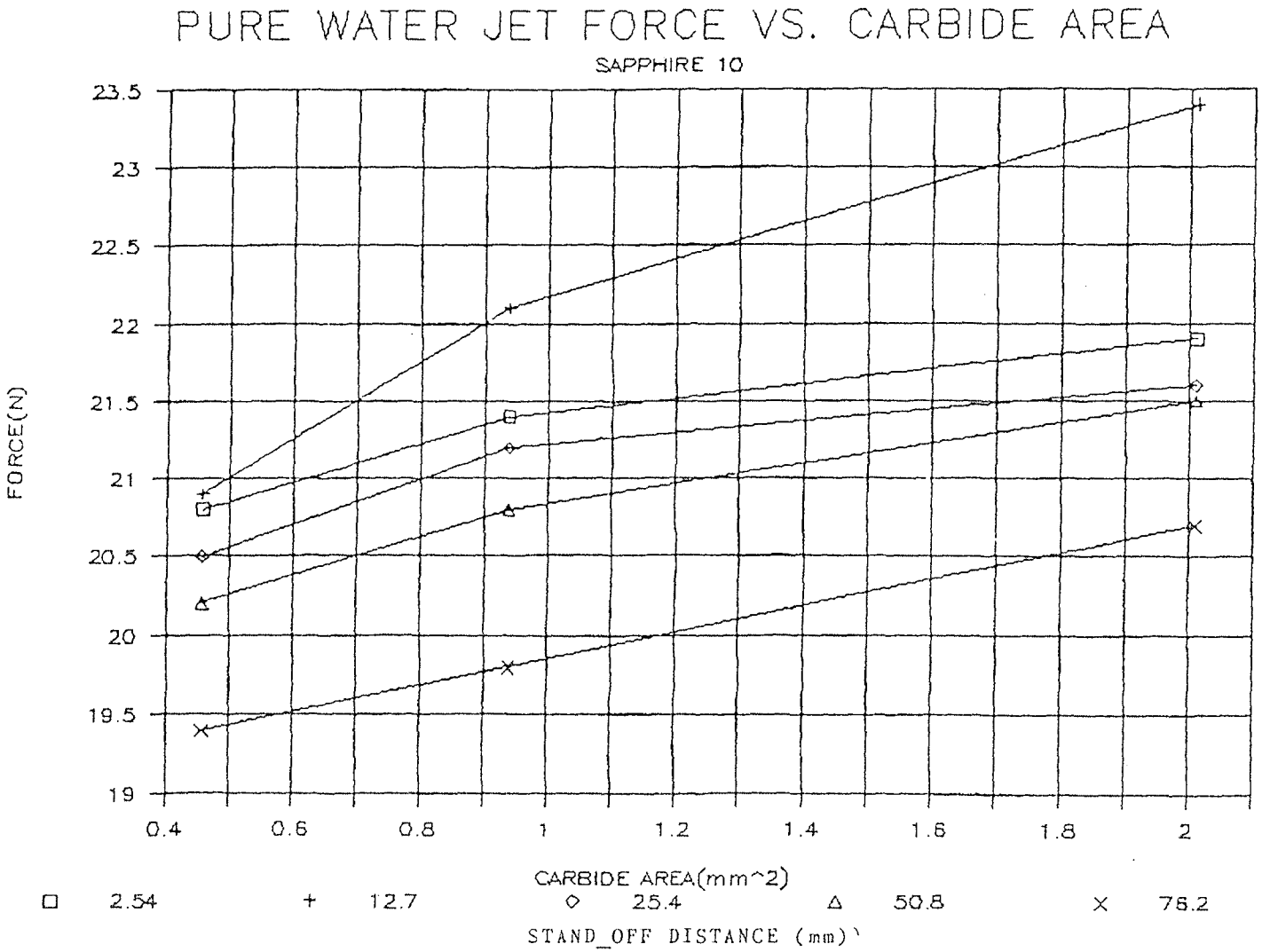
PURE WATER JET FORCE VS. CARBIDE AREA
SAPPHIRE 10
FORCE(N)
23.5
23
22.5
22
21.5
21
20.5
20
19.5
19
0.4
0.6
0.8
1
1.2
1.4
1.6
1.8
2
CARBIDE AREA(mm^2)
□ 2.54
+ 12.7
◇ 25.4
△ 50.8
× 76.2
STAND_OFF DISTANCE (mm)

FIGURE 6.13

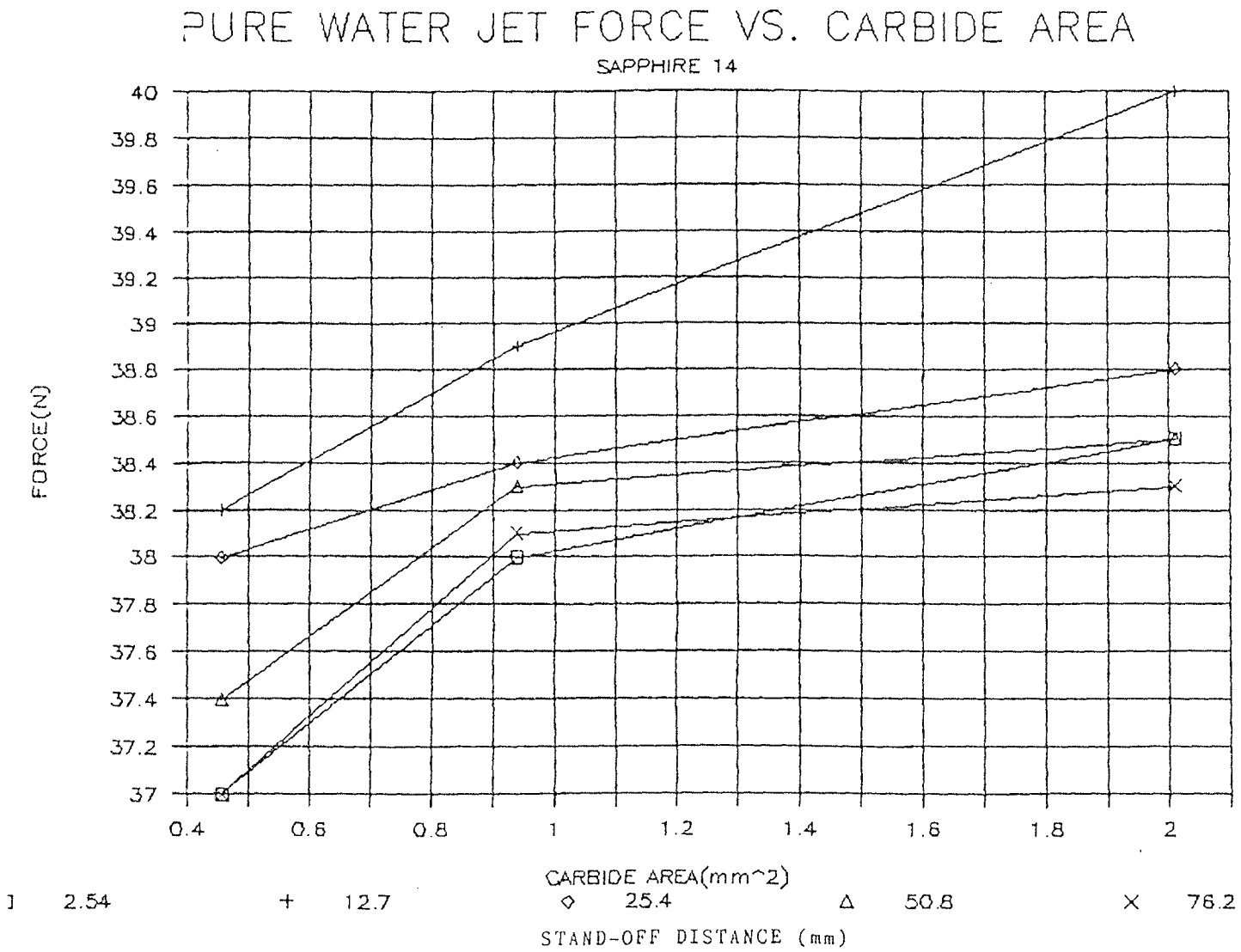
PURE WATER JET FORCE VS. CARBIDE AREA
SAPPHIRE 14
FORCE(N)
40
39.8
39.6
39.4
39.2
39
38.8
38.6
38.4
38.2
38
37.8
37.6
37.4
37.2
37
0.4
0.6
0.8
1
1.2
1.4
1.6
1.8
2
CARBIDE AREA(mm^2)
STAND-OFF DISTANCE (mm)
2.54
12.7
25.4
50.8
76.2

FIGURE 6.14

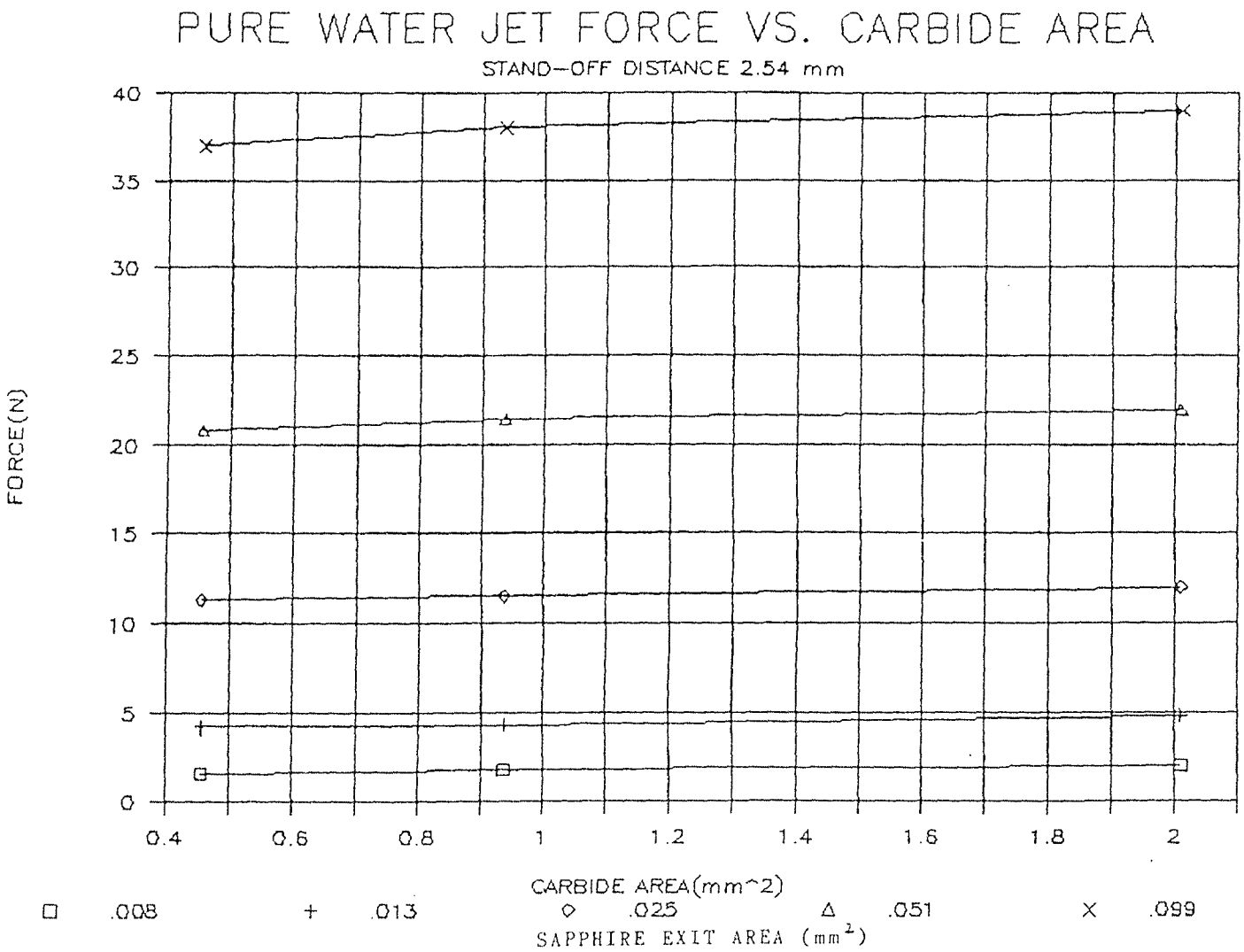
PURE WATER JET FORCE VS. CARBIDE AREA
STAND-OFF DISTANCE 2.54 mm
FORCE(N)
40
35
30
25
20
15
10
5
0
0.4
0.6
0.8
1
1.2
1.4
1.6
1.8
2
CARBIDE AREA(mm^2)
□ .008
+ .013
◇ .025
△ .051
× .099
SAPPHIRE EXIT AREA (mm²)

FIGURE 6.15

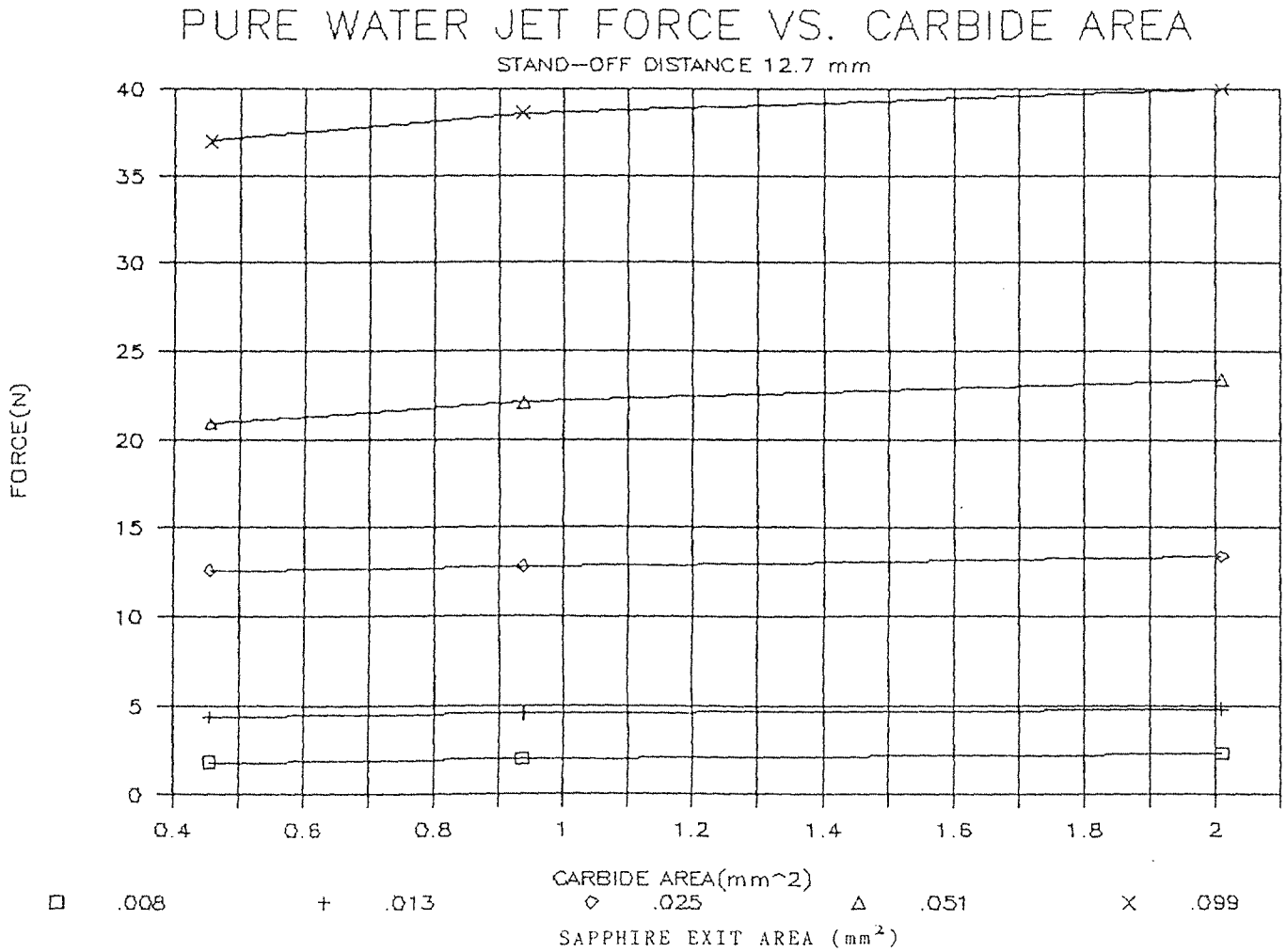
PURE WATER JET FORCE VS. CARBIDE AREA
STAND-OFF DISTANCE 12.7 mm
FORCE(N)
40
35
30
25
20
15
10
5
0
0.4
0.6
0.8
1
1.2
1.4
1.6
1.8
2
CARBIDE AREA(mm^2)
□ .008
+ .013
◇ .025
△ .051
× .099
SAPPHIRE EXIT AREA (mm²)

FIGURE 6.16

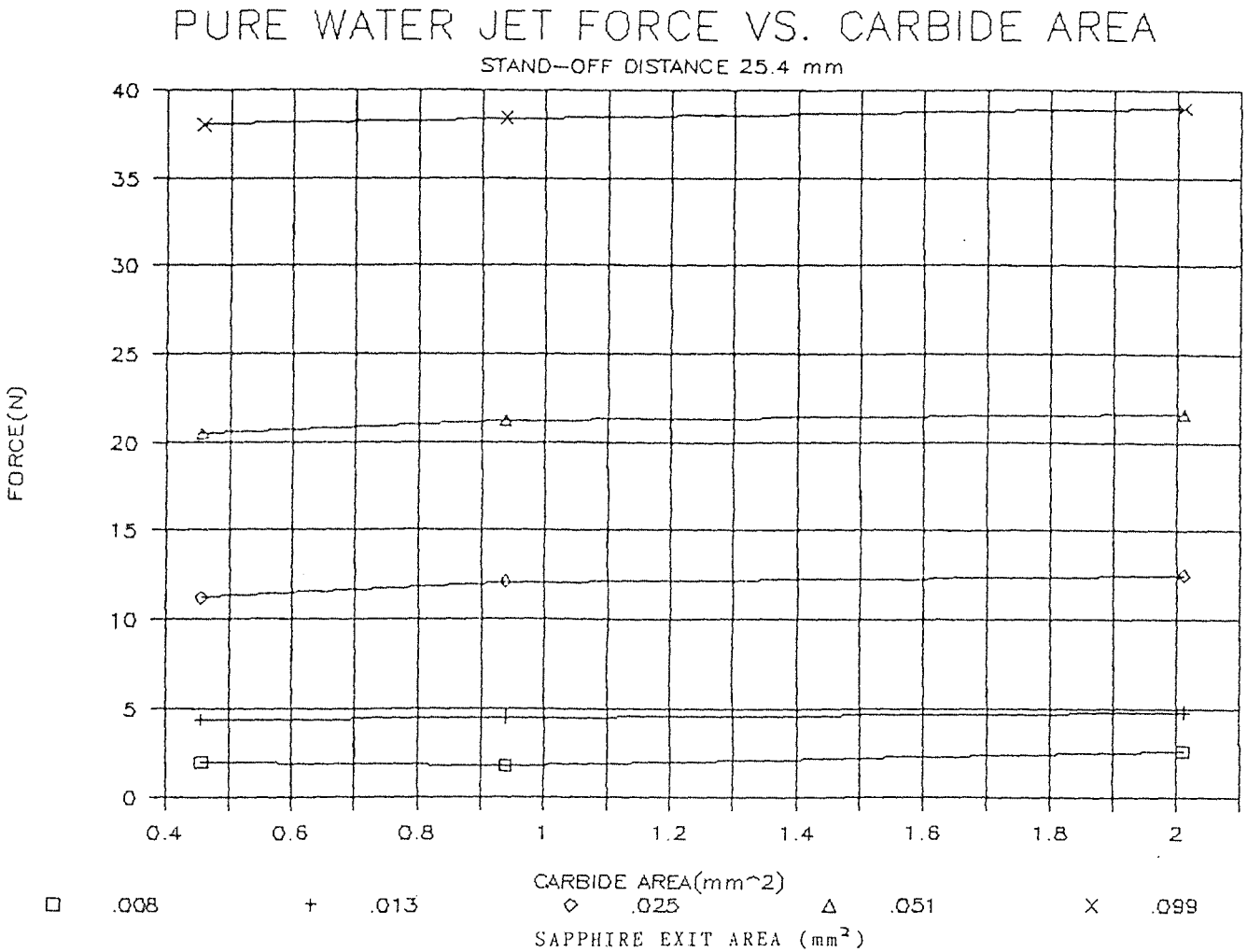
PURE WATER JET FORCE VS. CARBIDE AREA
STAND-OFF DISTANCE 25.4 mm
FORCE(N)
40
35
30
25
20
15
10
5
0
0.4
0.6
0.8
1
1.2
1.4
1.6
1.8
2
CARBIDE AREA(mm^2)
□ .008
+ .013
◇ .025
△ .051
X .099
SAPPHIRE EXIT AREA (mm²)

FIGURE 6.17

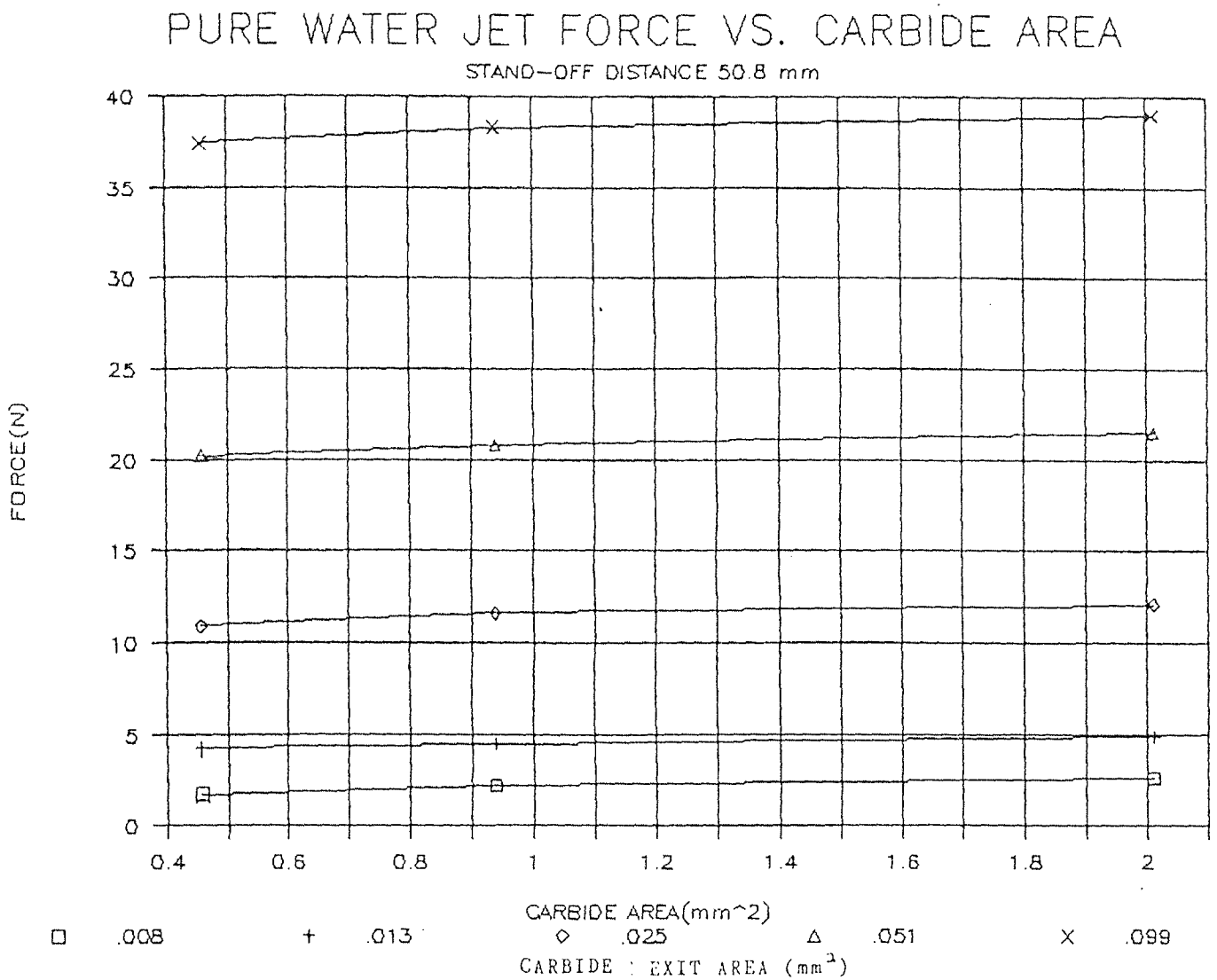
PURE WATER JET FORCE VS. CARBIDE AREA
STAND—OFF DISTANCE 50.8 mm
FORCE(N)
40
35
30
25
20
15
10
5
0
0.4
0.6
0.8
1
1.2
1.4
1.6
1.8
2
CARBIDE AREA(mm^2)
□ .008
+ .013
◇ .025
△ .051
X .099
CARBIDE : EXIT AREA (mm²)

FIGURE 6.18

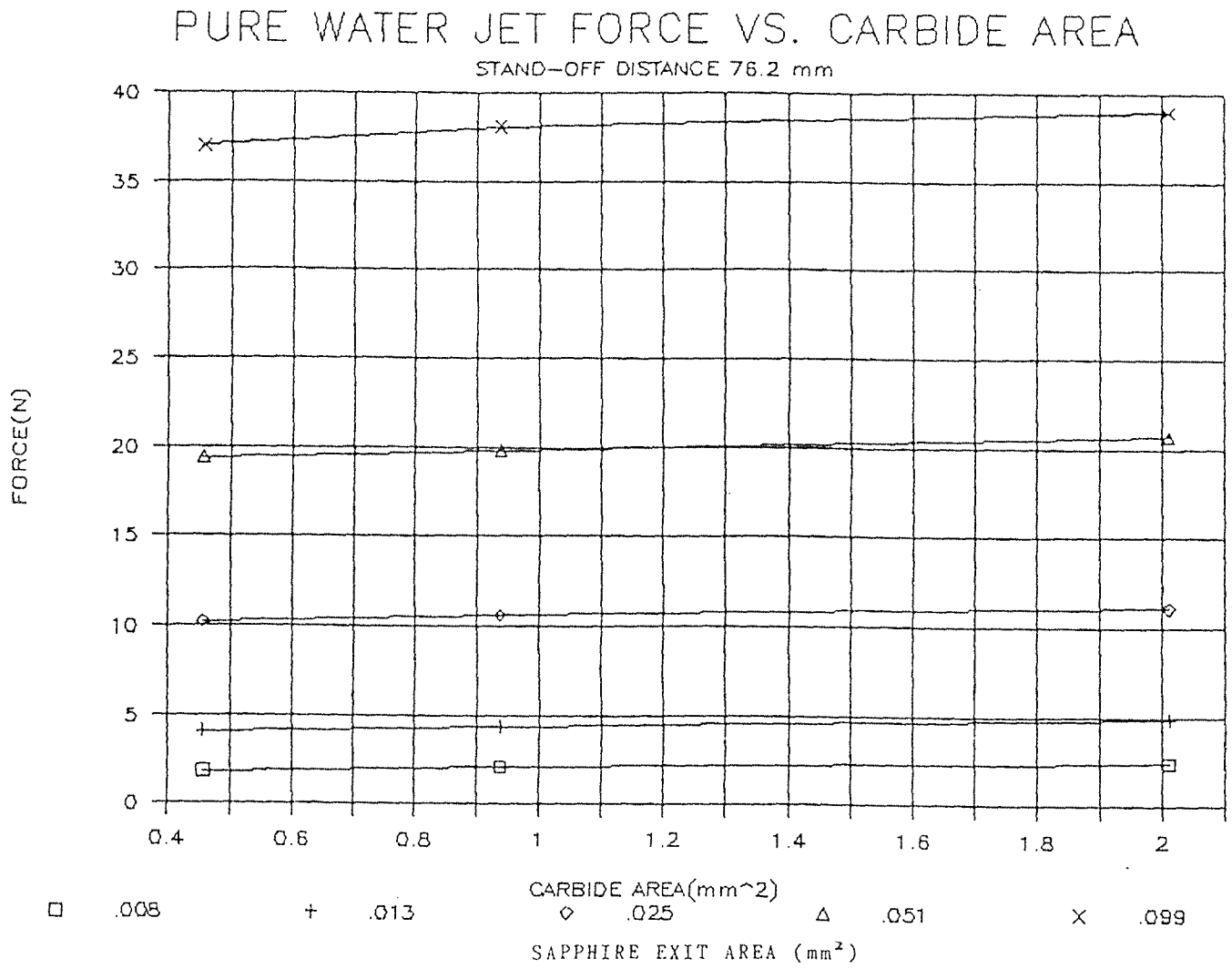
PURE WATER JET FORCE VS. CARBIDE AREA
STAND-OFF DISTANCE 76.2 mm
FORCE(N)
40
35
30
25
20
15
10
5
0
0.4
0.6
0.8
1
1.2
1.4
1.6
1.8
2
CARBIDE AREA(mm^2)
□ .008
+ .013
◇ .025
△ .051
× .099
SAPPHIRE EXIT AREA (mm²)

FIGURE 6.19

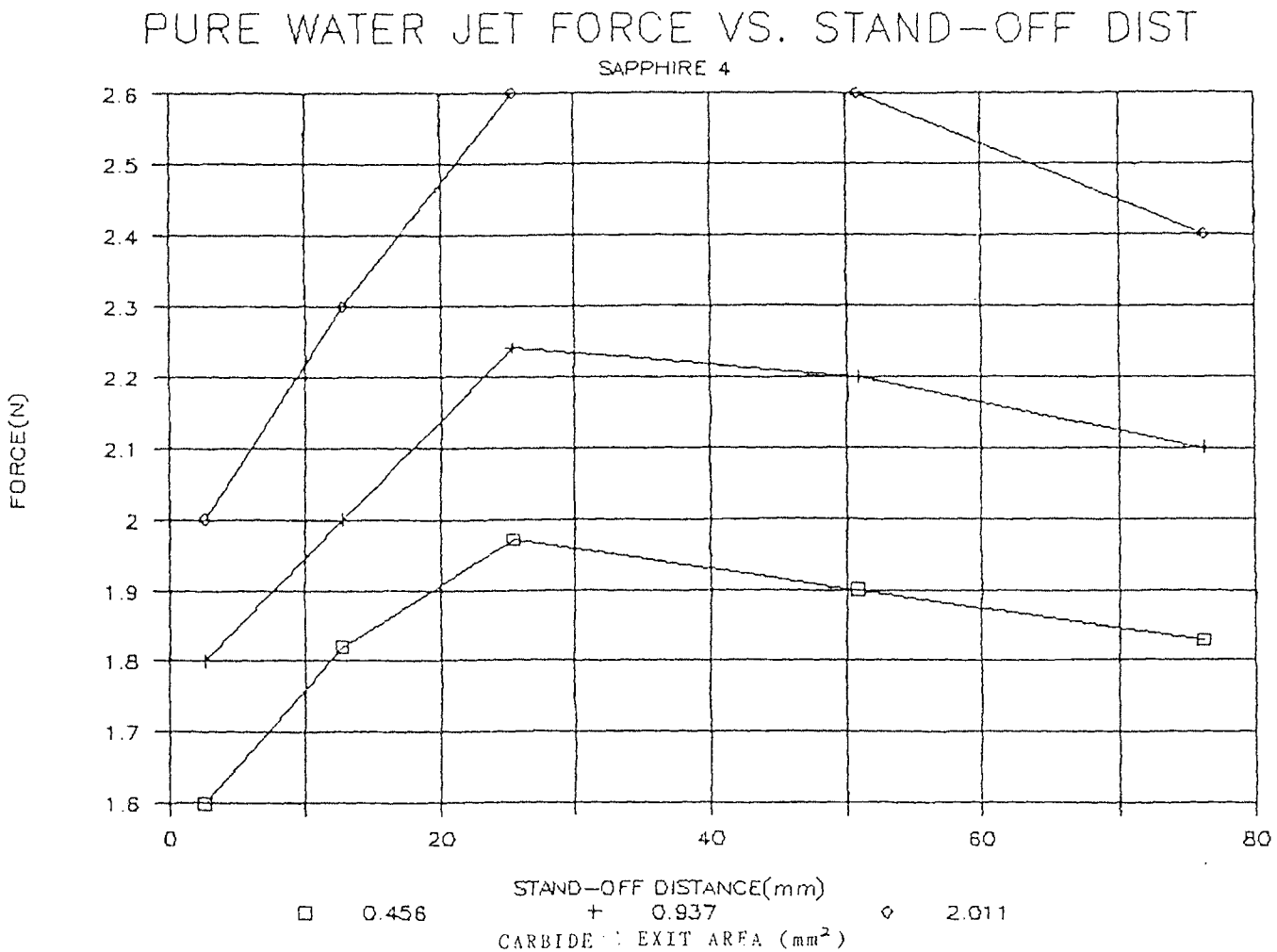
PURE WATER JET FORCE VS. STAND-OFF DIST
SAPPHIRE 4
FORCE(N)
2.6
2.5
2.4
2.3
2.2
2.1
2
1.9
1.8
1.7
1.6
0
20
40
60
80
STAND-OFF DISTANCE(mm)
□ 0.456
+ 0.937
◇ 2.011
CARBIDE EXIT AREA (mm²)

FIGURE 6.20

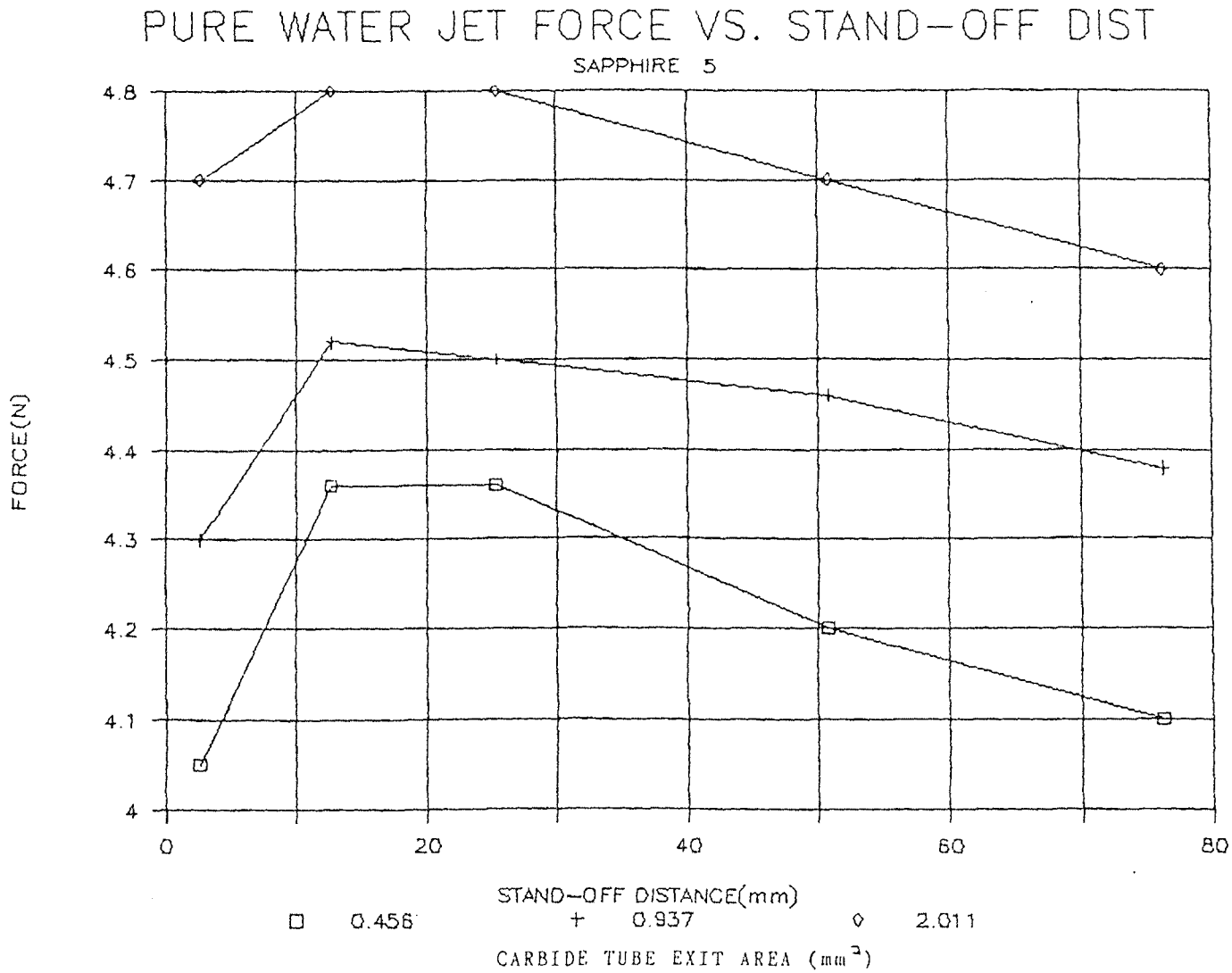
PURE WATER JET FORCE VS. STAND-OFF DIST
SAPPHIRE 5
FORCE(N)
4.8
4.7
4.6
4.5
4.4
4.3
4.2
4.1
4
0
20
40
60
80
STAND-OFF DISTANCE(mm)
□ 0.456
+ 0.937
◊ 2.011
CARBIDE TUBE EXIT AREA (mm²)

FIGURE 6.21.

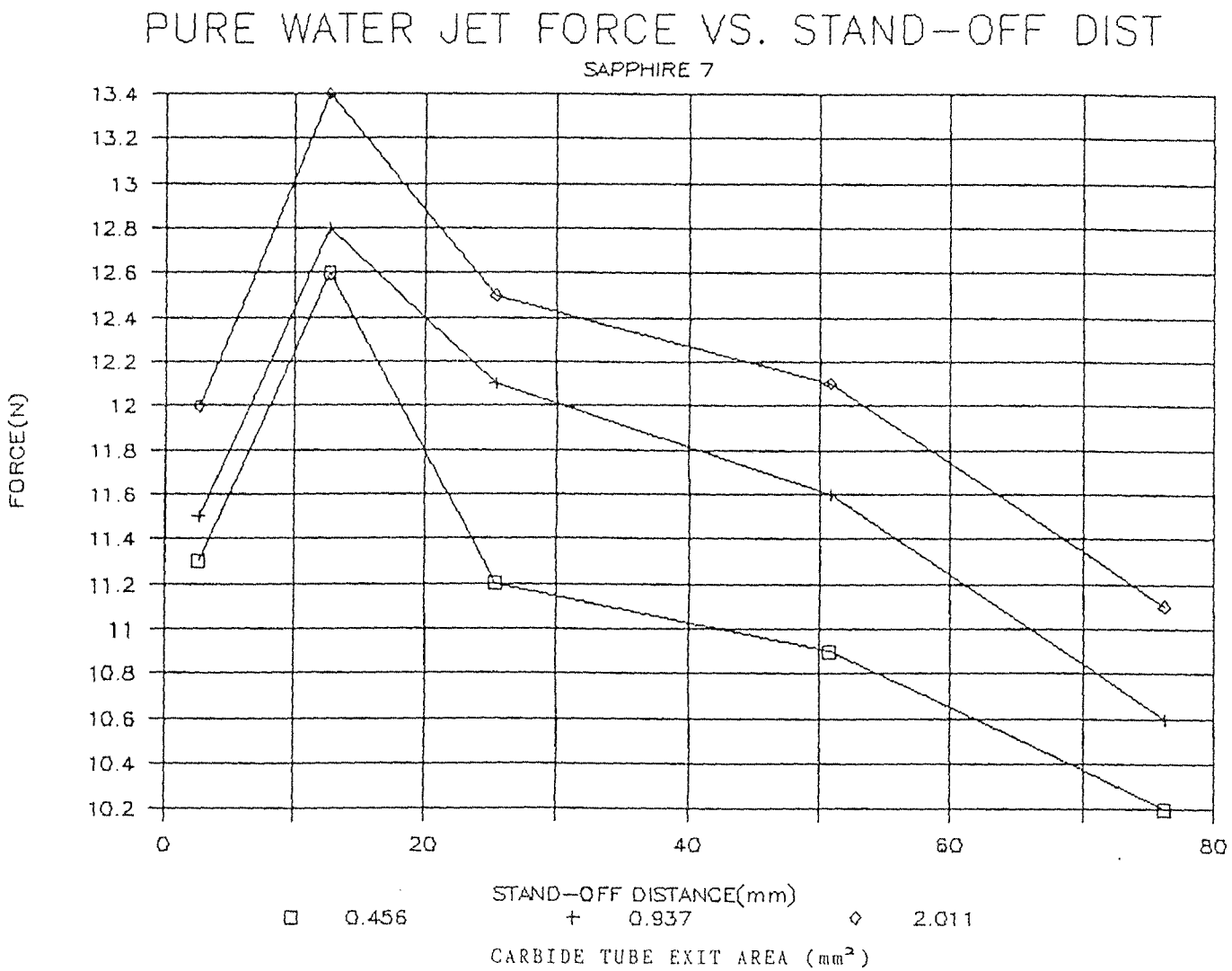
PURE WATER JET FORCE VS. STAND-OFF DIST
SAPPHIRE 7
FORCE(N)
13.4
13.2
13
12.8
12.6
12.4
12.2
12
11.8
11.6
11.4
11.2
11
10.8
10.6
10.4
10.2
0
20
40
60
80
STAND-OFF DISTANCE(mm)
□ 0.456
+ 0.937
◇ 2.011
CARBIDE TUBE EXIT AREA (mm²)

FIGURE #6.22

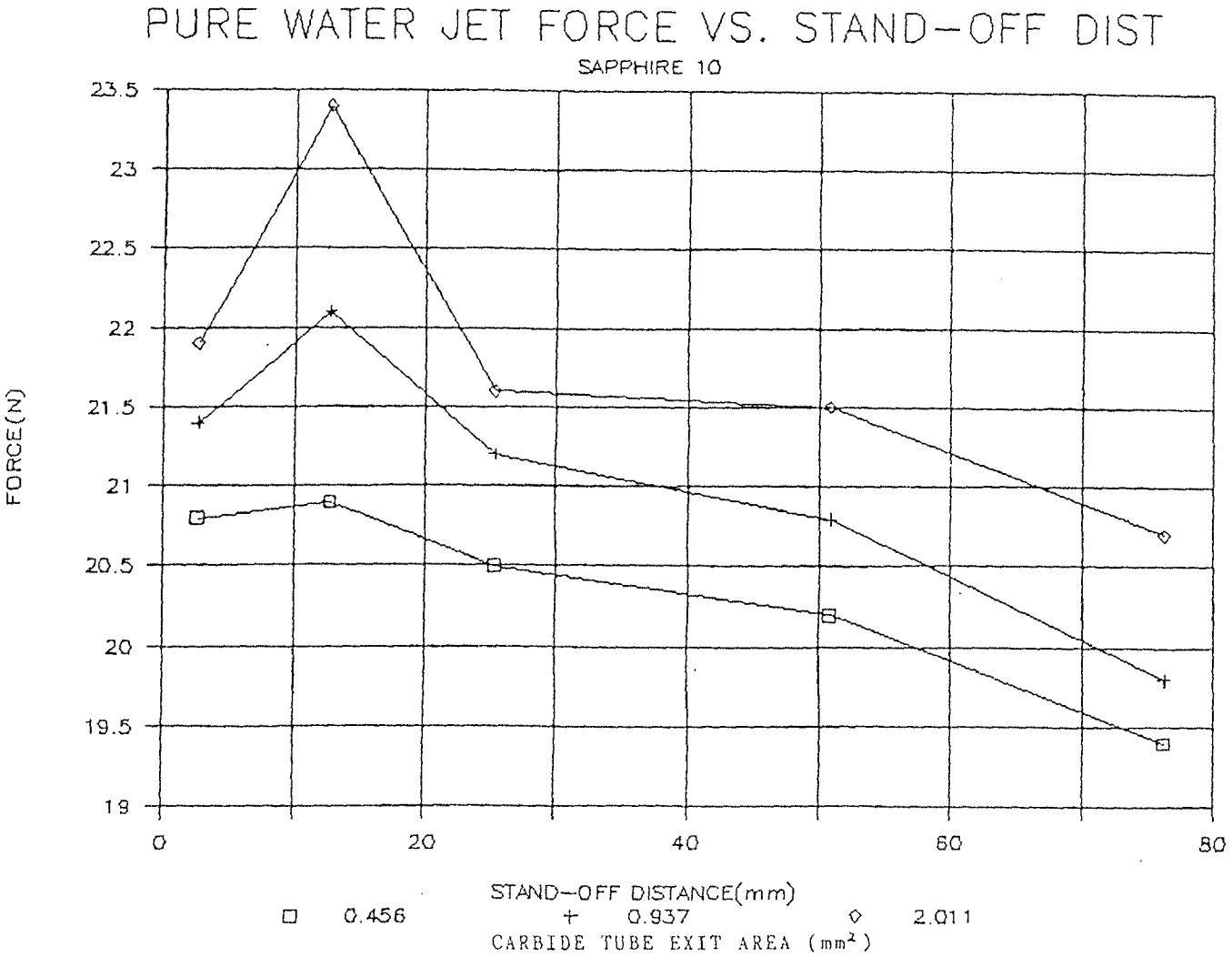
PURE WATER JET FORCE VS. STAND-OFF DIST
SAPPHIRE 10
FORCE(N)
23.5
23
22.5
22
21.5
21
20.5
20
19.5
19
0
20
40
60
80
STAND-OFF DISTANCE(mm)
□ 0.456
+ 0.937
◇ 2.011
CARBIDE TUBE EXIT AREA (mm²)

FIGURE 6.23

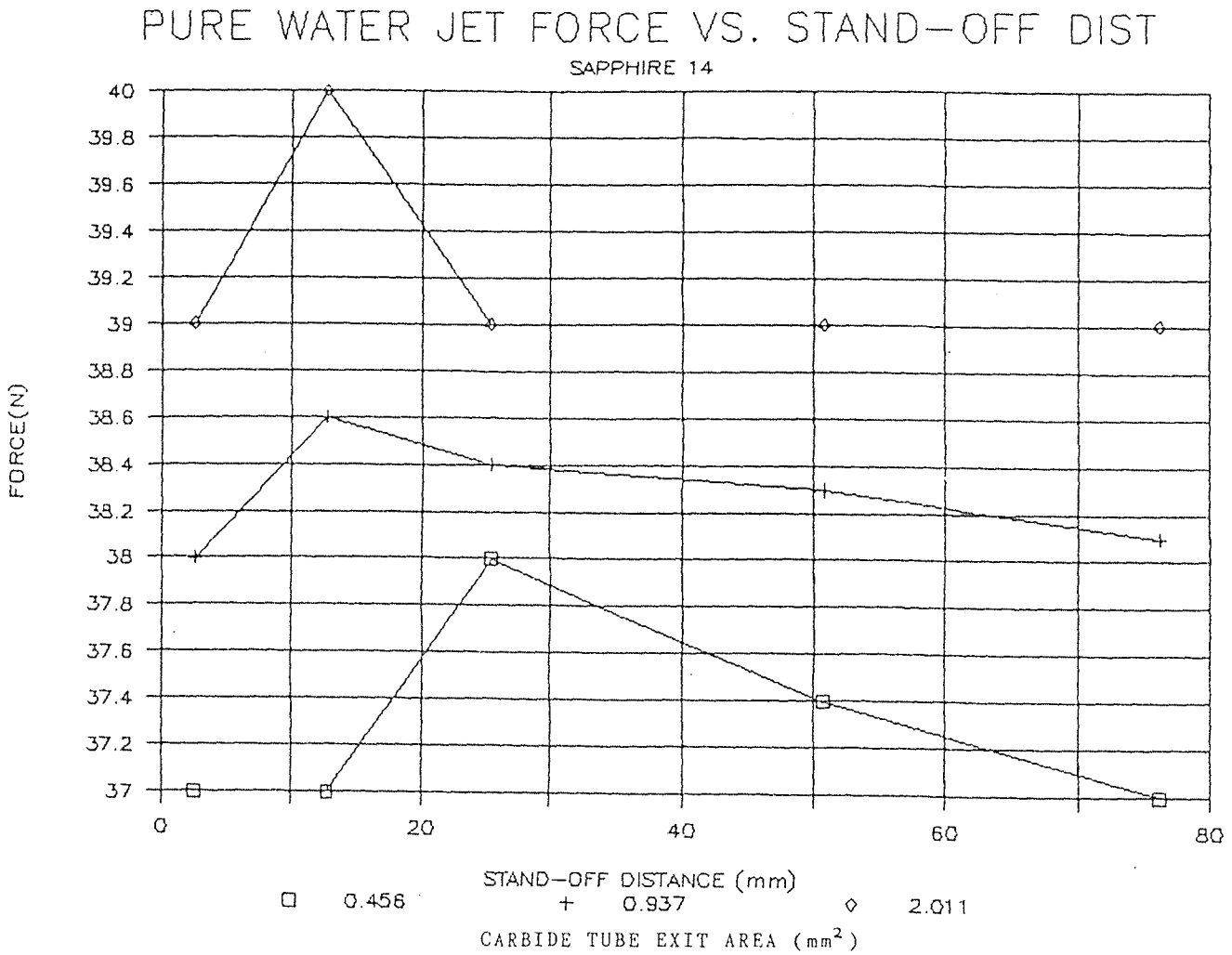
PURE WATER JET FORCE VS. STAND-OFF DIST
SAPPHIRE 14
FORCE(N)
40
39.8
39.6
39.4
39.2
39
38.8
38.6
38.4
38.2
38
37.8
37.6
37.4
37.2
37
0
20
40
60
80
STAND-OFF DISTANCE (mm)
□ 0.456
+ 0.937
◇ 2.011
CARBIDE TUBE EXIT AREA (mm²)

FIGURE 6.24.

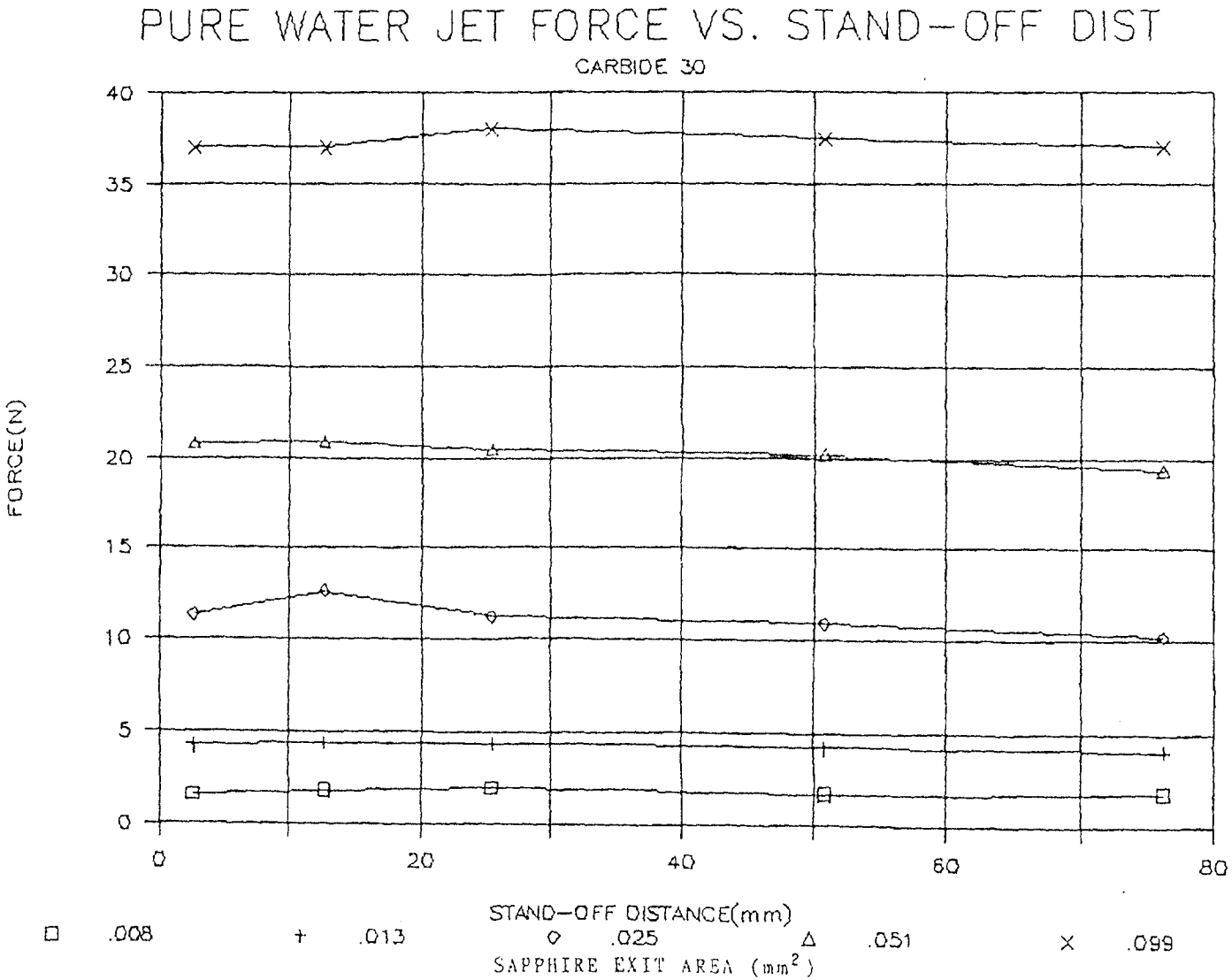
PURE WATER JET FORCE VS. STAND-OFF DIST
CARBIDE 30
FORCE(N)
40
35
30
25
20
15
10
5
0
0
20
40
60
80
STAND-OFF DISTANCE(mm)
□ .008
+ .013
◇ .025
△ .051
× .099
SAPPHIRE EXIT AREA (mm²)

FIGURE 6.25

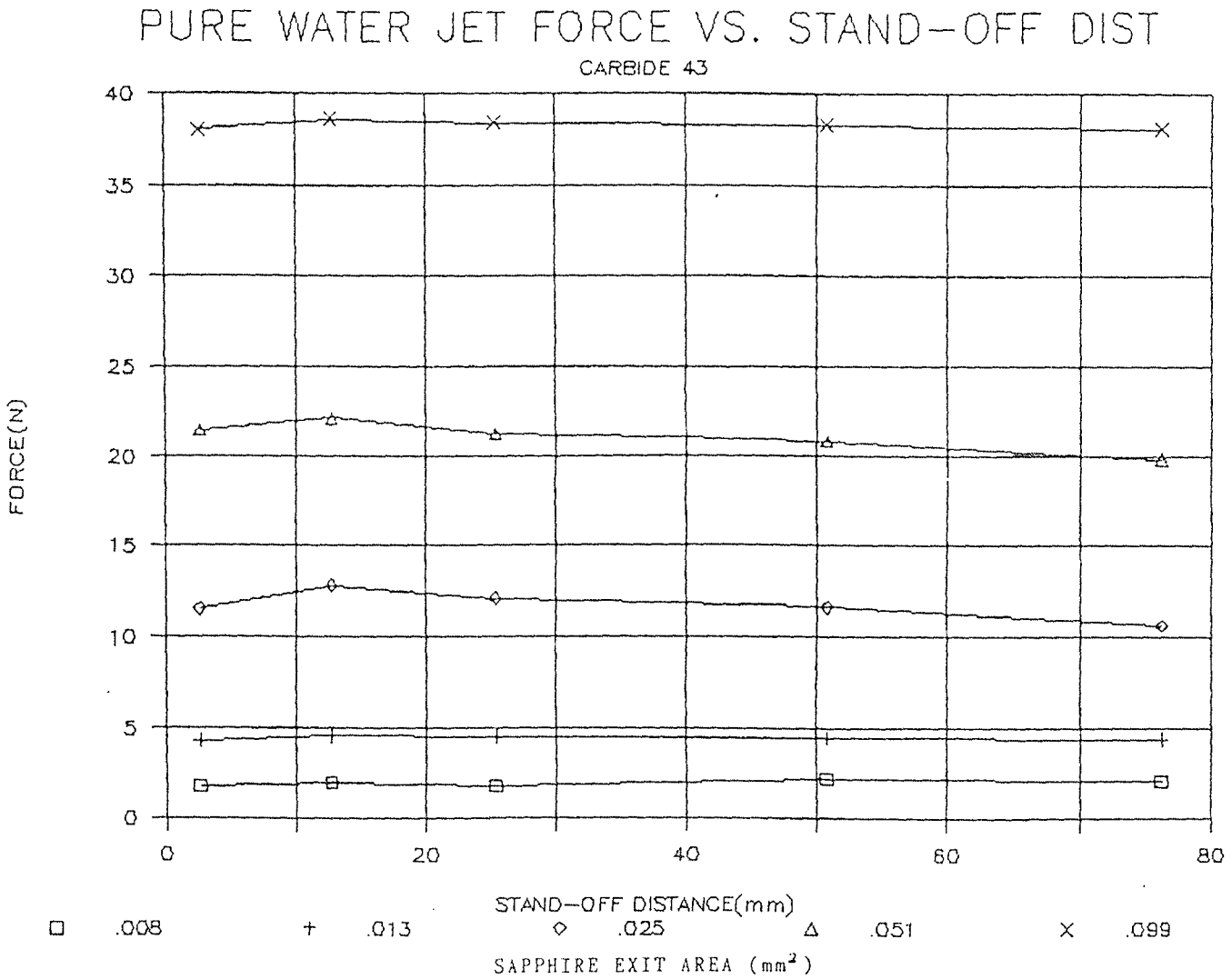
PURE WATER JET FORCE VS. STAND-OFF DIST
CARBIDE 43
FORCE(N)
40
35
30
25
20
15
10
5
0
0
20
40
60
80
STAND-OFF DISTANCE(mm)
□ .008
+ .013
◇ .025
△ .051
× .099
SAPPHIRE EXIT AREA (mm²)

FIGURE 6.26

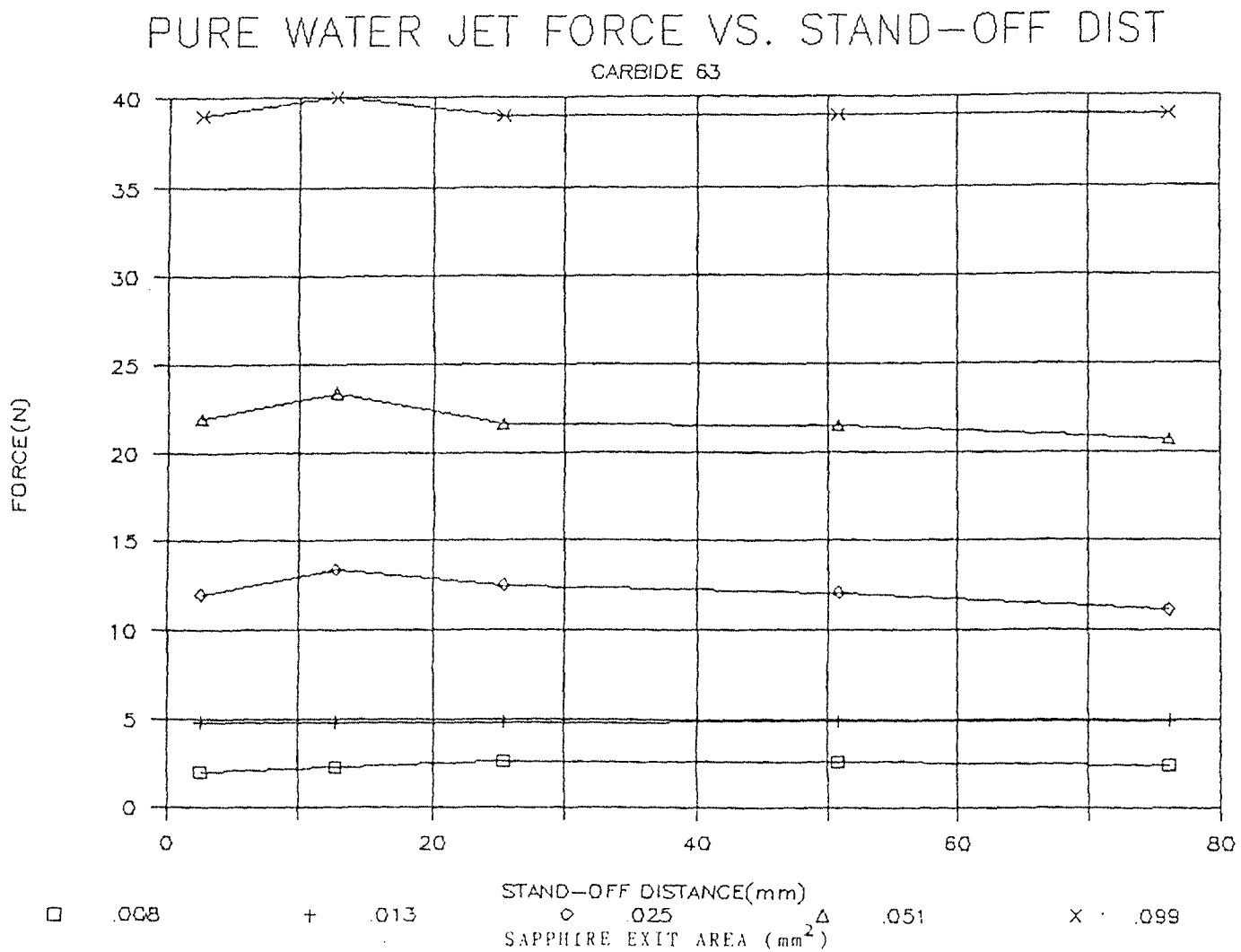
PURE WATER JET FORCE VS. STAND-OFF DIST
CARBIDE 63
FORCE(N)
40
35
30
25
20
15
10
5
0
0
20
40
60
80
STAND-OFF DISTANCE(mm)
□ .008
+ .013
◇ .025
△ .051
X .099
SAPPHIRE EXIT AREA (mm²)

FIGURE 6.27

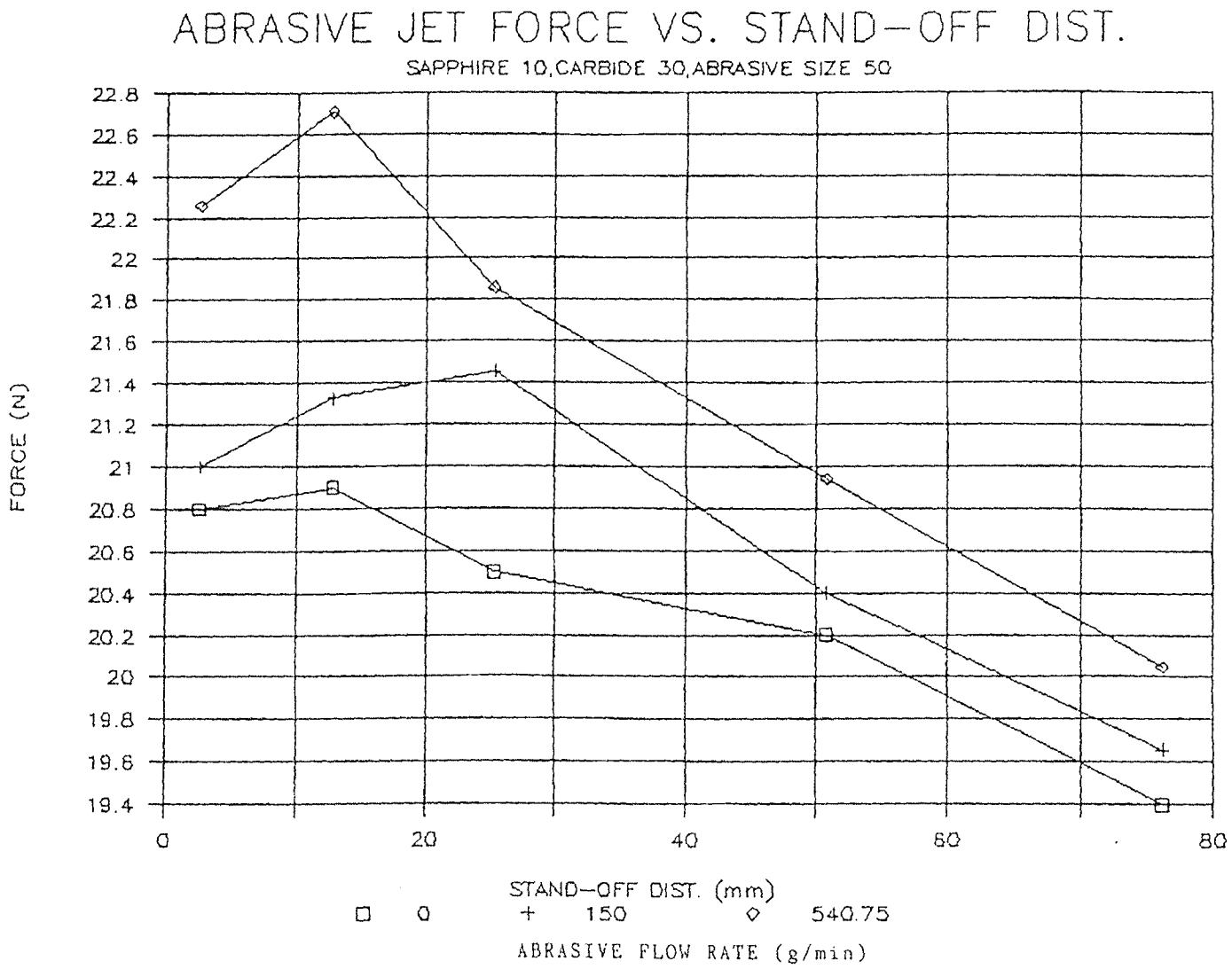
ABRASIVE JET FORCE VS. STAND-OFF DIST.
SAPPHIRE 10,CARBIDE 30,ABRASIVE SIZE 50
FORCE (N)
22.8
22.6
22.4
22.2
22
21.8
21.6
21.4
21.2
21
20.8
20.6
20.4
20.2
20
19.8
19.6
19.4
0
20
40
60
80
STAND-OFF DIST. (mm)
□ 0 + 150 ◇ 540.75
ABRASIVE FLOW RATE (g/min)

FIGURE 6.28

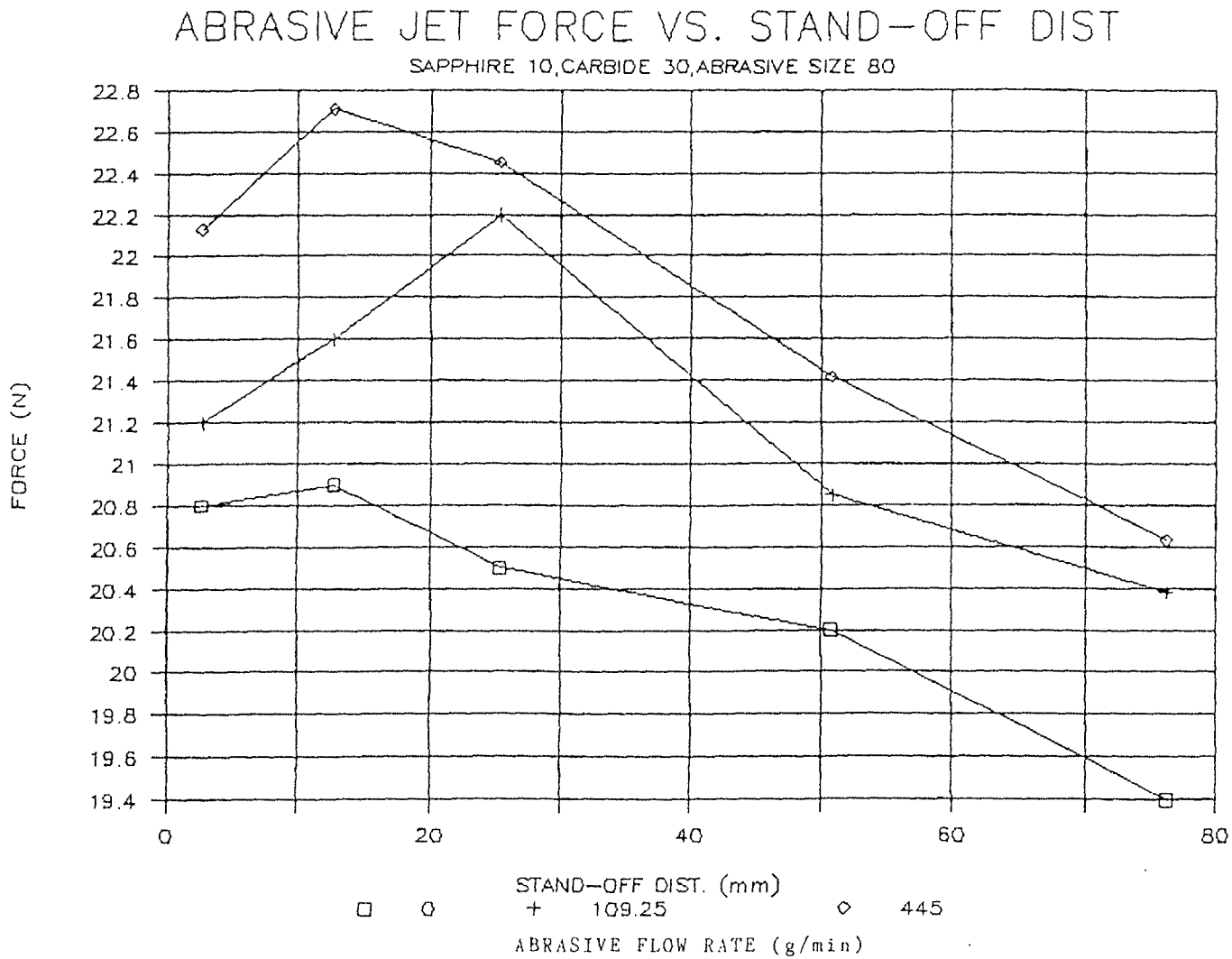
ABRASIVE JET FORCE VS. STAND-OFF DIST
SAPPHIRE 10,CARBIDE 30,ABRASIVE SIZE 80
FORCE (N)
22.8
22.6
22.4
22.2
22
21.8
21.6
21.4
21.2
21
20.8
20.6
20.4
20.2
20
19.8
19.6
19.4
0
20
40
60
80
STAND-OFF DIST. (mm)
□ 0
+ 109.25
◇ 445
ABRASIVE FLOW RATE (g/min)

FIGURE 6.29

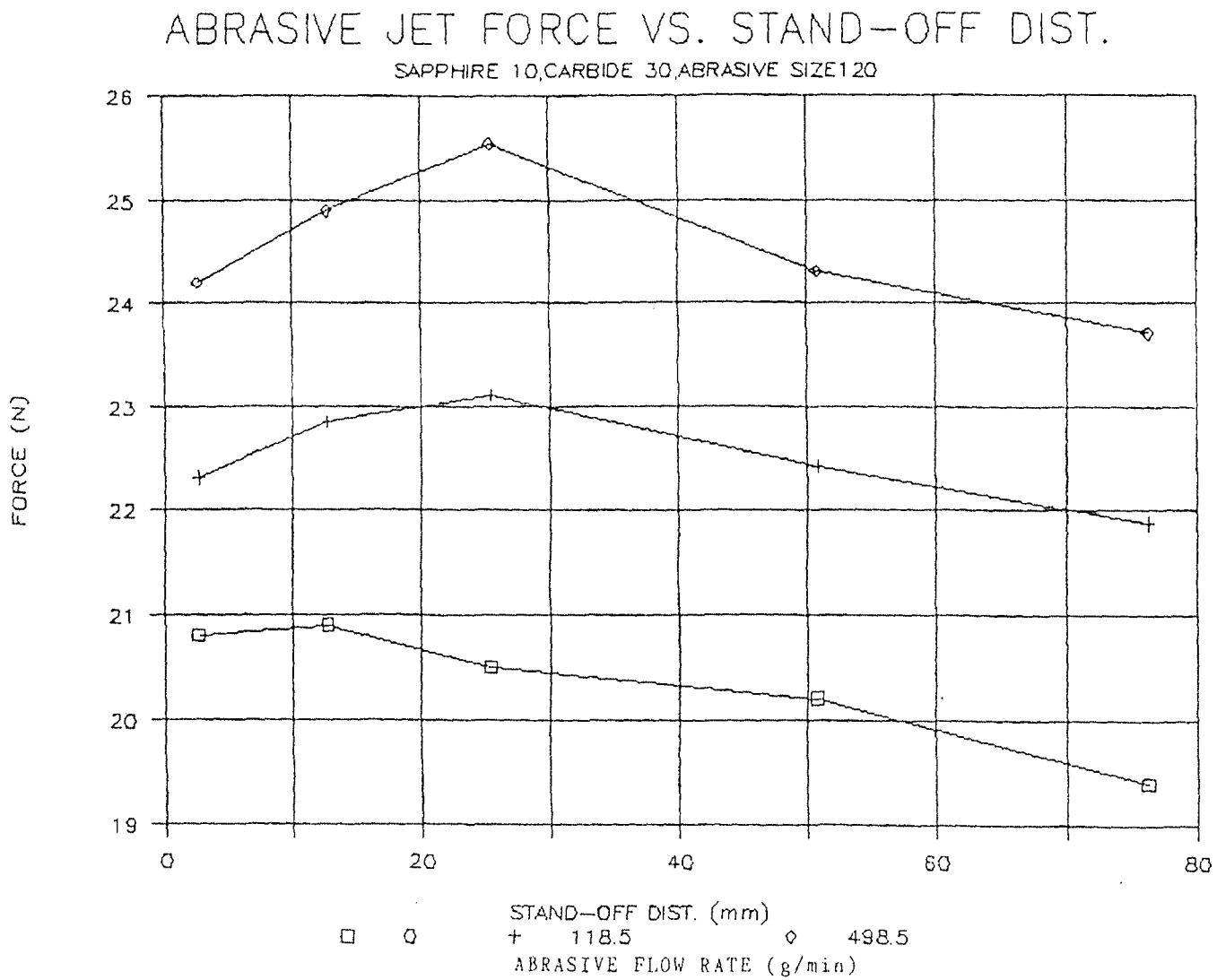
ABRASIVE JET FORCE VS. STAND-OFF DIST.
SAPPHIRE 10,CARBIDE 30,ABRASIVE SIZE120
FORCE (N)
26
25
24
23
22
21
20
19
0
20
40
60
80
STAND-OFF DIST. (mm)
□ 0
+ 118.5
◇ 498.5
ABRASIVE FLOW RATE (g/min)

FIGURE 6.30

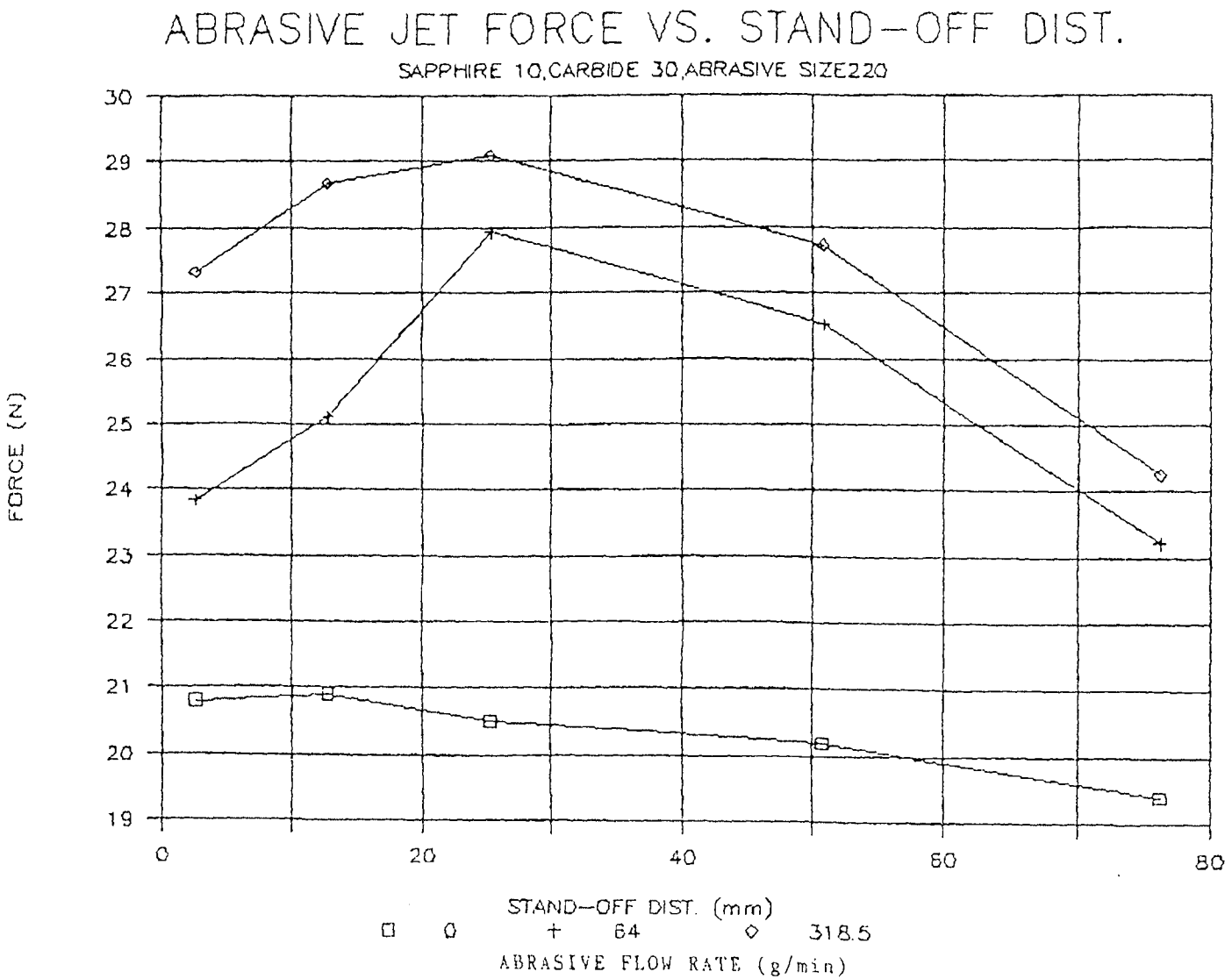
ABRASIVE JET FORCE VS. STAND-OFF DIST.
SAPPHIRE 10,CARBIDE 30,ABRASIVE SIZE220
FORCE (N)
30
29
28
27
26
25
24
23
22
21
20
19
0
20
40
60
80
STAND-OFF DIST. (mm)
□ 0 + 64 ◇ 318.5
ABRASIVE FLOW RATE (g/min)

FIGURE 6.31

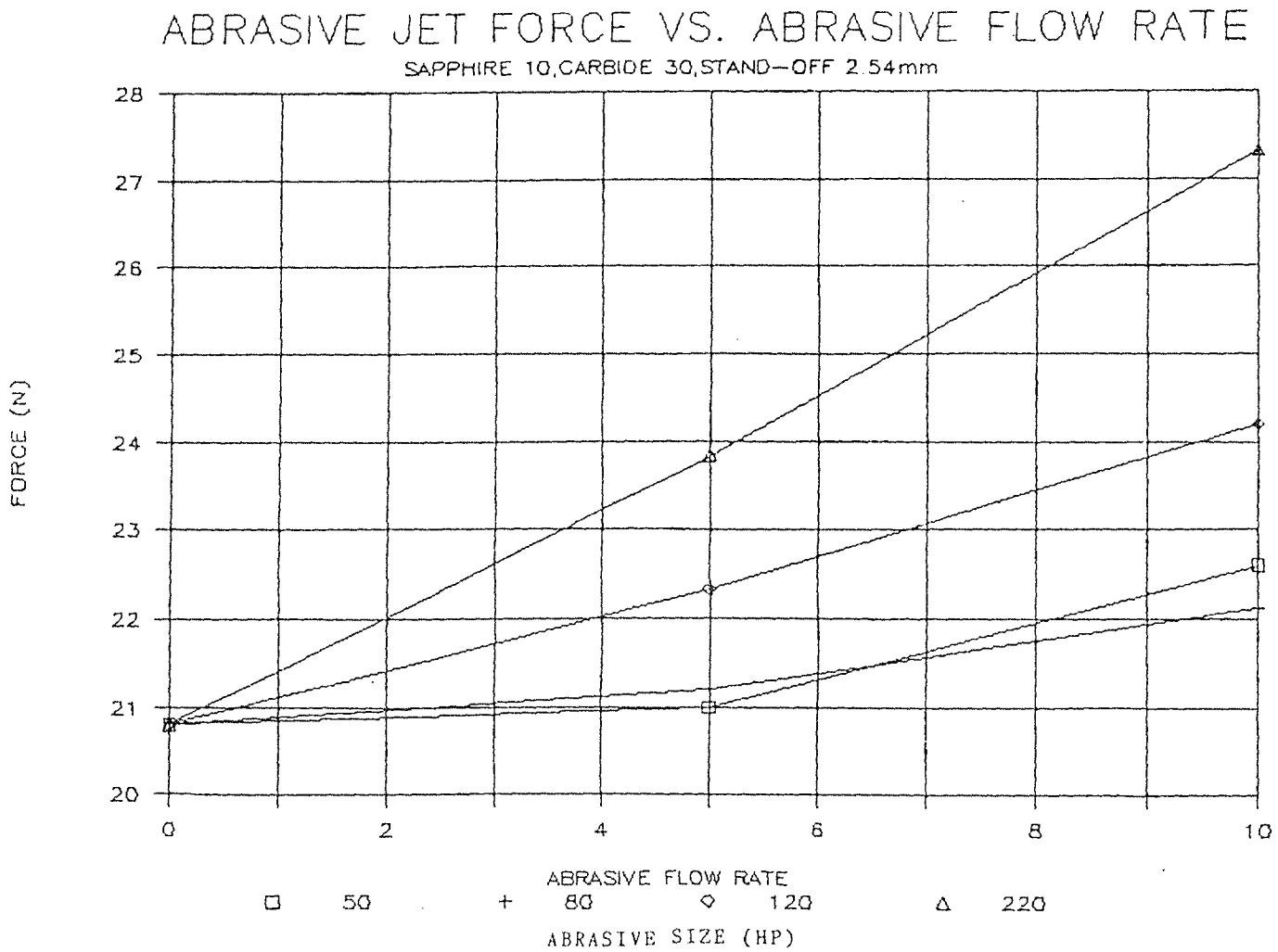
ABRASIVE JET FORCE VS. ABRASIVE FLOW RATE
SAPPHIRE 10,CARBIDE 30,STAND-OFF 2.54mm
FORCE (N)
28
27
26
25
24
23
22
21
20
0
2
4
6
8
10
ABRASIVE FLOW RATE
□ 50
+ 80
◇ 120
△ 220
ABRASIVE SIZE (HP)

FIGURE 6.32

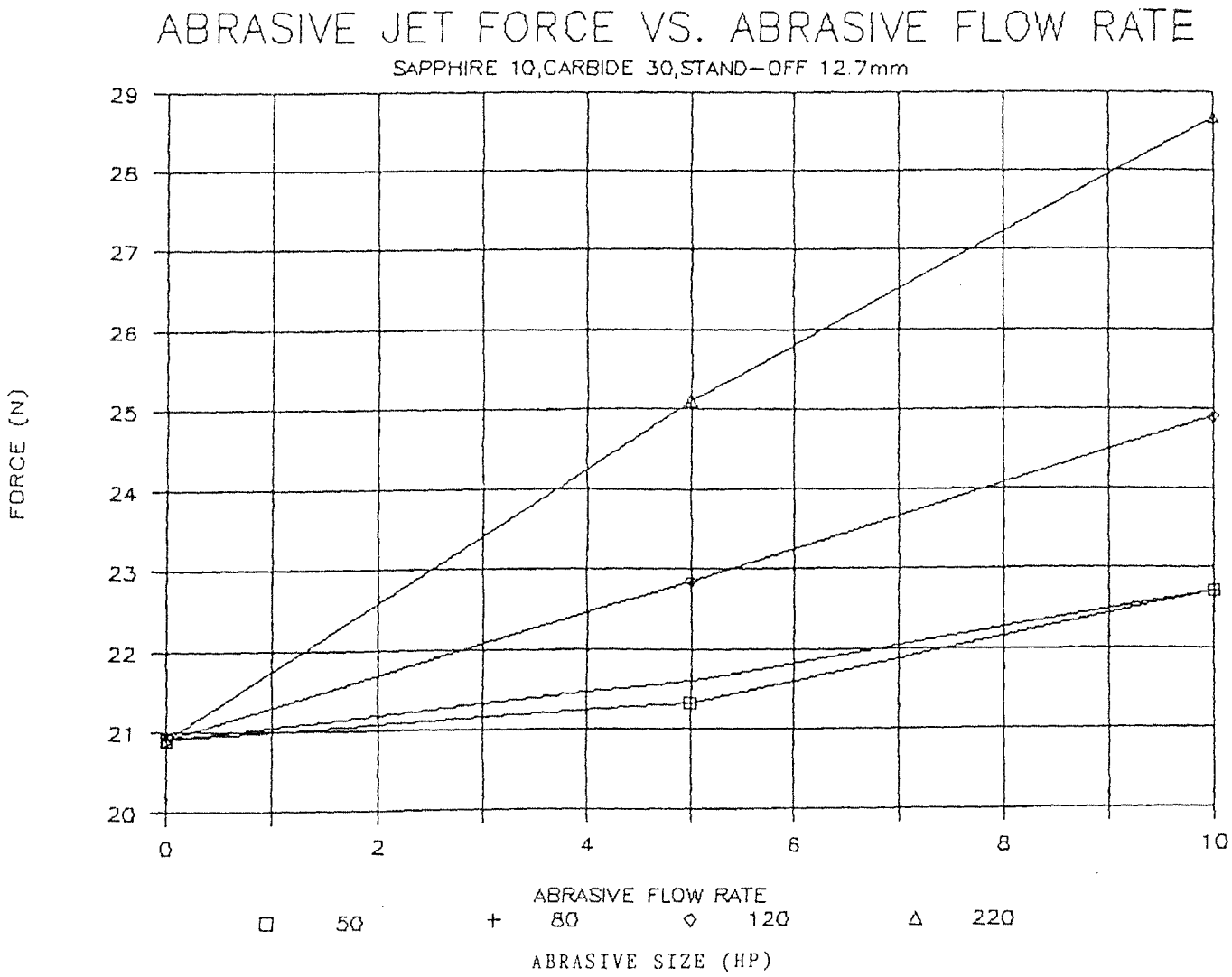
ABRASIVE JET FORCE VS. ABRASIVE FLOW RATE
SAPPHIRE 10,CARBIDE 30,STAND-OFF 12.7mm
FORCE (N)
29
28
27
26
25
24
23
22
21
20
0
2
4
6
8
10
ABRASIVE FLOW RATE
□ 50
+ 80
◇ 120
△ 220
ABRASIVE SIZE (HP)

FIGURE 6.33

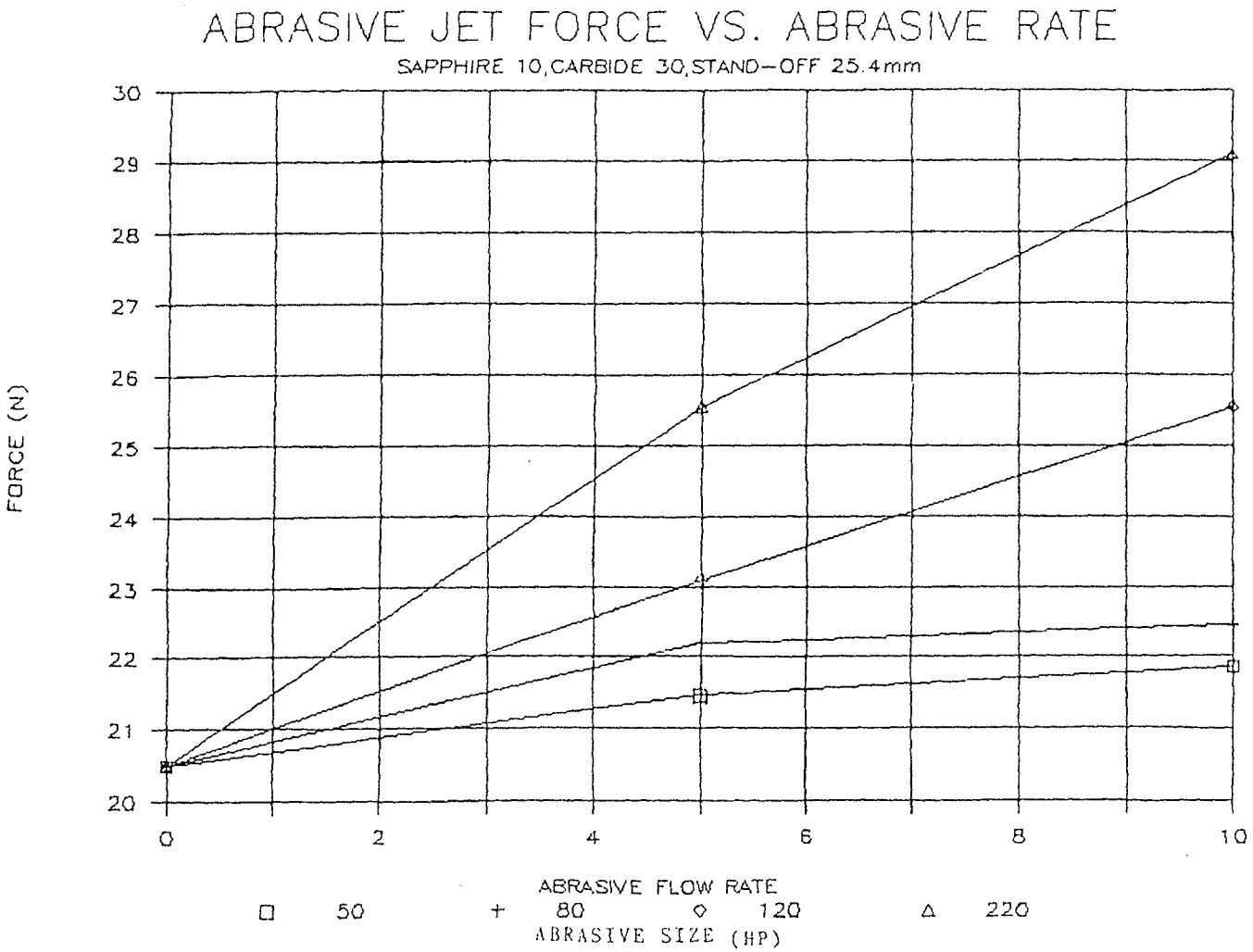
ABRASIVE JET FORCE VS. ABRASIVE RATE
SAPPHIRE 10,CARBIDE 30,STAND-OFF 25.4mm
FORCE (N)
30
29
28
27
26
25
24
23
22
21
20
0
2
4
6
8
10
ABRASIVE FLOW RATE
□ 50
+ 80
◇ 120
△ 220
ABRASIVE SIZE (HP)

FIGURE 6.34

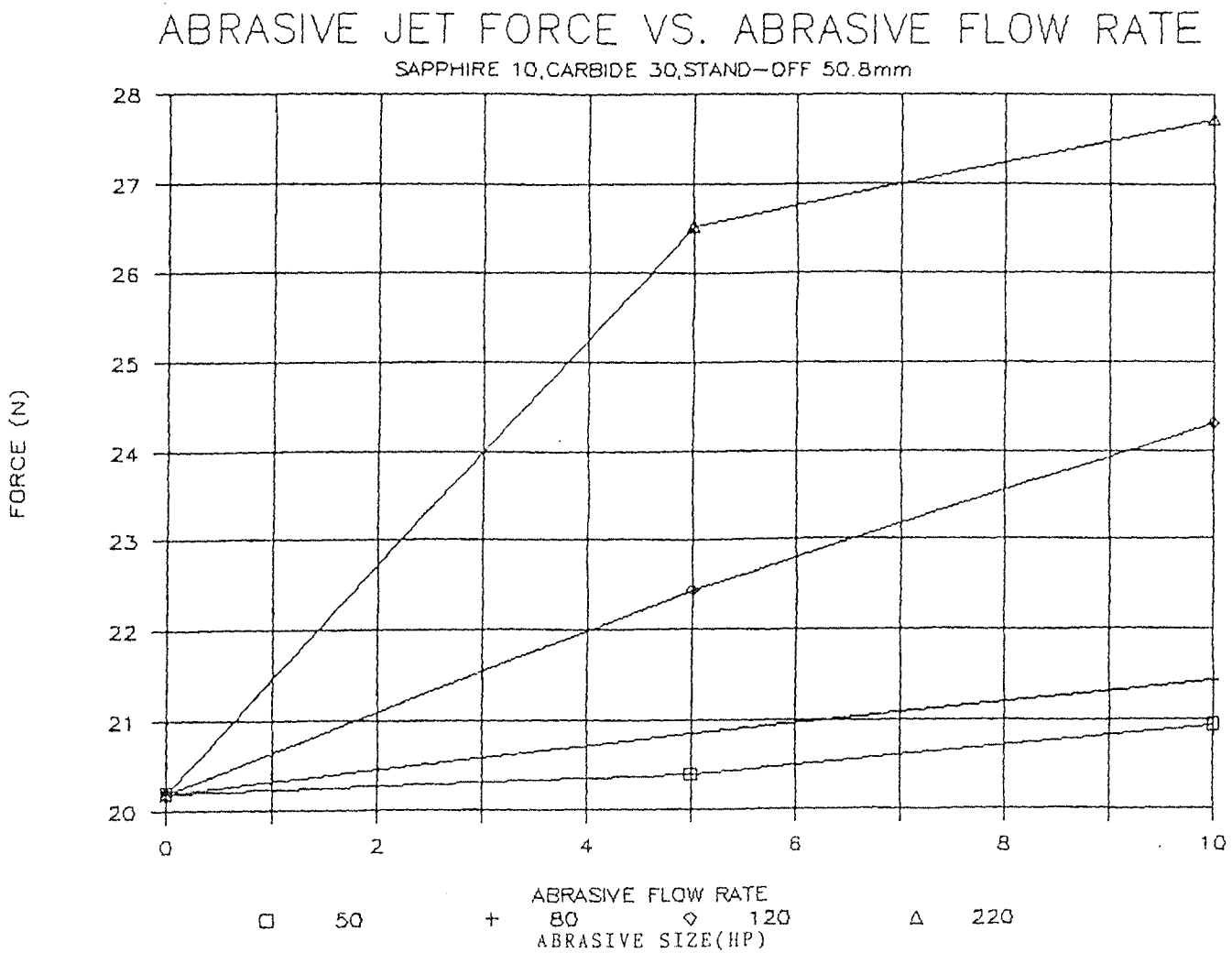
ABRASIVE JET FORCE VS. ABRASIVE FLOW RATE
SAPPHIRE 10,CARBIDE 30,STAND-OFF 50.8mm
FORCE (N)
28
27
26
25
24
23
22
21
20
0
2
4
6
8
10
ABRASIVE FLOW RATE
□ 50
+ 80
◇ 120
△ 220
ABRASIVE SIZE(HP)

FIGURE 6.35

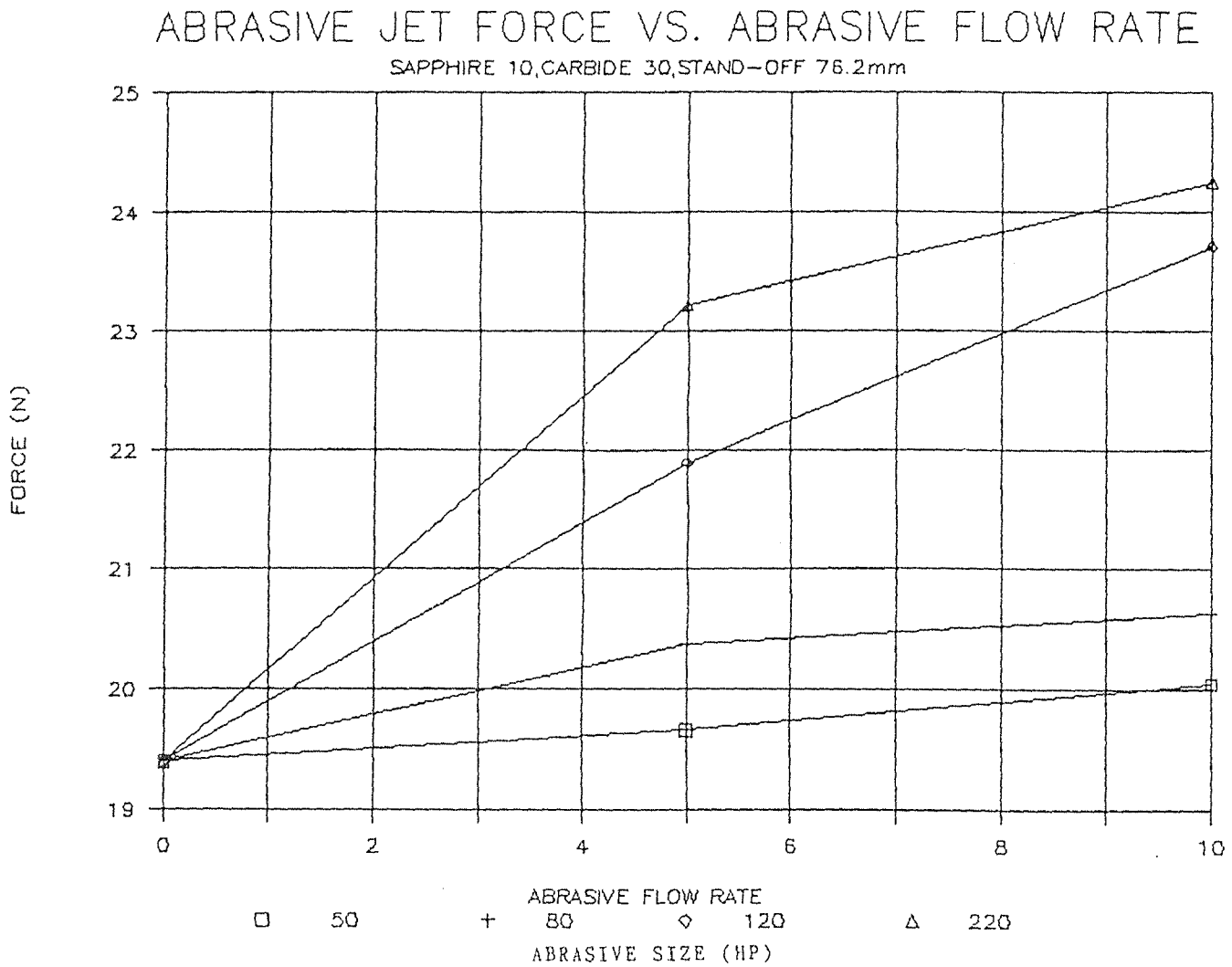
ABRASIVE JET FORCE VS. ABRASIVE FLOW RATE
SAPPHIRE 10,CARBIDE 30,STAND-OFF 76.2mm
FORCE (N)
25
24
23
22
21
20
19
0
2
4
6
8
10
ABRASIVE FLOW RATE
□ 50
+ 80
◇ 120
△ 220
ABRASIVE SIZE (MP)

FIGURE 6.36

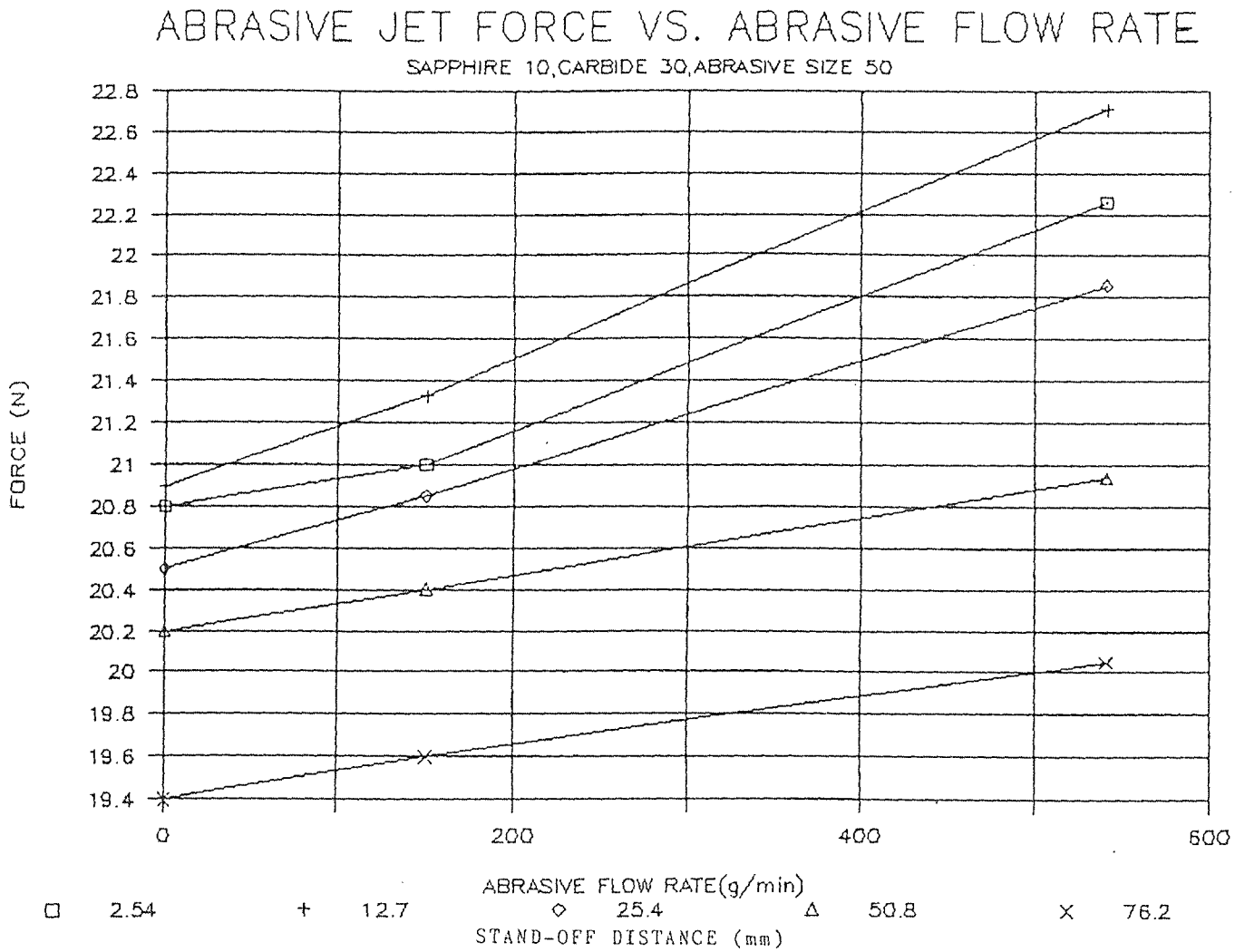
ABRASIVE JET FORCE VS. ABRASIVE FLOW RATE
SAPPHIRE 10,CARBIDE 30,ABRASIVE SIZE 50
FORCE (N)
22.8
22.6
22.4
22.2
22
21.8
21.6
21.4
21.2
21
20.8
20.6
20.4
20.2
20
19.8
19.6
19.4
0
200
400
600
ABRASIVE FLOW RATE(g/min)
□ 2.54
+ 12.7
◇ 25.4
Δ 50.8
× 76.2
STAND-OFF DISTANCE (mm)

FIGURE 6.37

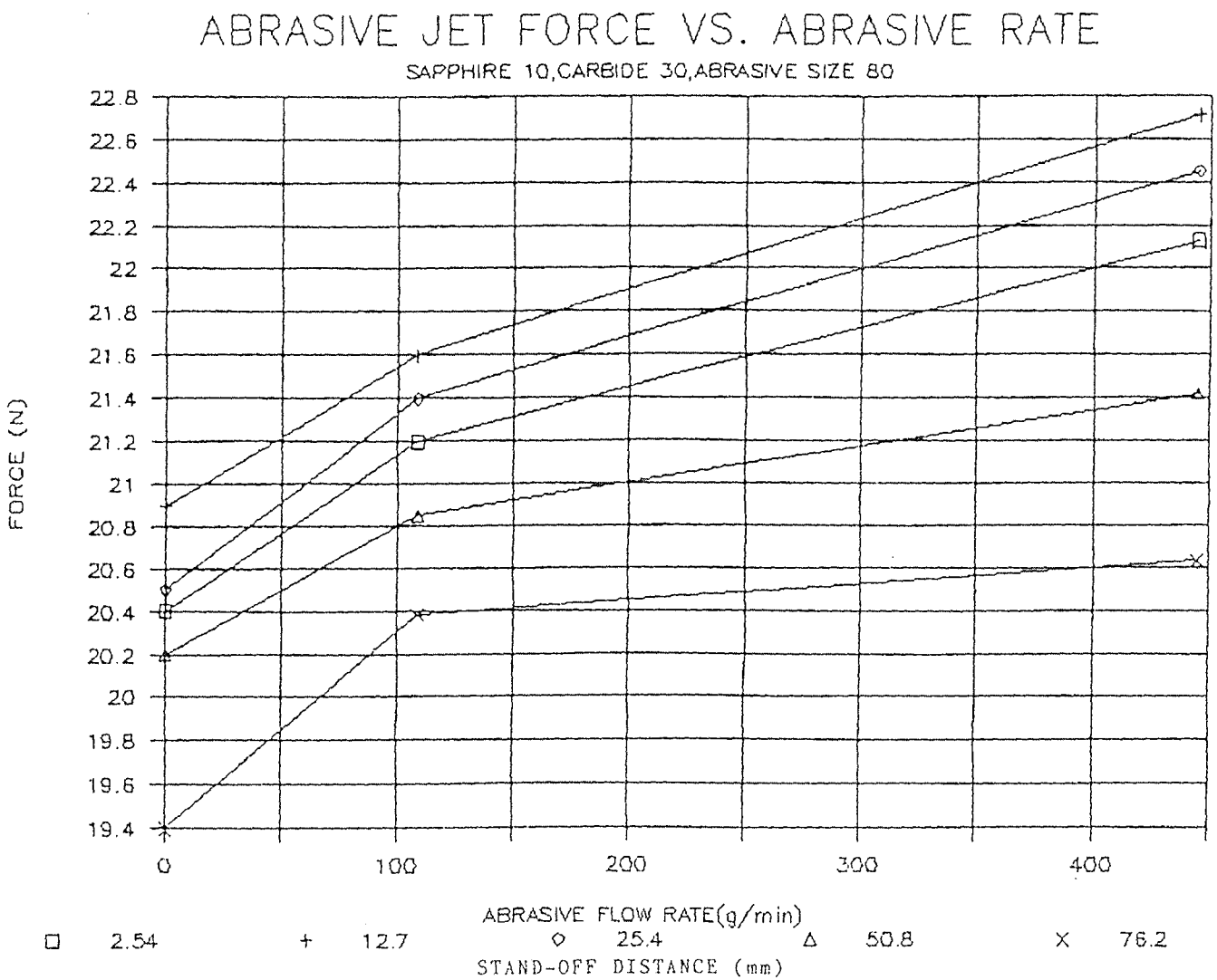
ABRASIVE JET FORCE VS. ABRASIVE RATE
SAPPHIRE 10,CARBIDE 30,ABRASIVE SIZE 80
FORCE (N)
22.8
22.6
22.4
22.2
22
21.8
21.6
21.4
21.2
21
20.8
20.6
20.4
20.2
20
19.8
19.6
19.4
0
100
200
300
400
ABRASIVE FLOW RATE(g/min)
□ 2.54
+ 12.7
◇ 25.4
△ 50.8
X 76.2
STAND-OFF DISTANCE (mm)

FIGURE 6.38

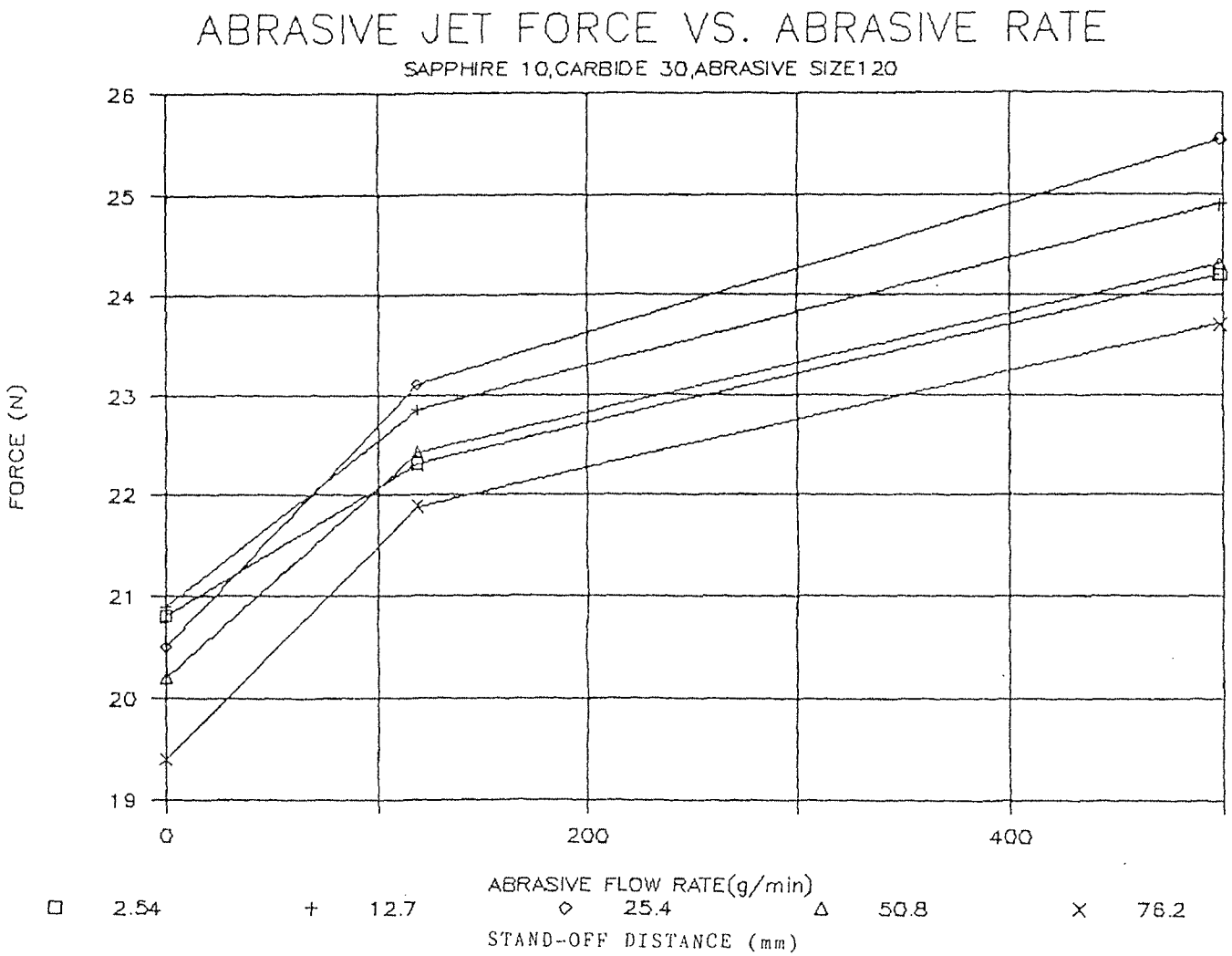
ABRASIVE JET FORCE VS. ABRASIVE RATE
SAPPHIRE 10,CARBIDE 30,ABRASIVE SIZE120
FORCE (N)
26
25
24
23
22
21
20
19
0
200
400
ABRASIVE FLOW RATE(g/min)
□ 2.54
+ 12.7
◇ 25.4
Δ 50.8
× 76.2
STAND-OFF DISTANCE (mm)

FIGURE 6.39

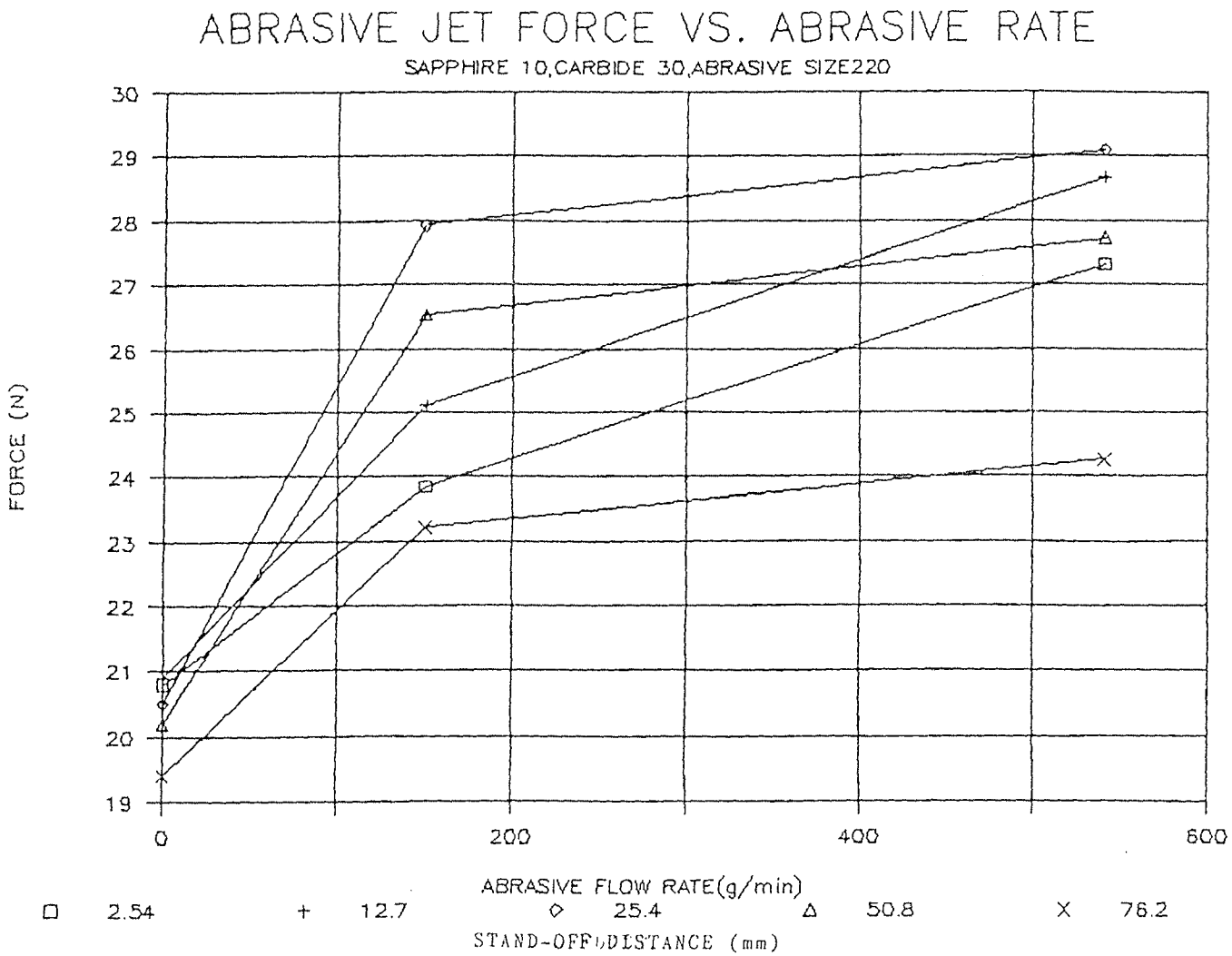
ABRASIVE JET FORCE VS. ABRASIVE RATE
SAPPHIRE 10,CARBIDE 30,ABRASIVE SIZE220
FORCE (N)
30
29
28
27
26
25
24
23
22
21
20
19
0
200
400
600
ABRASIVE FLOW RATE(g/min)
□ 2.54
+ 12.7
◇ 25.4
△ 50.8
X 76.2
STAND-OFF DISTANCE (mm)

FIGURE 6.40

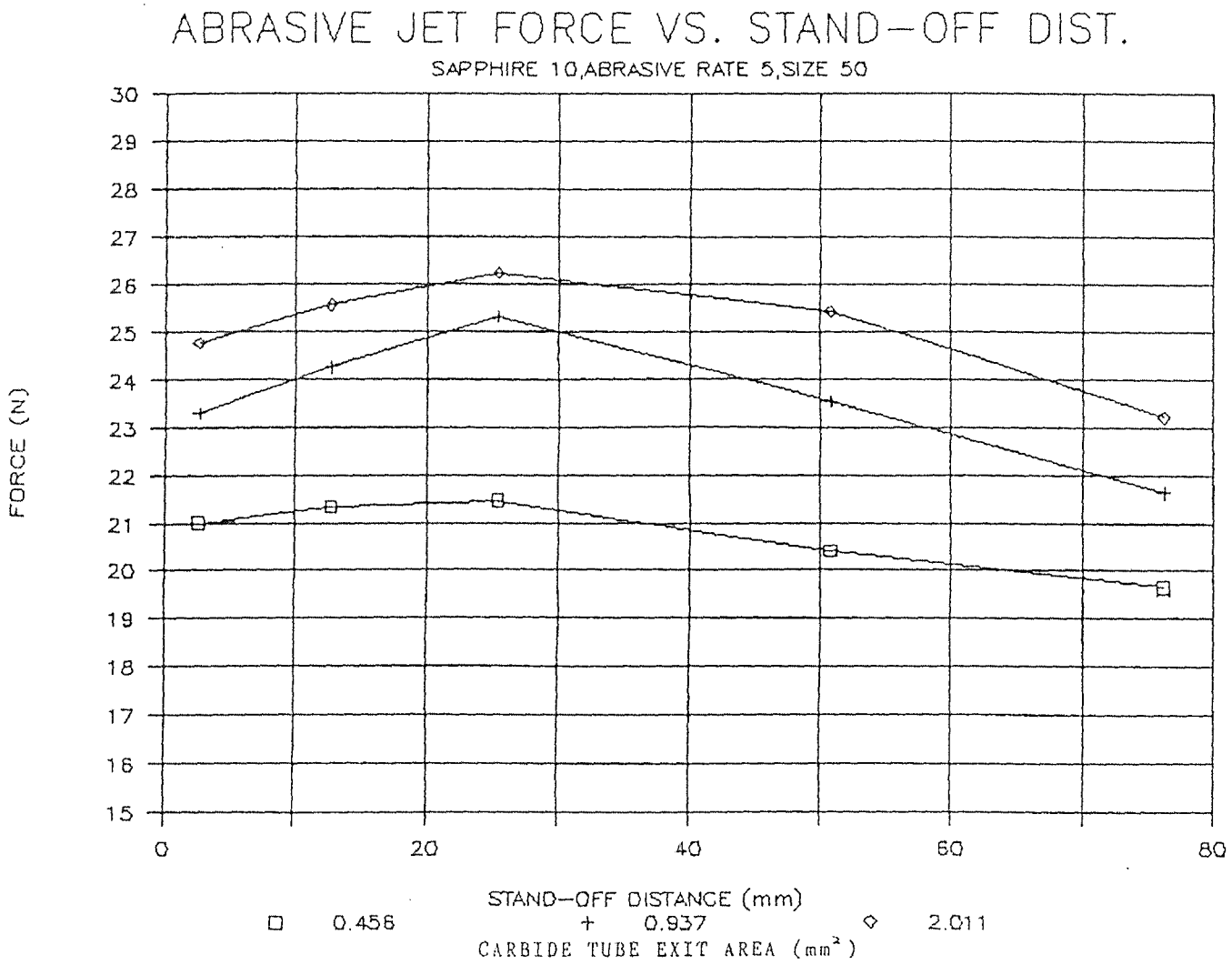
ABRASIVE JET FORCE VS. STAND-OFF DIST.
SAPPHIRE 10,ABRASIVE RATE 5,SIZE 50
FORCE (N)
30
29
28
27
26
25
24
23
22
21
20
19
18
17
16
15
0
20
40
60
80
STAND-OFF DISTANCE (mm)
□ 0.456
+ 0.937
◇ 2.011
CARBIDE TUBE EXIT AREA (mm²)

FIGURE 6.41

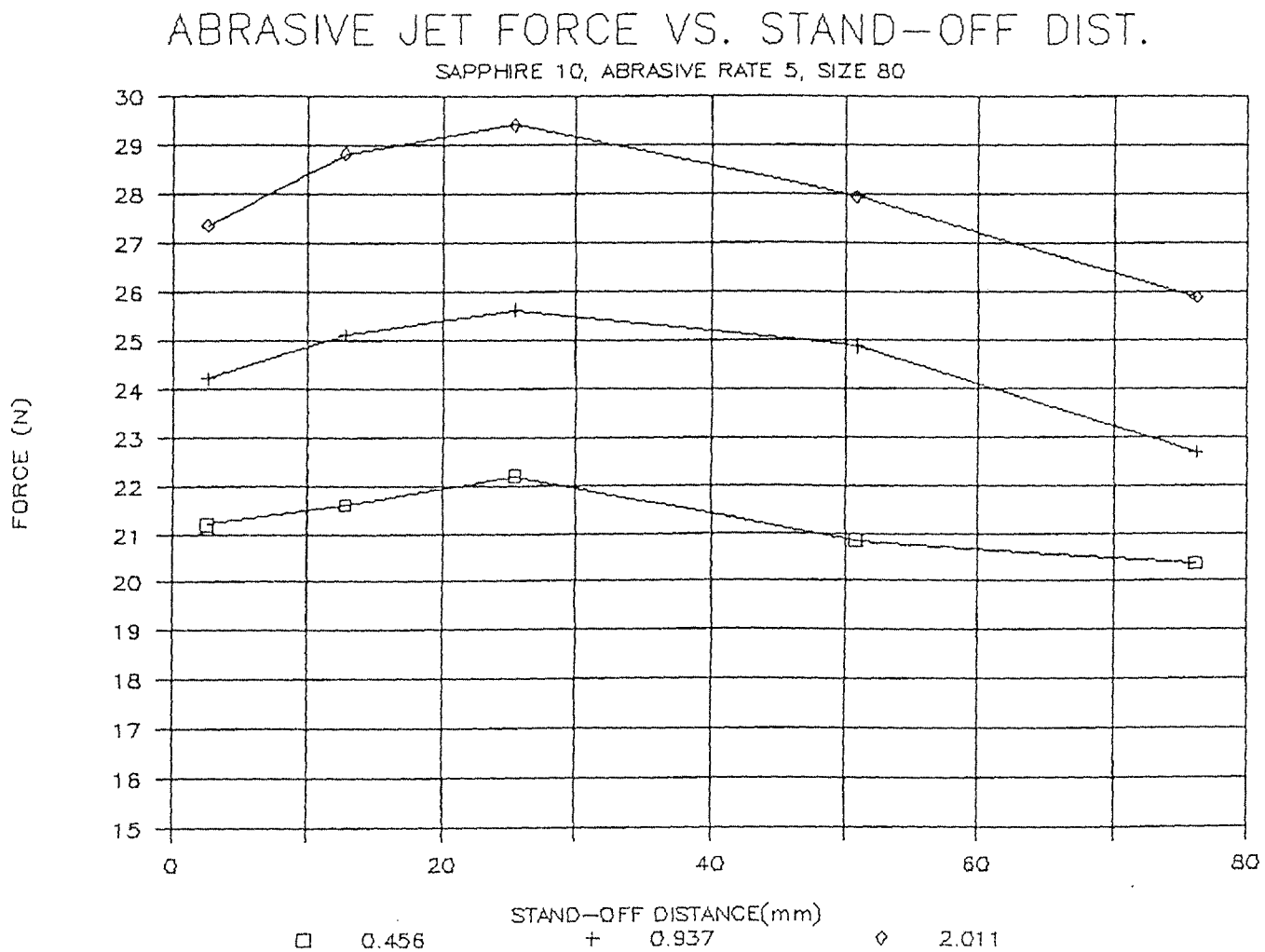
ABRASIVE JET FORCE VS. STAND-OFF DIST.
SAPPHIRE 10, ABRASIVE RATE 5, SIZE 80
FORCE (N)
30
29
28
27
26
25
24
23
22
21
20
19
18
17
16
15
0
20
40
60
80
STAND-OFF DISTANCE(mm)
□ 0.456
+ 0.937
◇ 2.011
CARBIDE TUBE EXIT AREA (mm²)

FIGURE 6.42

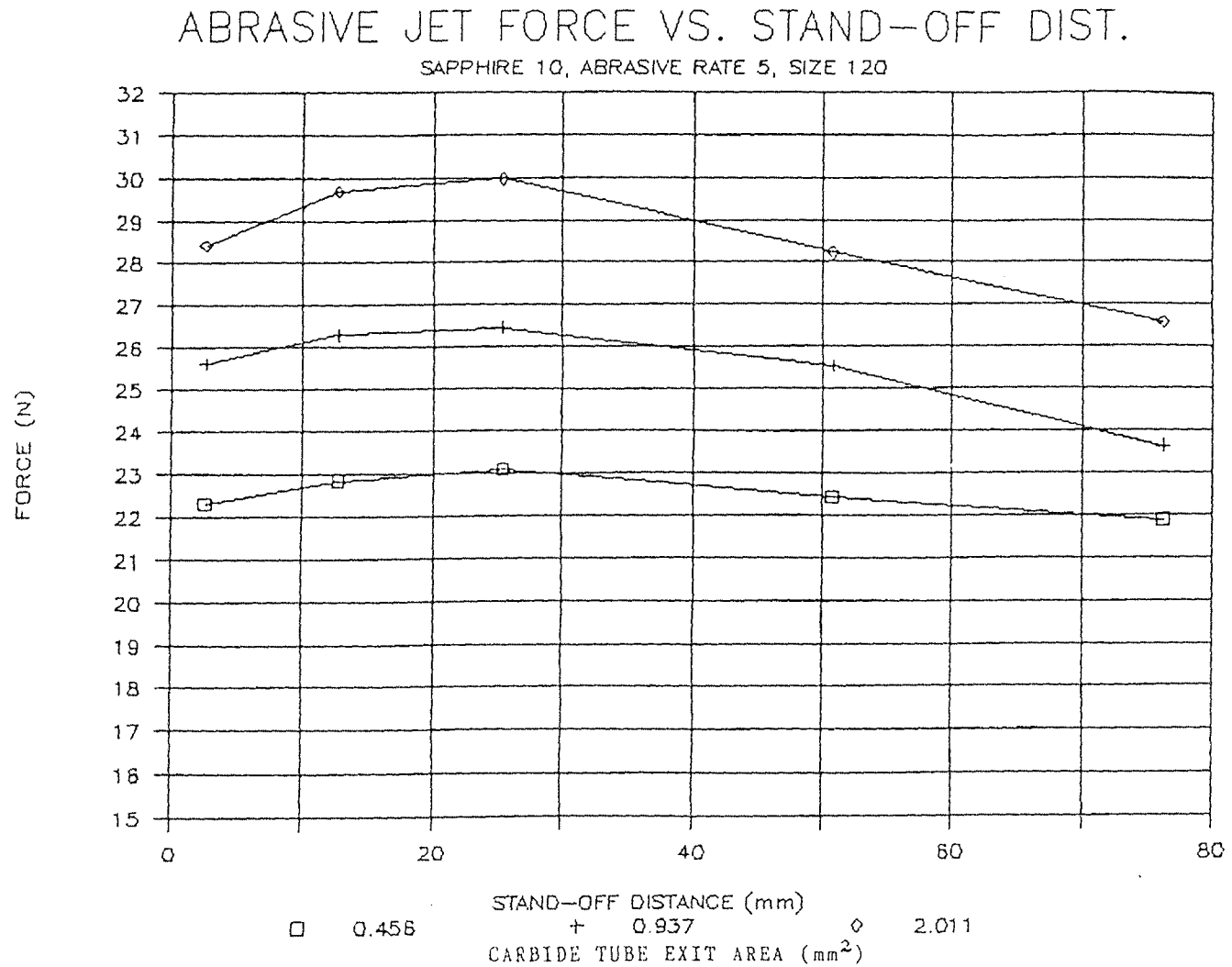
ABRASIVE JET FORCE VS. STAND-OFF DIST.
SAPPHIRE 10, ABRASIVE RATE 5, SIZE 120
FORCE (N)
32
31
30
29
28
27
26
25
24
23
22
21
20
19
18
17
16
15
0
20
40
60
80
STAND-OFF DISTANCE (mm)
□ 0.456
+ 0.937
◇ 2.011
CARBIDE TUBE EXIT AREA (mm²)

FIGURE 6.43

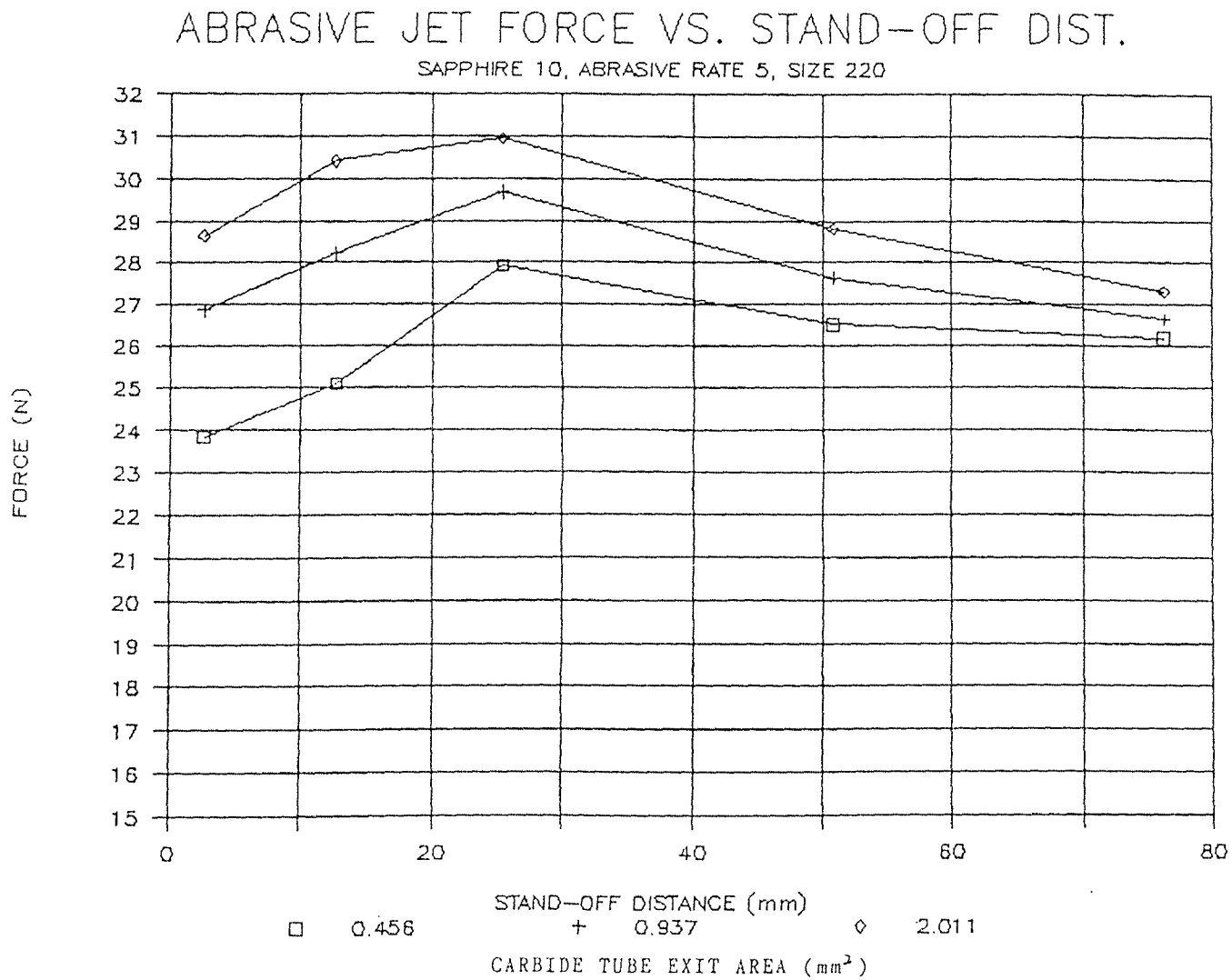
ABRASIVE JET FORCE VS. STAND-OFF DIST.
SAPPHIRE 10, ABRASIVE RATE 5, SIZE 220
FORCE (N)
32
31
30
29
28
27
26
25
24
23
22
21
20
19
18
17
16
15
0
20
40
60
80
STAND-OFF DISTANCE (mm)
□ 0.456
+ 0.937
◊ 2.011
CARBIDE TUBE EXIT AREA (mm²)

FIGURE 6.44

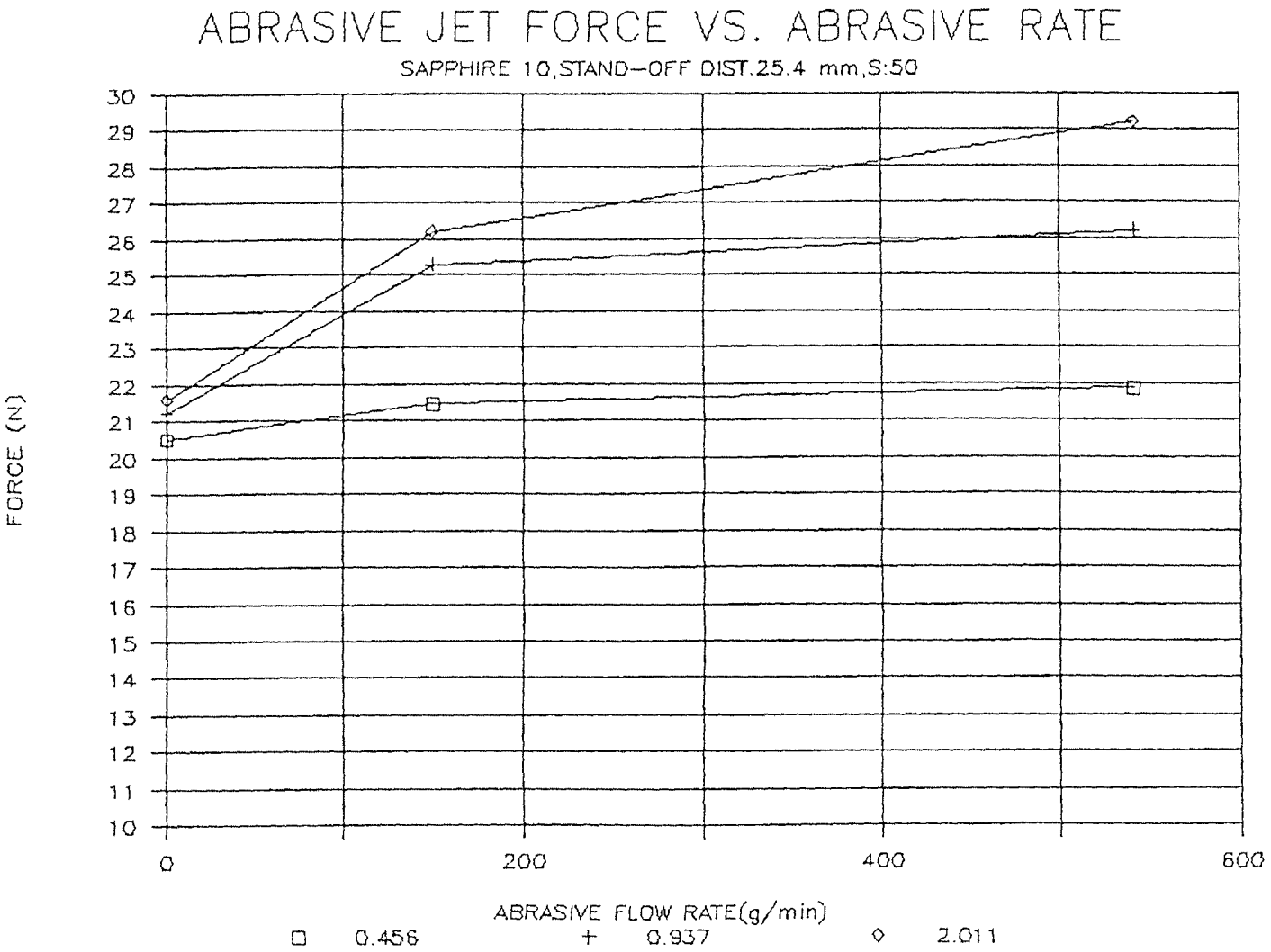
ABRASIVE JET FORCE VS. ABRASIVE RATE
SAPPHIRE 10,STAND-OFF DIST.25.4 mm,S:50
FORCE (N)
30
29
28
27
26
25
24
23
22
21
20
19
18
17
16
15
14
13
12
11
10
0
200
400
600
ABRASIVE FLOW RATE(g/min)
□ 0.456
+ 0.937
◇ 2.011
CARBIDE TUBE EXIT AREA (mm²)

FIGURE 6.45

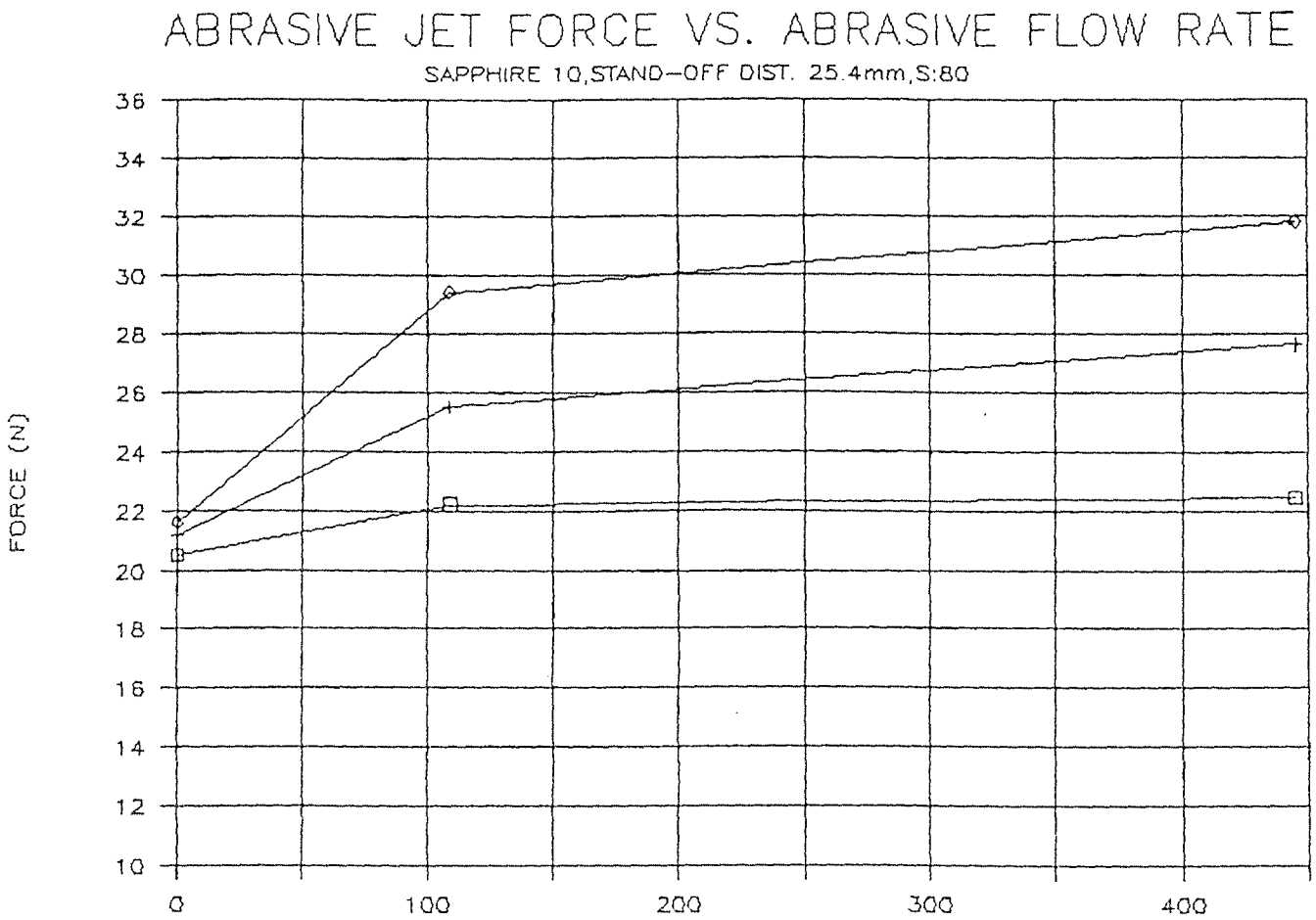
ABRASIVE JET FORCE VS. ABRASIVE FLOW RATE
SAPPHIRE 10,STAND-OFF DIST. 25.4mm,S:80
FORCE (N)
36
34
32
30
28
26
24
22
20
18
16
14
12
10
0
100
200
300
400
ABRASIVE FLOW RATE(g/min)
□ 0.456
+ 0.937
◇ 2.011
CARBIDE TUBE EXIT AREA (mm²)

FIGURE 6.46

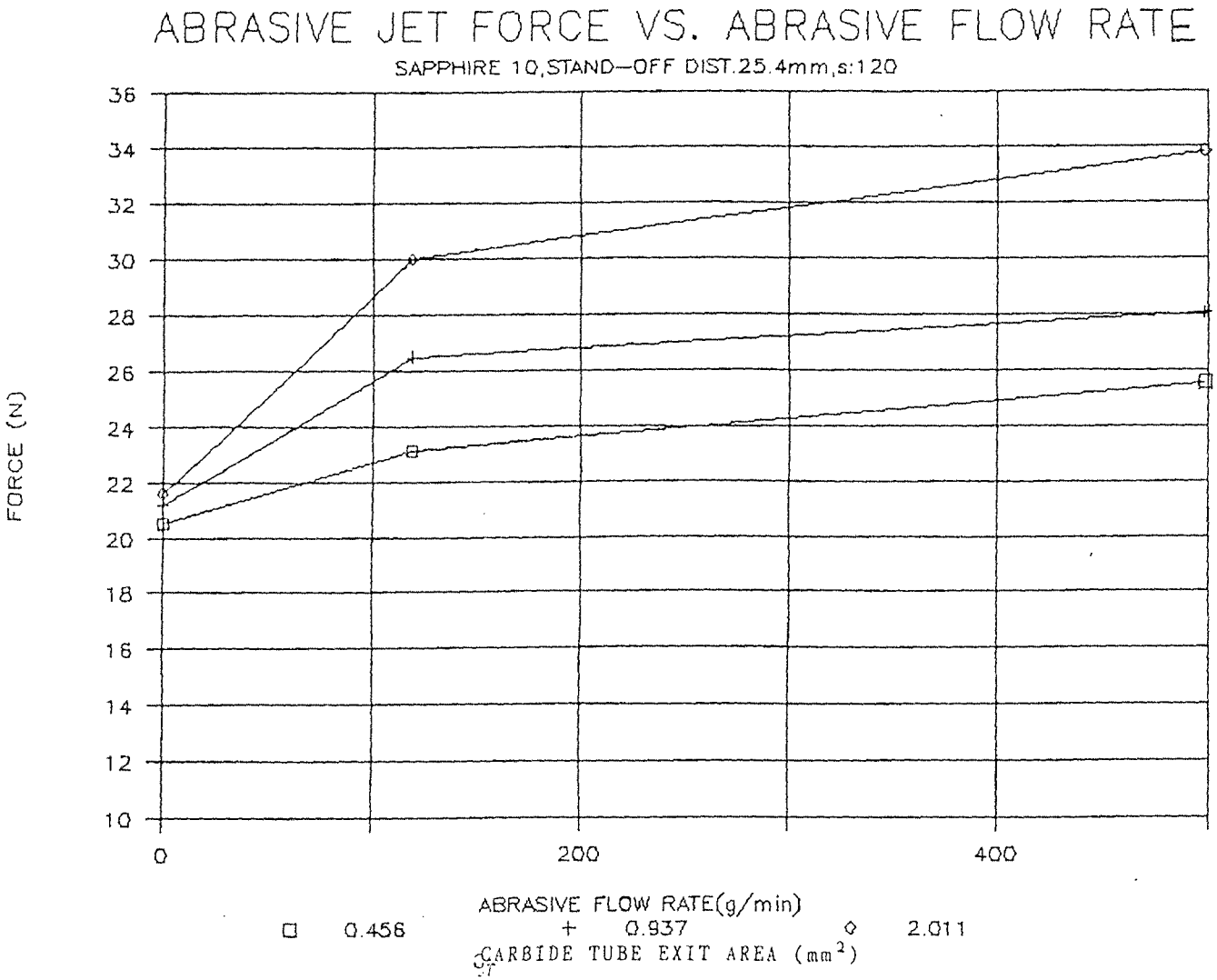
ABRASIVE JET FORCE VS. ABRASIVE FLOW RATE
SAPPHIRE 10,STAND—OFF DIST.25.4mm,s:120
FORCE (N)
36
34
32
30
28
26
24
22
20
18
16
14
12
10
0
200
400
ABRASIVE FLOW RATE(g/min)
□ 0.456
+ 0.937
◇ 2.011
CARBIDE TUBE EXIT AREA (mm²)

FIGURE 6.47

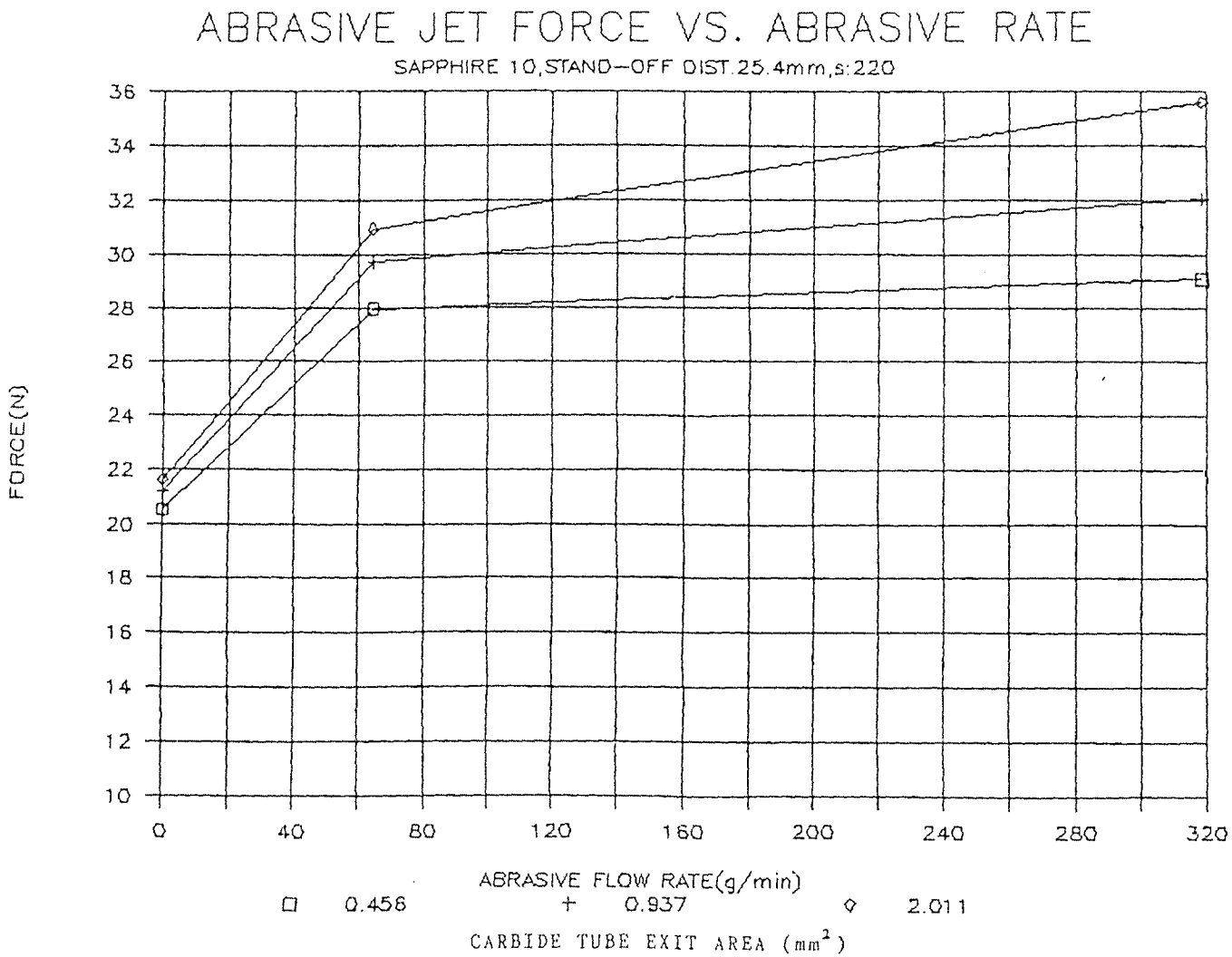
ABRASIVE JET FORCE VS. ABRASIVE RATE
SAPPHIRE 10,STAND-OFF DIST.25.4mm,s:220
FORCE(N)
36
34
32
30
28
26
24
22
20
18
16
14
12
10
0
40
80
120
160
200
240
280
320
ABRASIVE FLOW RATE(g/min)
□ 0.456
+ 0.937
◇ 2.011
CARBIDE TUBE EXIT AREA (mm²)

FIGURE 6.48

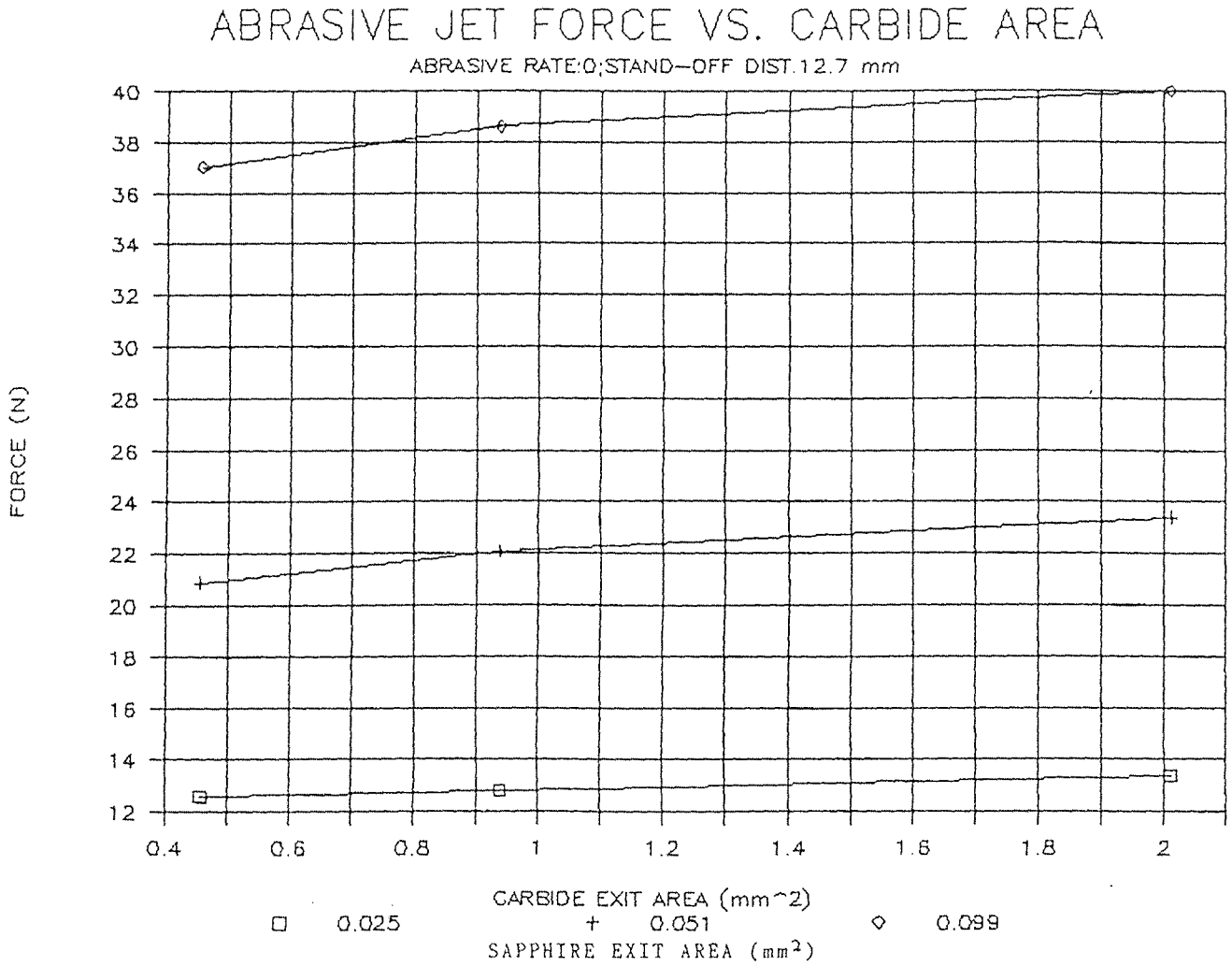
ABRASIVE JET FORCE VS. CARBIDE AREA
ABRASIVE RATE:0;STAND-OFF DIST.12.7 mm
FORCE (N)
40
38
36
34
32
30
28
26
24
22
20
18
16
14
12
0.4
0.6
0.8
1
1.2
1.4
1.6
1.8
2
CARBIDE EXIT AREA (mm^2)
□ 0.025
+ 0.051
◇ 0.099
SAPPHIRE EXIT AREA (mm²)

FIGURE 6.49

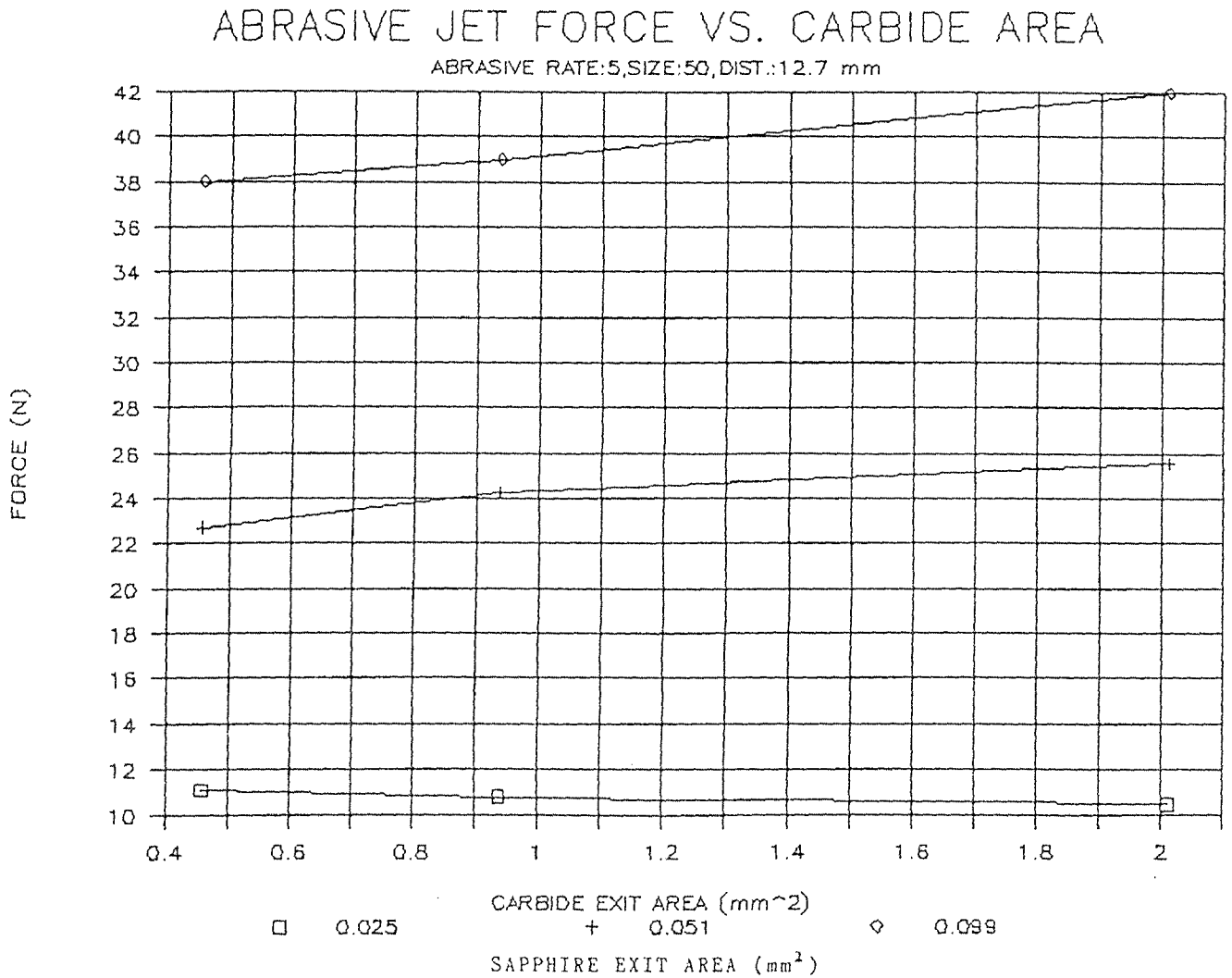
ABRASIVE JET FORCE VS. CARBIDE AREA
ABRASIVE RATE:5,SIZE:50,DIST.:12.7 mm
FORCE (N)
42
40
38
36
34
32
30
28
26
24
22
20
18
16
14
12
10
0.4
0.6
0.8
1
1.2
1.4
1.6
1.8
2
CARBIDE EXIT AREA (mm^2)
0.025
0.051
0.099
SAPPHIRE EXIT AREA (mm²)

FIGURE 6.50

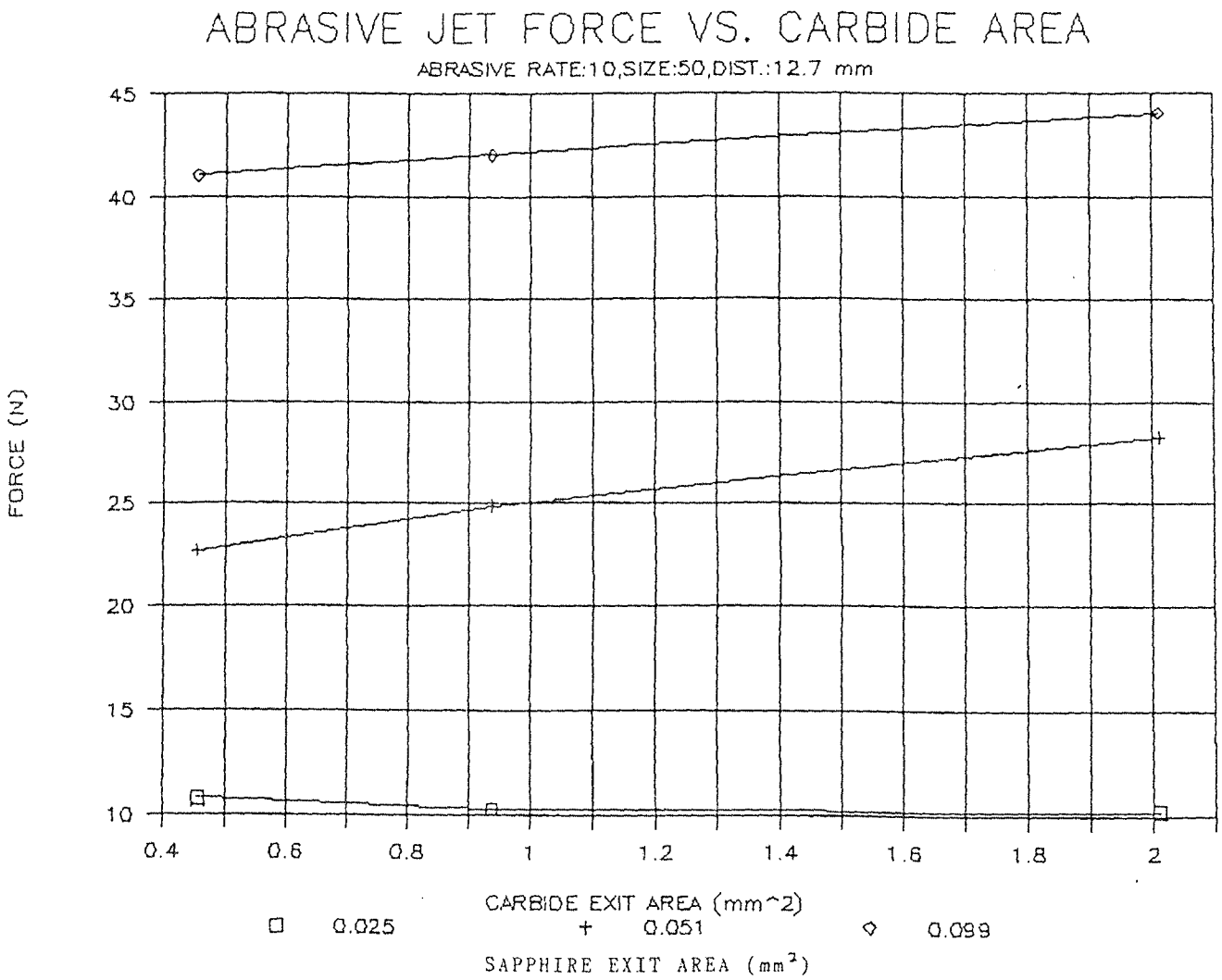
ABRASIVE JET FORCE VS. CARBIDE AREA
ABRASIVE RATE:10,SIZE:50,DIST.:12.7 mm
FORCE (N)
45
40
35
30
25
20
15
10
0.4
0.6
0.8
1
1.2
1.4
1.6
1.8
2
CARBIDE EXIT AREA (mm^2)
0.025
0.051
0.099
SAPPHIRE EXIT AREA (mm²)

FIGURE 6.51

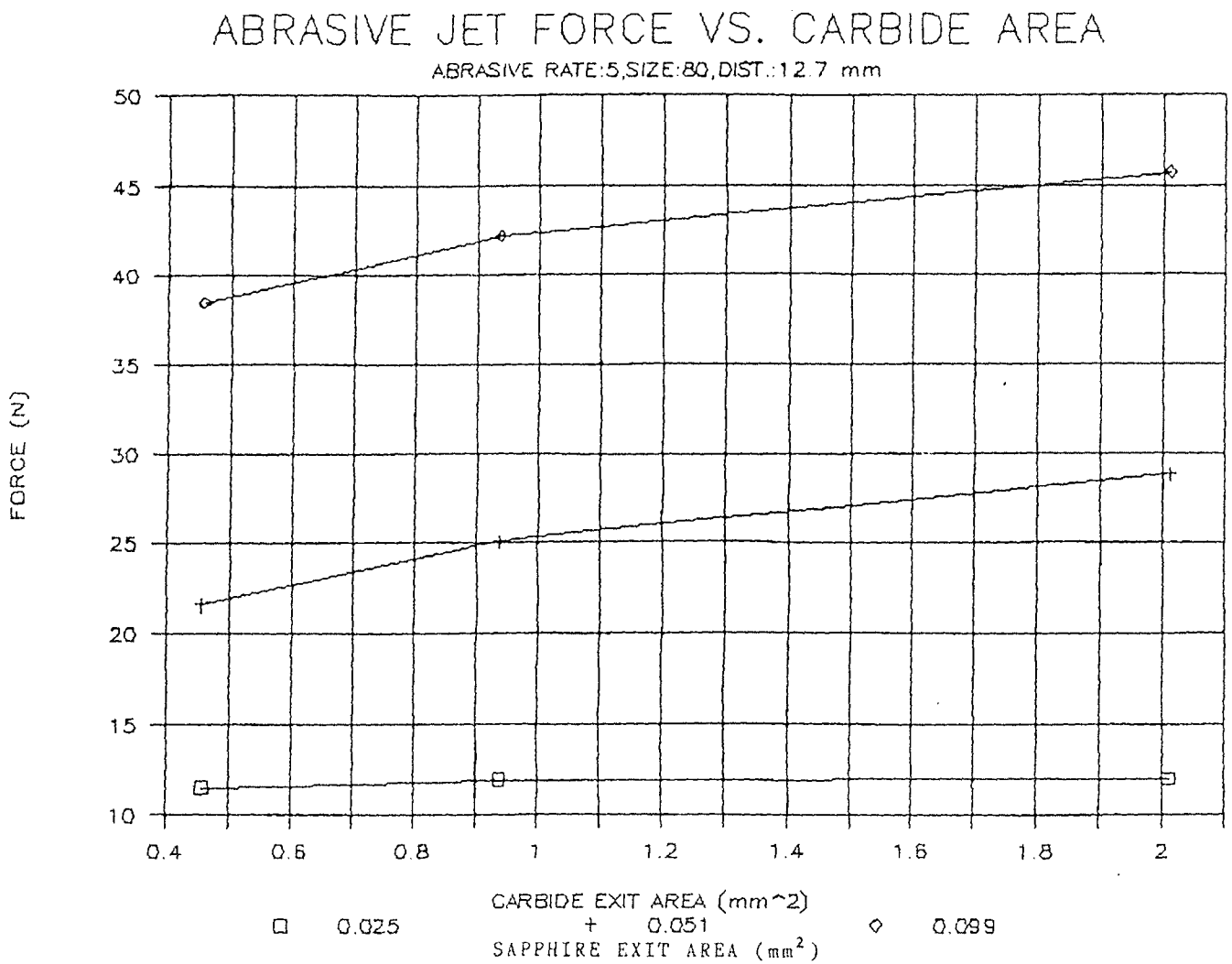
ABRASIVE JET FORCE VS. CARBIDE AREA
ABRASIVE RATE:5,SIZE:80,DIST.:12.7 mm
FORCE (N)
50
45
40
35
30
25
20
15
10
0.4
0.6
0.8
1
1.2
1.4
1.6
1.8
2
CARBIDE EXIT AREA (mm^2)
□ 0.025
+ 0.051
◇ 0.099
SAPPHIRE EXIT AREA (mm²)

FIGURE 6.52

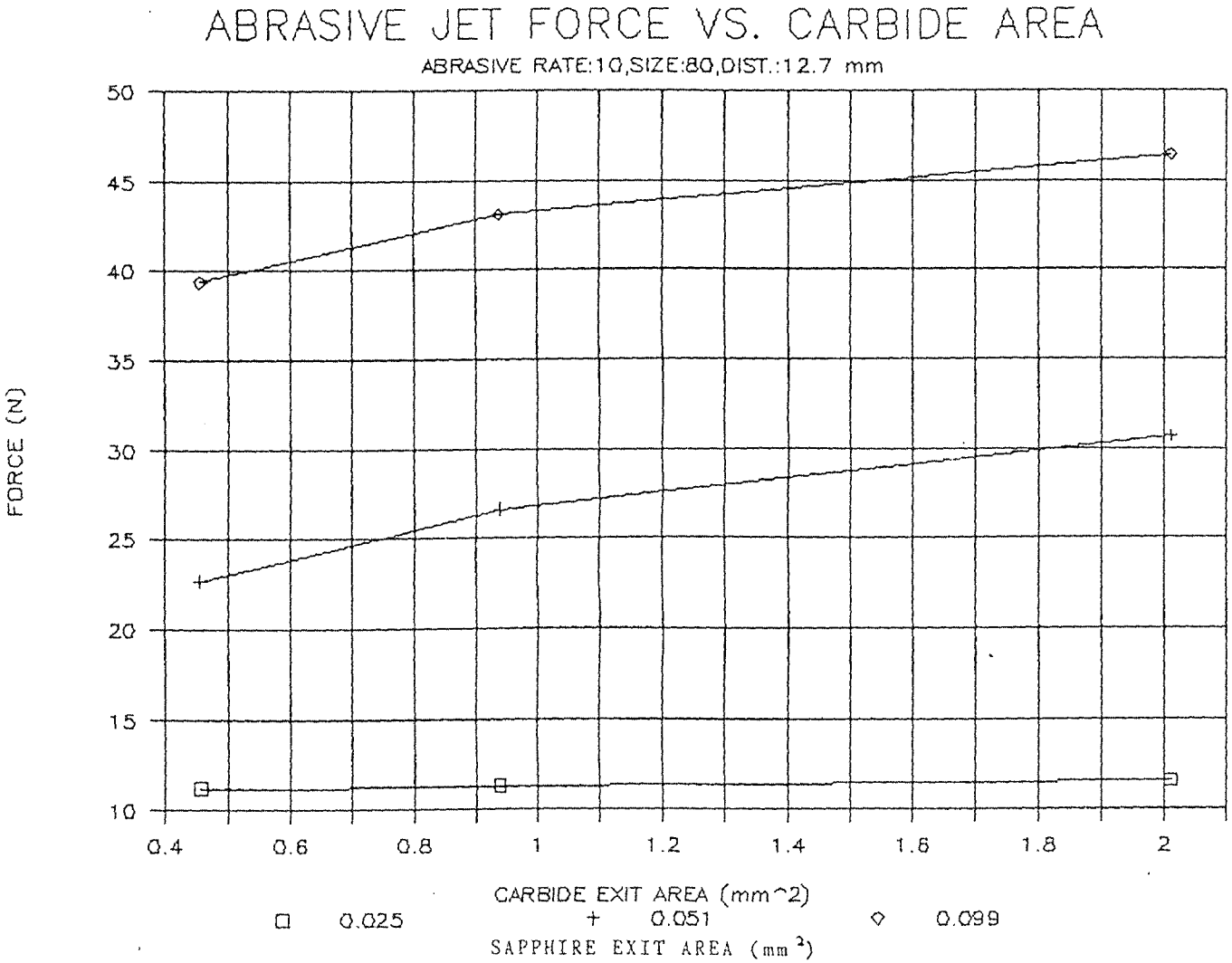
ABRASIVE JET FORCE VS. CARBIDE AREA
ABRASIVE RATE:10,SIZE:80,DIST.:12.7 mm
FORCE (N)
50
45
40
35
30
25
20
15
10
0.4
0.6
0.8
1
1.2
1.4
1.6
1.8
2
CARBIDE EXIT AREA (mm^2)
0.025
0.051
0.099
SAPPHIRE EXIT AREA (mm²)

FIGURE 6.53

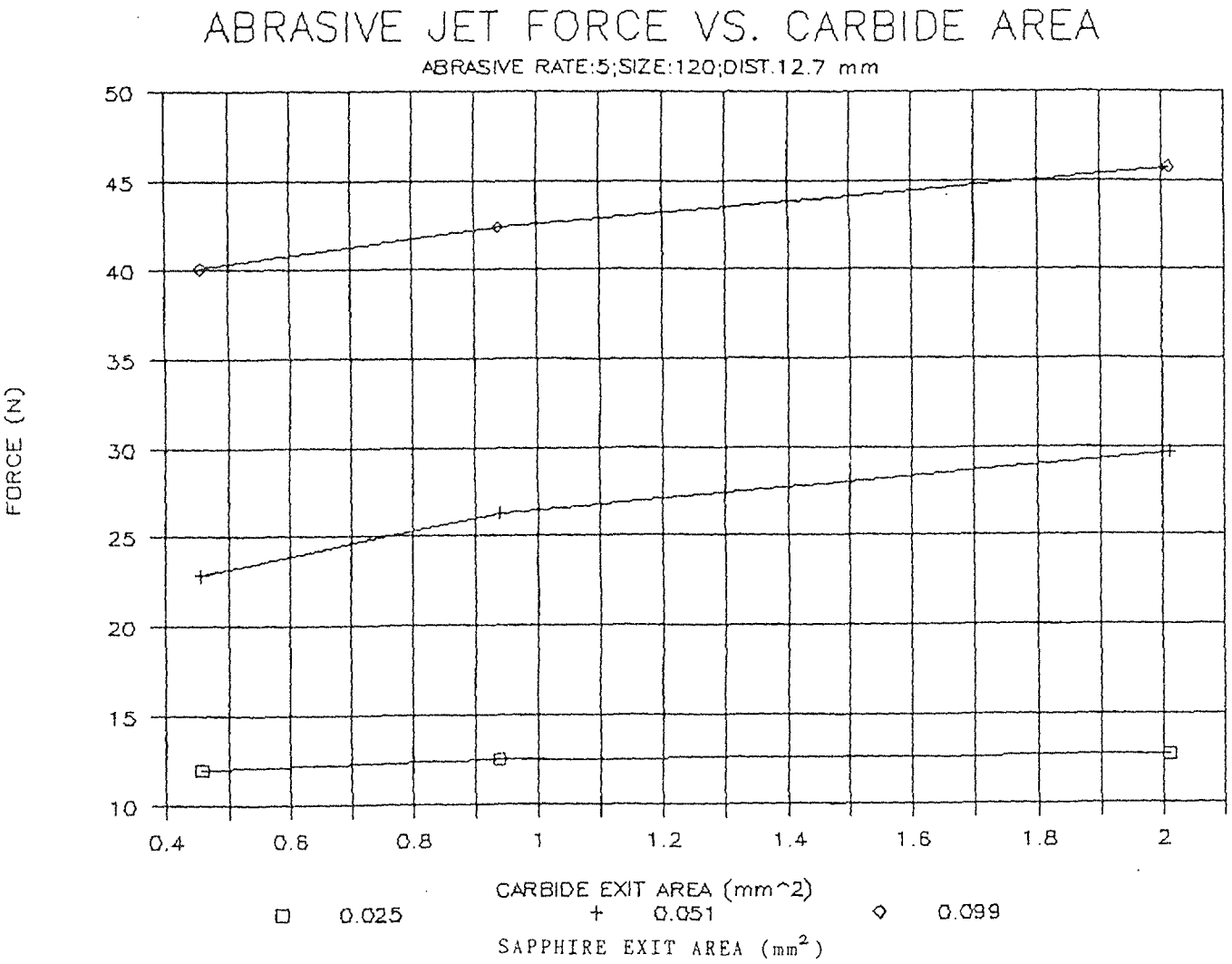
ABRASIVE JET FORCE VS. CARBIDE AREA
ABRASIVE RATE:5;SIZE:120;DIST.12.7 mm
FORCE (N)
50
45
40
35
30
25
20
15
10
0.4
0.6
0.8
1
1.2
1.4
1.6
1.8
2
CARBIDE EXIT AREA (mm^2)
0.025
0.051
0.099
SAPPHIRE EXIT AREA (mm²)

FIGURE 6.54

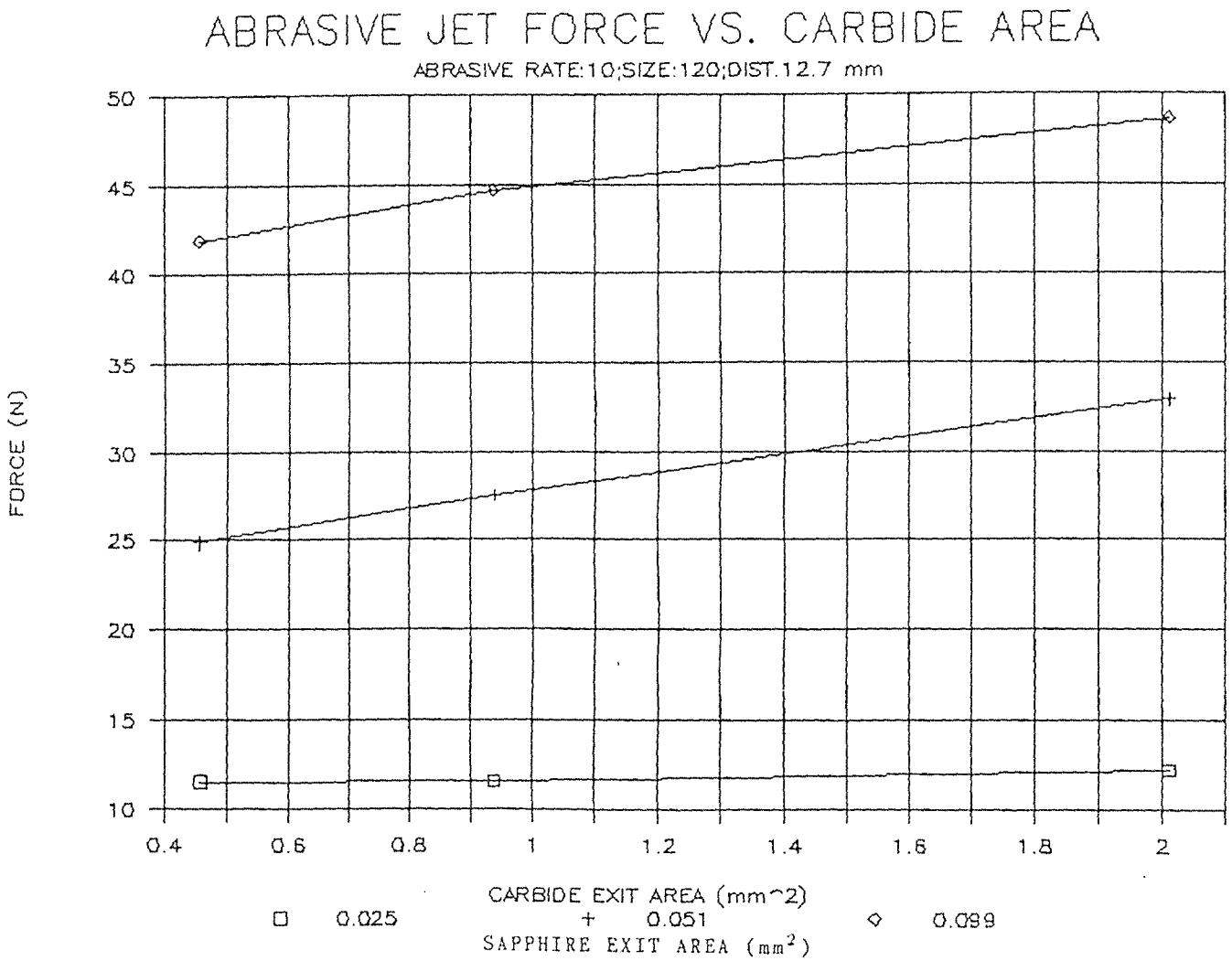
ABRASIVE JET FORCE VS. CARBIDE AREA
ABRASIVE RATE:10;SIZE:120;DIST.12.7 mm
FORCE (N)
50
45
40
35
30
25
20
15
10
0.4
0.6
0.8
1
1.2
1.4
1.6
1.8
2
CARBIDE EXIT AREA (mm^2)
0.025
0.051
0.099
SAPPHIRE EXIT AREA (mm²)

FIGURE 6.55

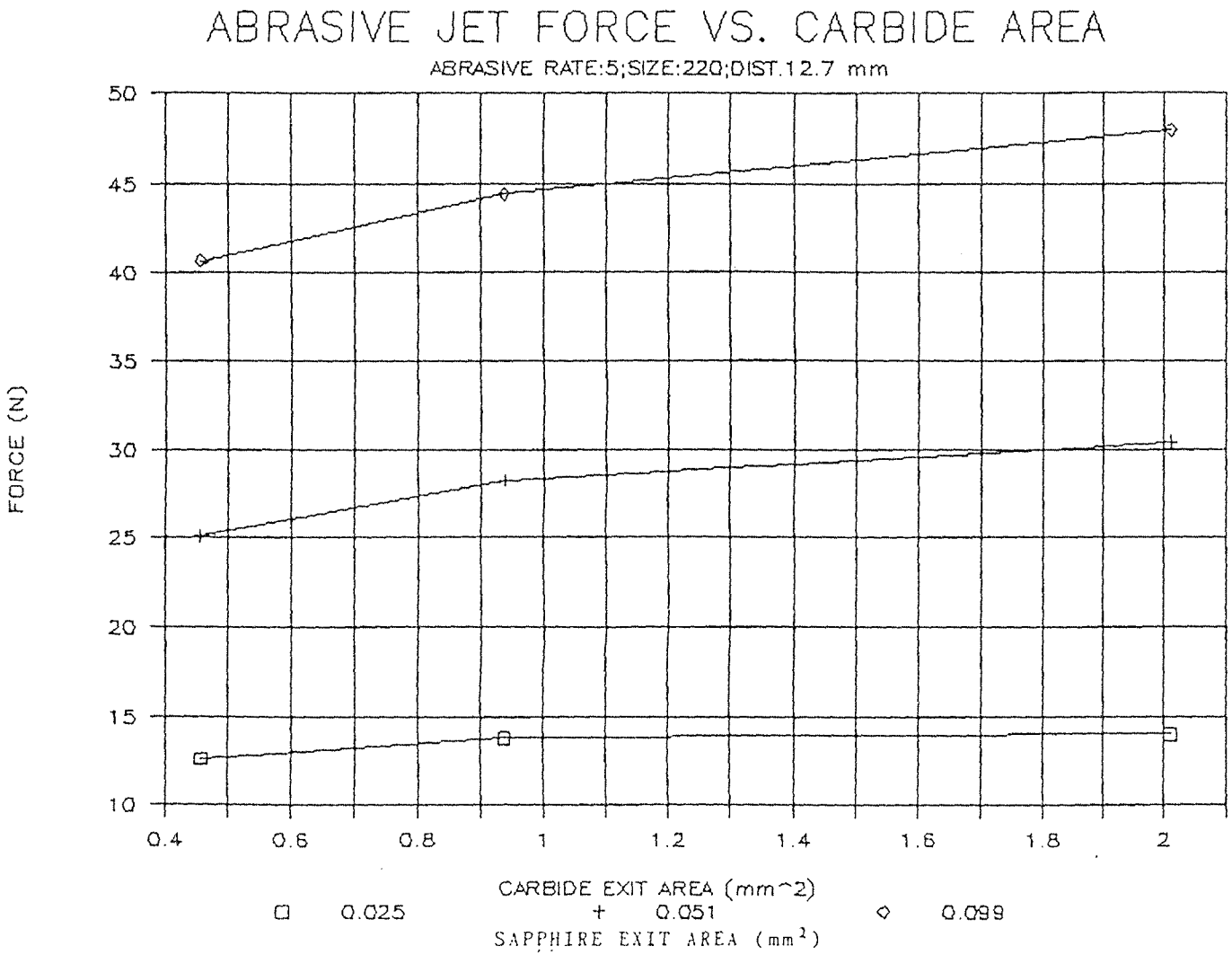
ABRASIVE JET FORCE VS. CARBIDE AREA
ABRASIVE RATE:5;SIZE:220;DIST.12.7 mm
FORCE (N)
50
45
40
35
30
25
20
15
10
0.4
0.6
0.8
1
1.2
1.4
1.6
1.8
2
CARBIDE EXIT AREA (mm^2)
0.025
0.051
0.099
SAPPHIRE EXIT AREA (mm²)

FIGURE 6.5a

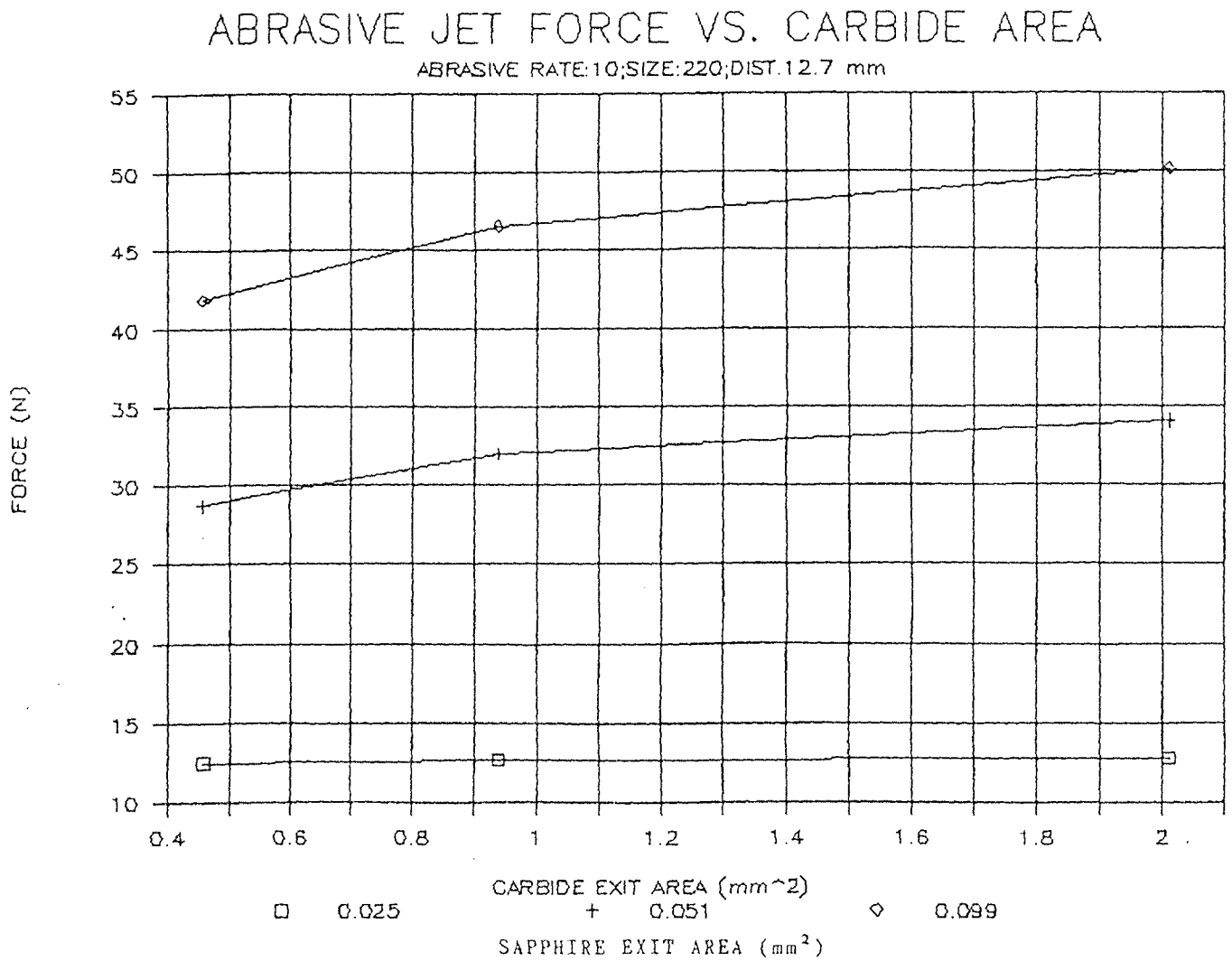
ABRASIVE JET FORCE VS. CARBIDE AREA
ABRASIVE RATE:10;SIZE:220;DIST.12.7 mm
FORCE (N)
55
50
45
40
35
30
25
20
15
10
0.4
0.6
0.8
1
1.2
1.4
1.6
1.8
2
CARBIDE EXIT AREA (mm^2)
0.025
0.051
0.099
SAPPHIRE EXIT AREA (mm²)

FIGURE 6.57

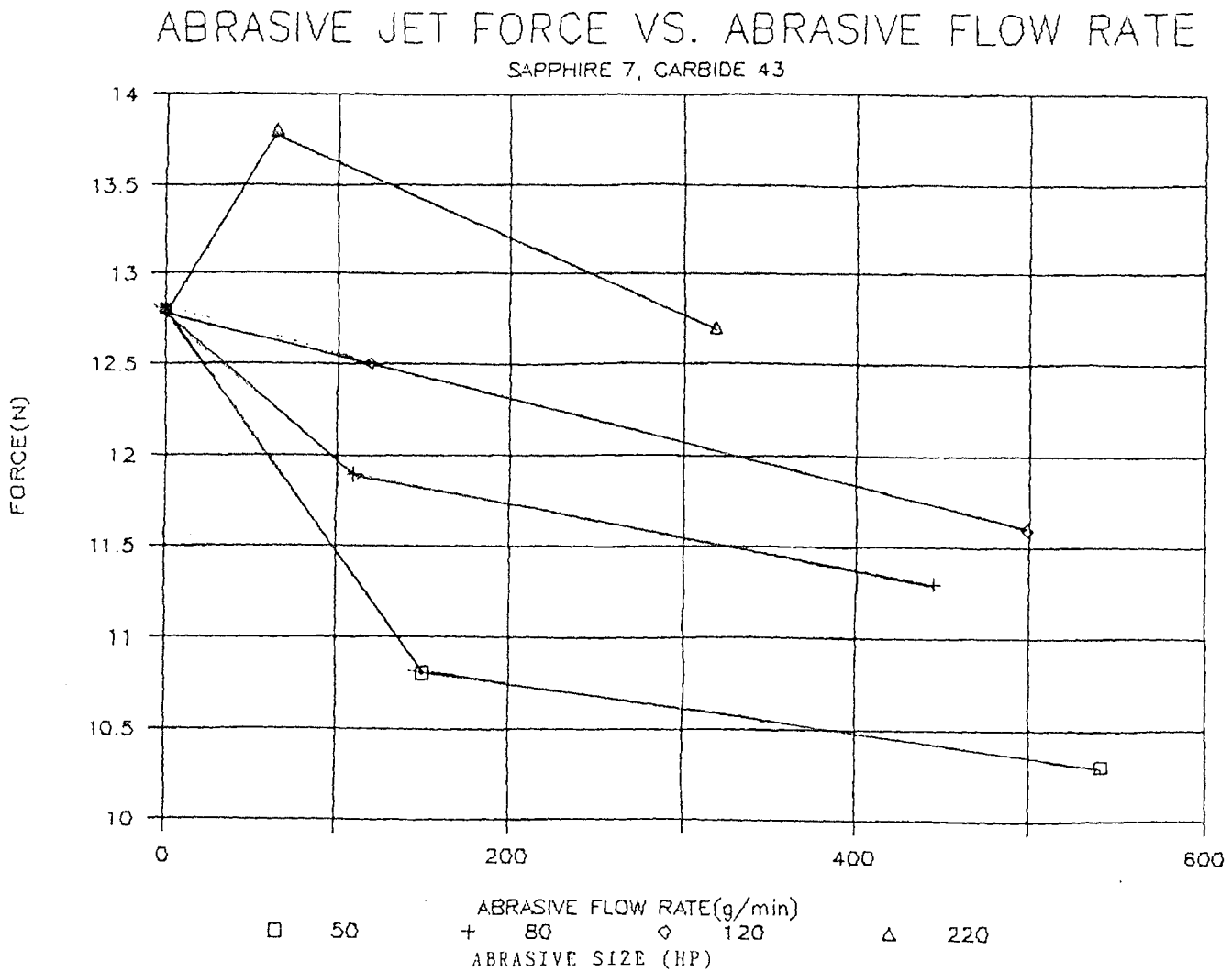
ABRASIVE JET FORCE VS. ABRASIVE FLOW RATE
SAPPHIRE 7, CARBIDE 43
FORCE(N)
14
13.5
13
12.5
12
11.5
11
10.5
10
0
200
400
600
ABRASIVE FLOW RATE(g/min)
□ 50
+ 80
◇ 120
△ 220
ABRASIVE SIZE (HP)

FIGURE 6.58

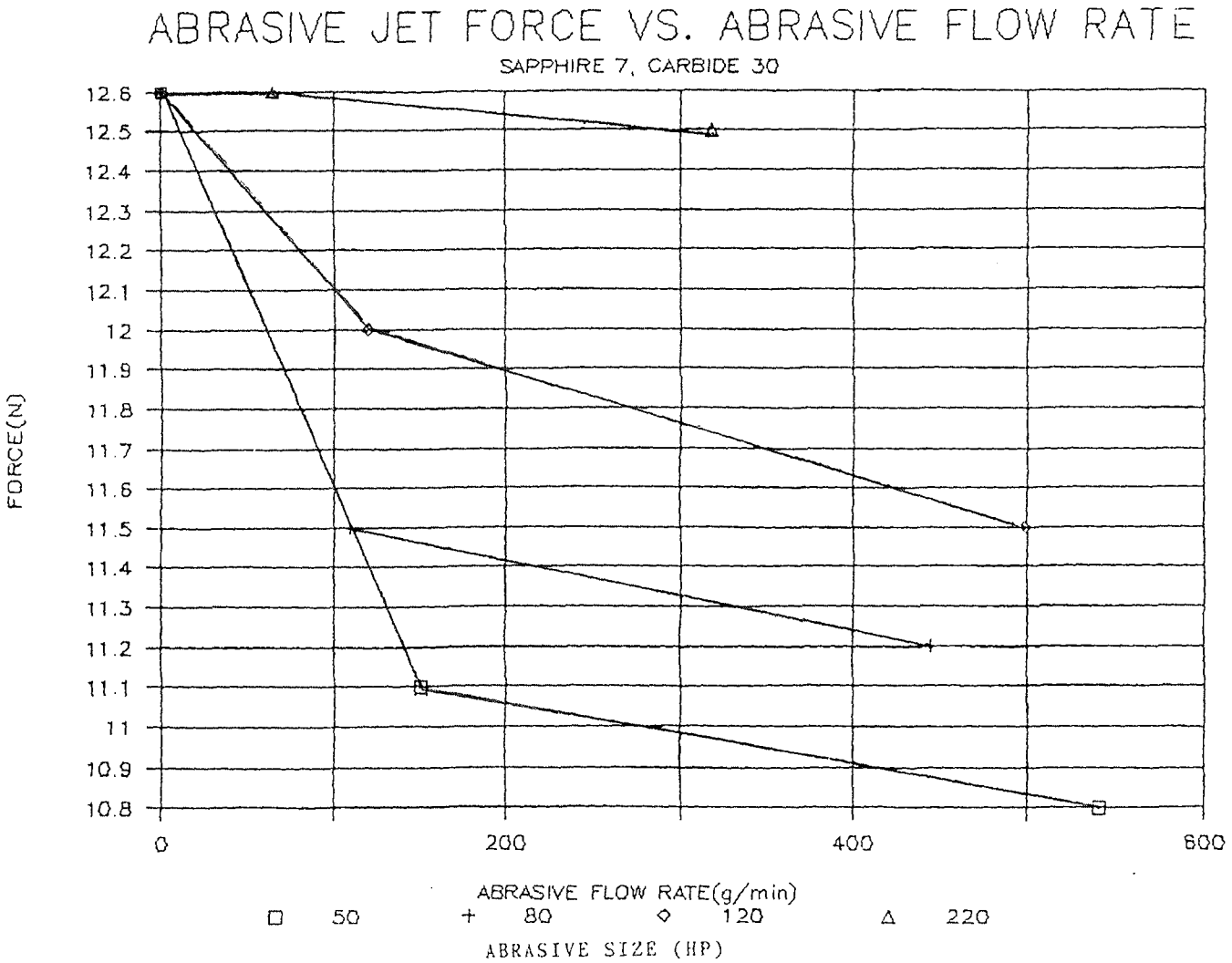
ABRASIVE JET FORCE VS. ABRASIVE FLOW RATE
SAPPHIRE 7, CARBIDE 30
FORCE(N)
12.6
12.5
12.4
12.3
12.2
12.1
12
11.9
11.8
11.7
11.6
11.5
11.4
11.3
11.2
11.1
11
10.9
10.8
0
200
400
600
ABRASIVE FLOW RATE(g/min)
□ 50
+ 80
◇ 120
Δ 220
ABRASIVE SIZE (HP)

FIGURE 6.59

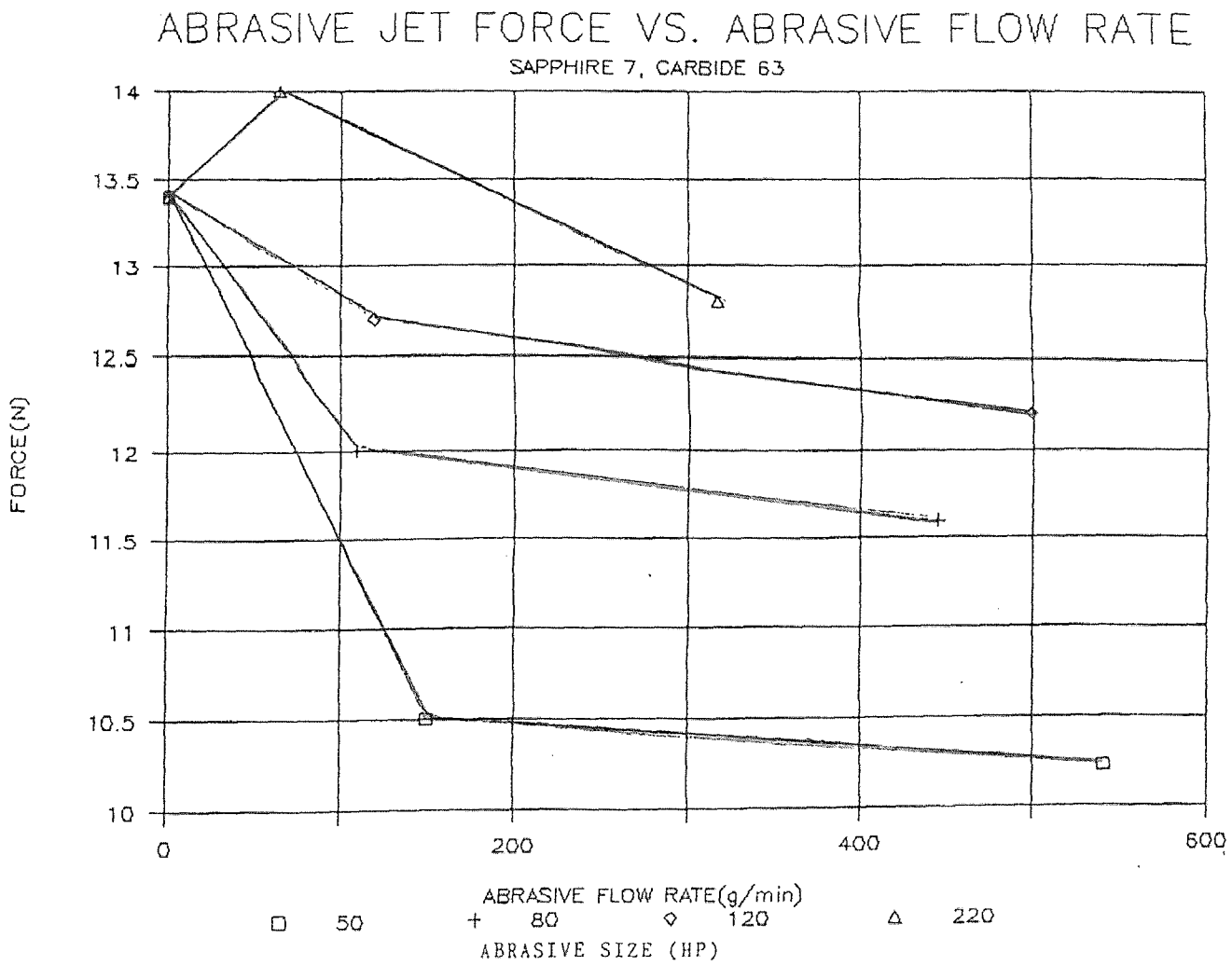
ABRASIVE JET FORCE VS. ABRASIVE FLOW RATE
SAPPHIRE 7, CARBIDE 63
FORCE(N)
14
13.5
13
12.5
12
11.5
11
10.5
10
0
200
400
600
ABRASIVE FLOW RATE(g/min)
50
80
120
220
ABRASIVE SIZE (HP)

FIGURE 6.60

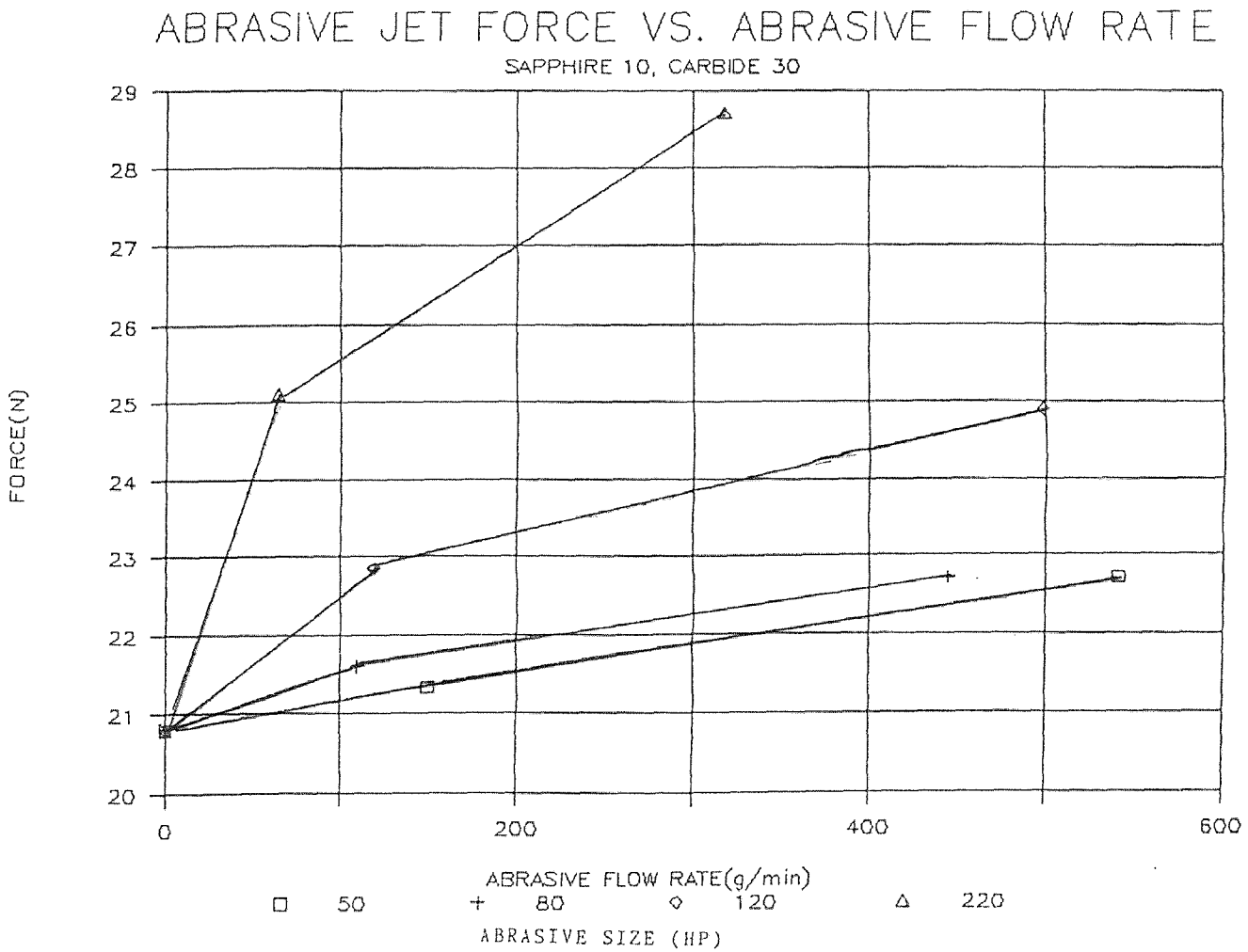
ABRASIVE JET FORCE VS. ABRASIVE FLOW RATE
SAPPHIRE 10, CARBIDE 30
FORCE(N)
29
28
27
26
25
24
23
22
21
20
0
200
400
600
ABRASIVE FLOW RATE(g/min)
50
80
120
220
ABRASIVE SIZE (HP)

FIGURE 6.61

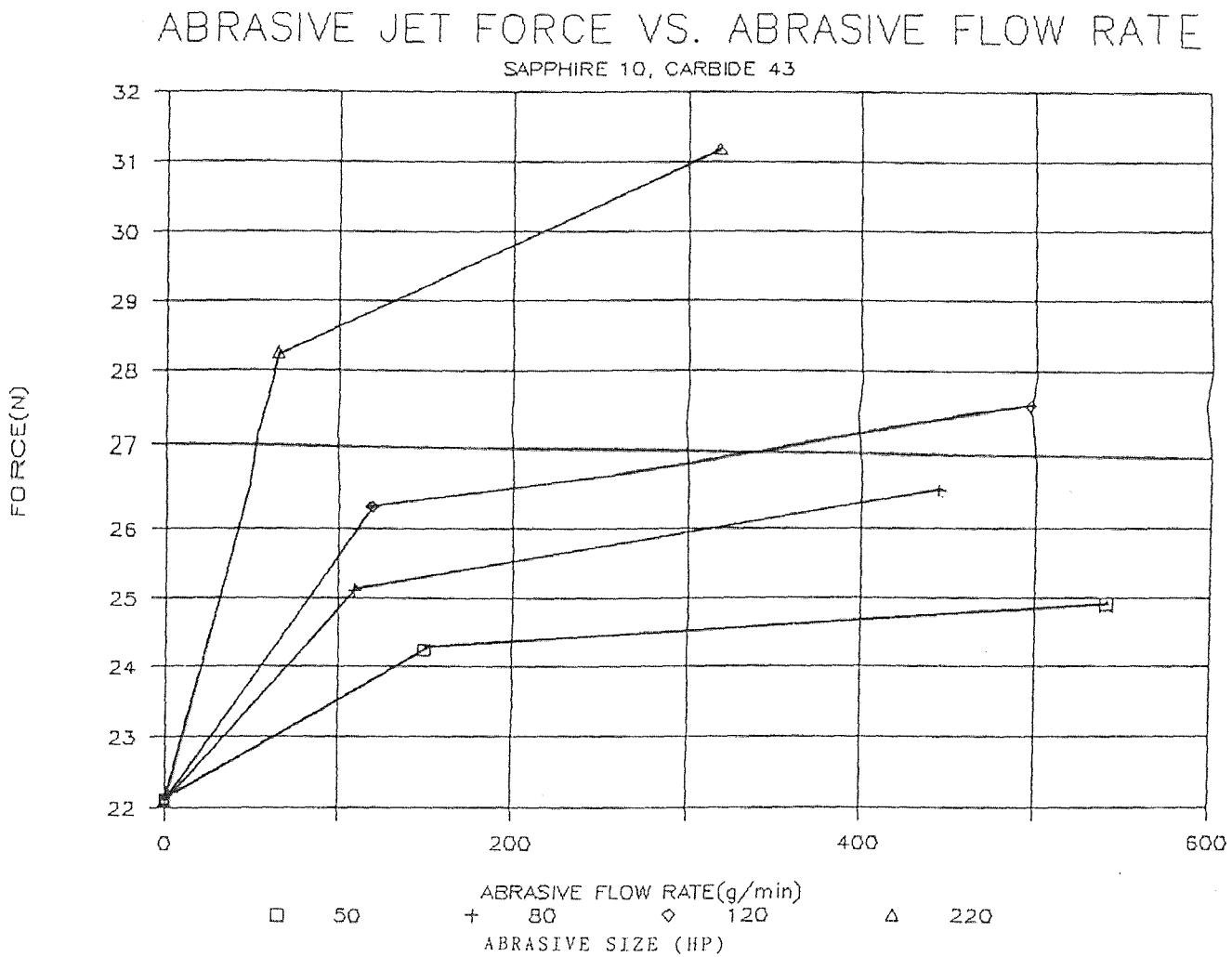
ABRASIVE JET FORCE VS. ABRASIVE FLOW RATE
SAPPHIRE 10, CARBIDE 43
FORCE(N)
32
31
30
29
28
27
26
25
24
23
22
0
200
400
600
ABRASIVE FLOW RATE(g/min)
□ 50
+ 80
◇ 120
△ 220
ABRASIVE SIZE (HP)

FIGURE 6.62

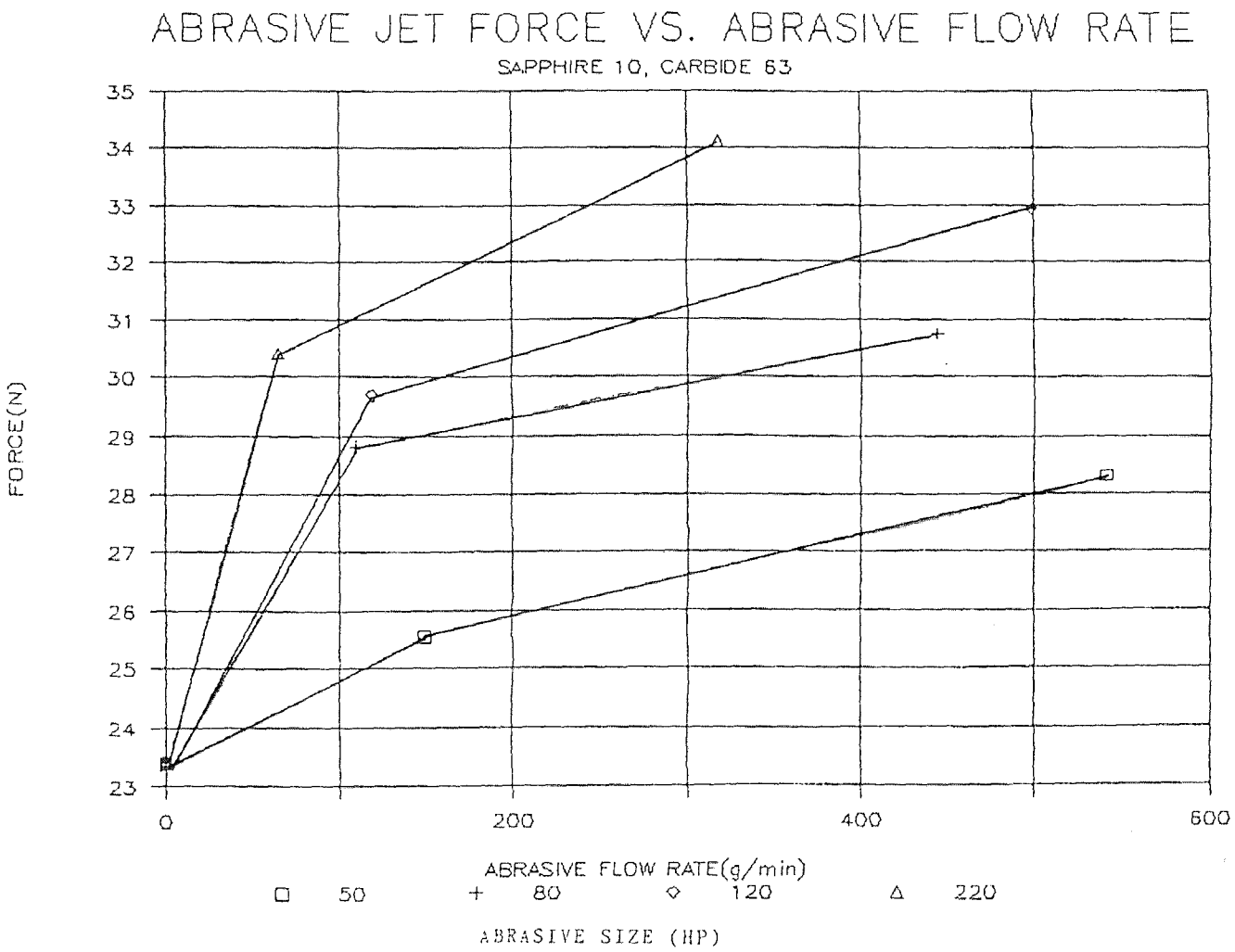
ABRASIVE JET FORCE VS. ABRASIVE FLOW RATE
SAPPHIRE 10, CARBIDE 63
FORCE(N)
35
34
33
32
31
30
29
28
27
26
25
24
23
0
200
400
600
ABRASIVE FLOW RATE(g/min)
□ 50
+ 80
◇ 120
△ 220
ABRASIVE SIZE (HP)

FIGURE 6.63

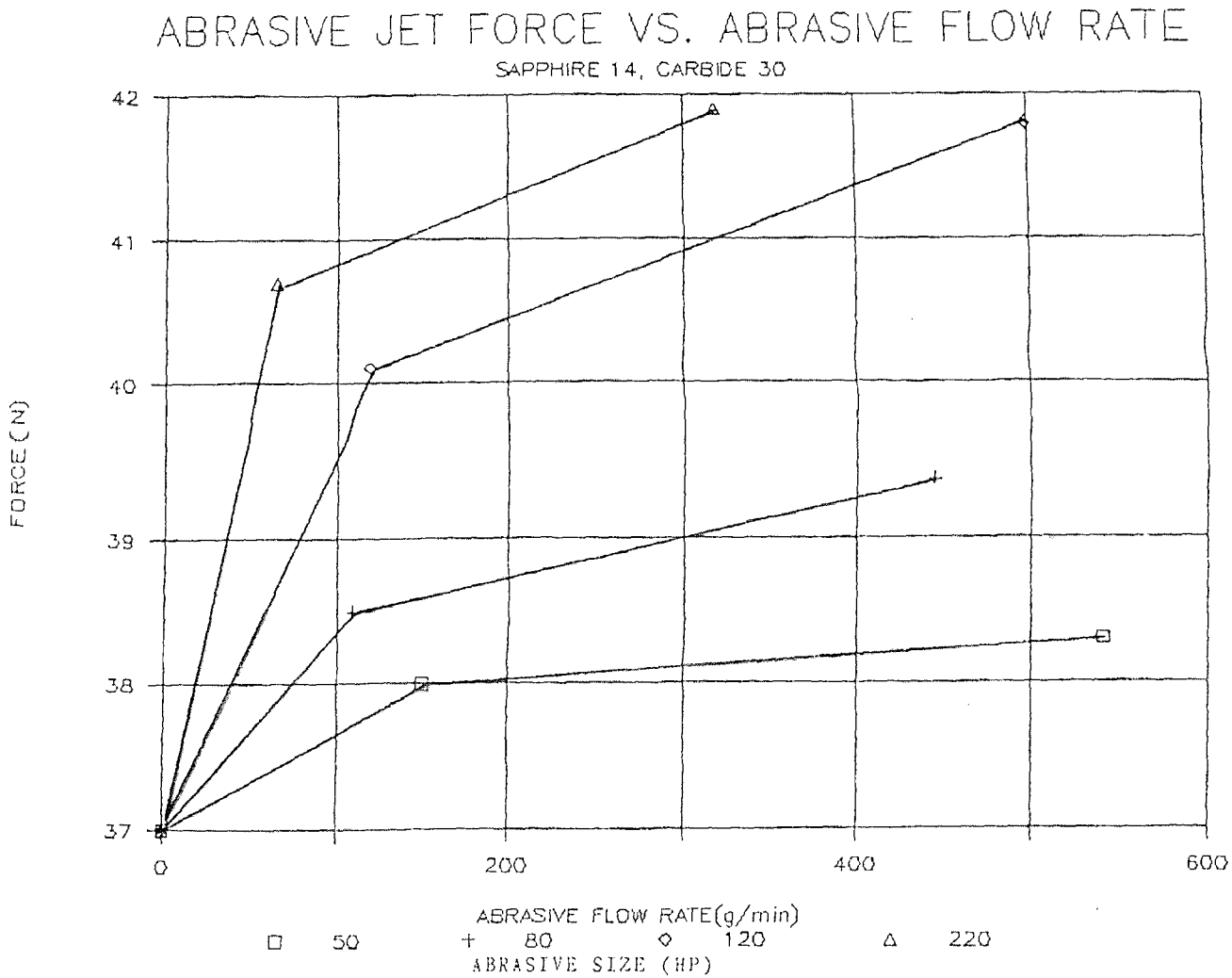
ABRASIVE JET FORCE VS. ABRASIVE FLOW RATE
SAPPHIRE 14, CARBIDE 30
FORCE (N)
42
41
40
39
38
37
0
200
400
600
ABRASIVE FLOW RATE(g/min)
50
80
120
220
ABRASIVE SIZE (HP)

FIGURE 6.64

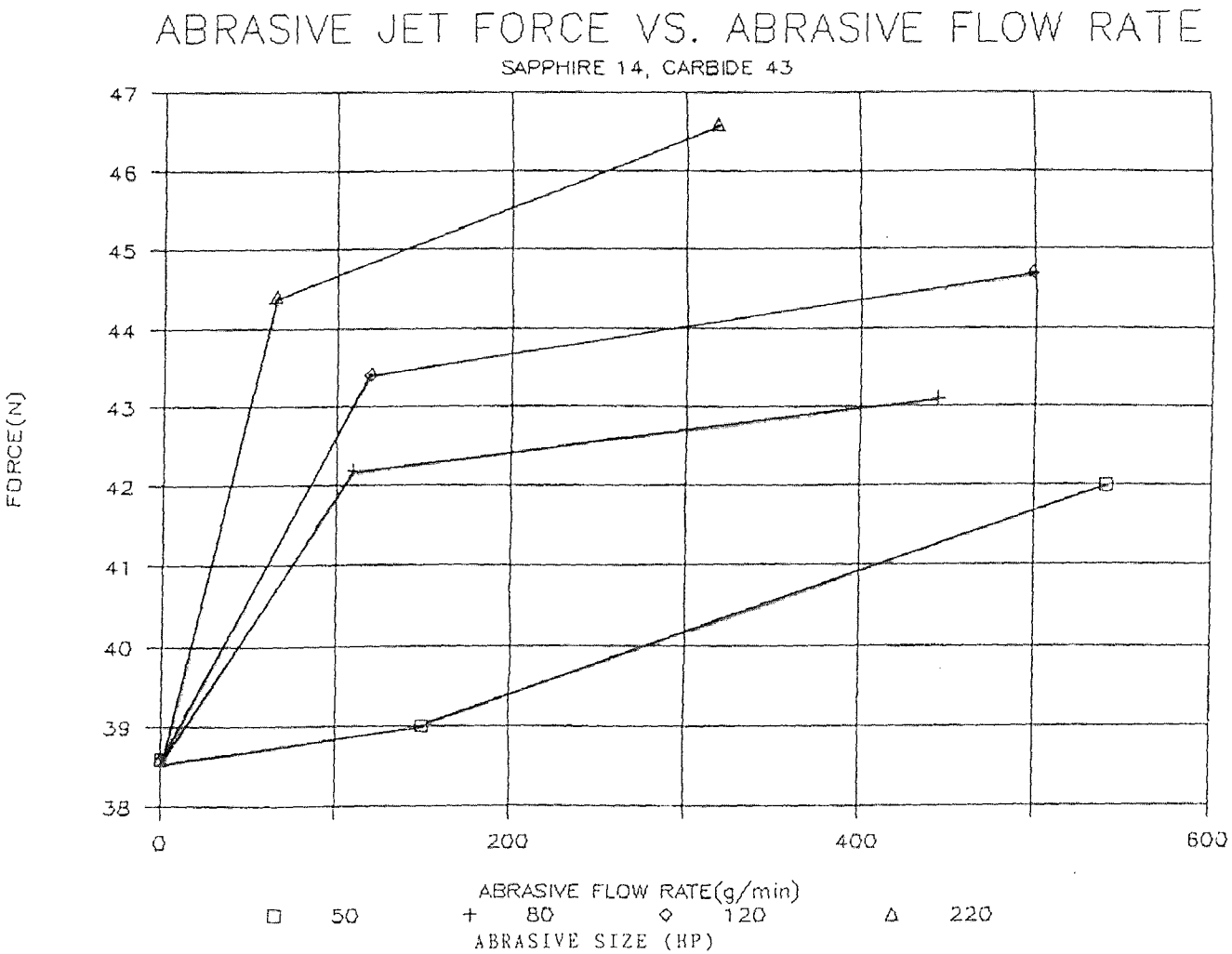
ABRASIVE JET FORCE VS. ABRASIVE FLOW RATE
SAPPHIRE 14, CARBIDE 43
FORCE(N)
47
46
45
44
43
42
41
40
39
38
0
200
400
600
ABRASIVE FLOW RATE(g/min)
□ 50
+ 80
◇ 120
△ 220
ABRASIVE SIZE (MP)

FIGURE 6.65

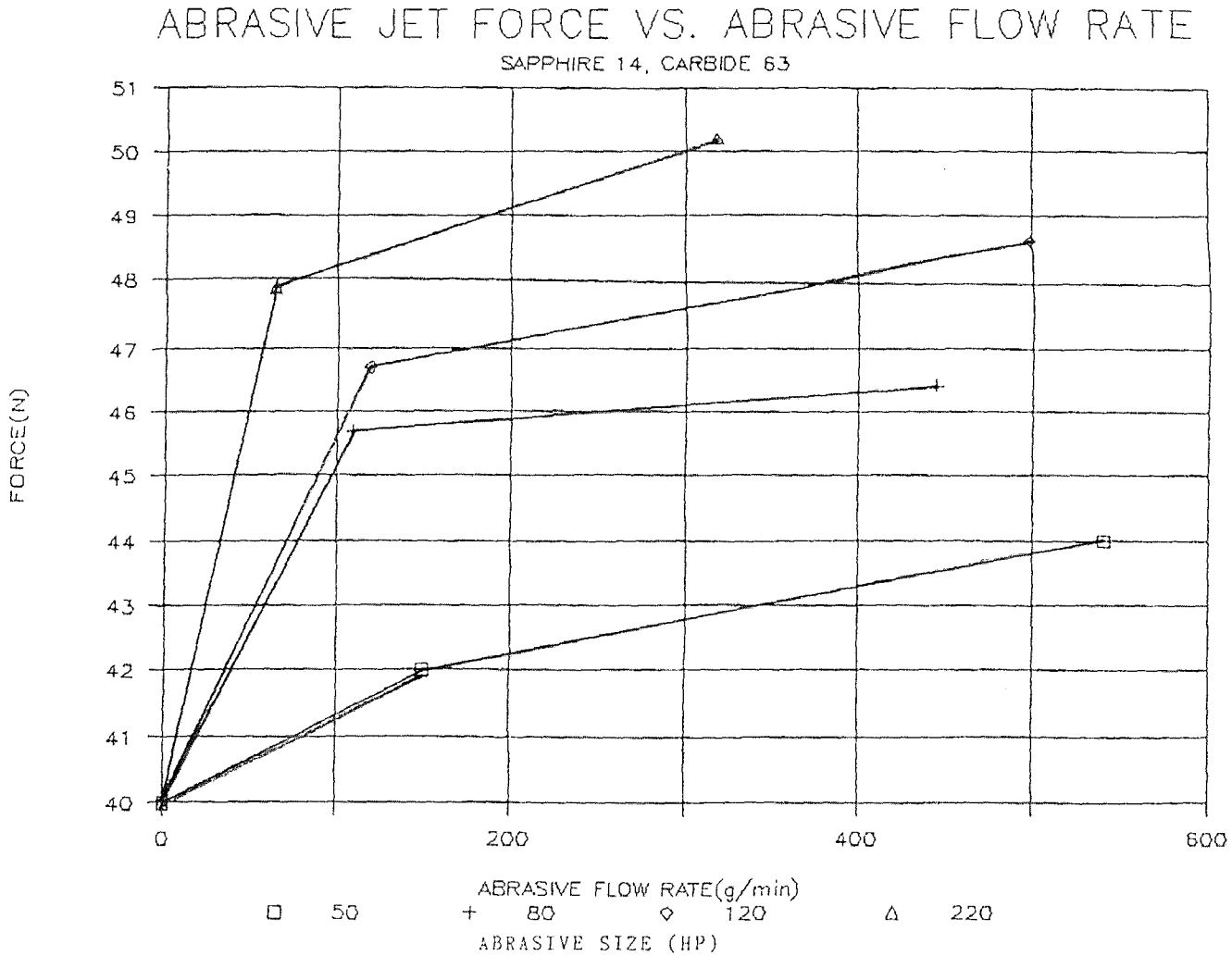
ABRASIVE JET FORCE VS. ABRASIVE FLOW RATE
SAPPHIRE 14, CARBIDE 63
FORCE(N)
51
50
49
48
47
46
45
44
43
42
41
40
0
200
400
600
ABRASIVE FLOW RATE(g/min)
□ 50
+ 80
◇ 120
Δ 220
ABRASIVE SIZE (HP)

FIGURE 6.66

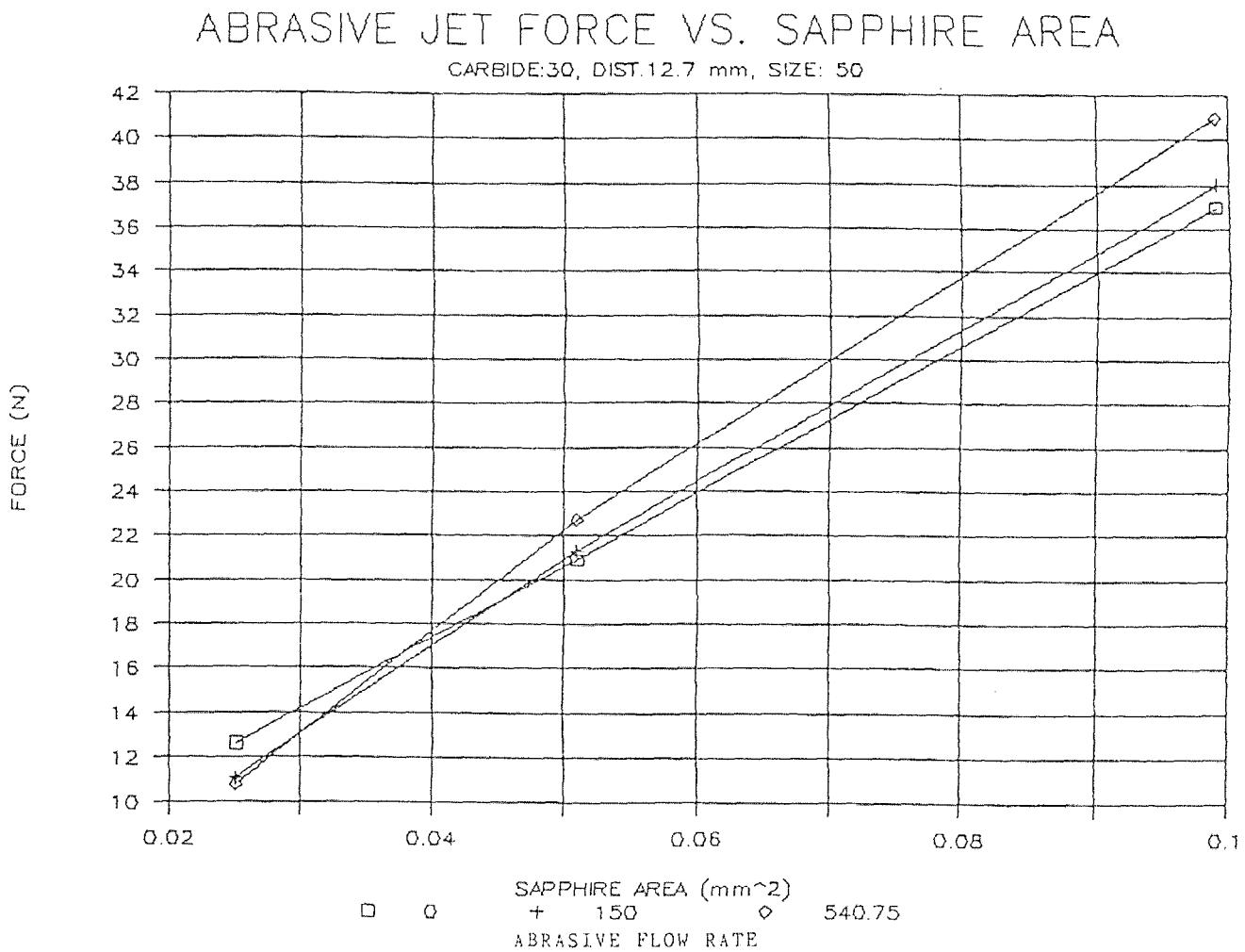
ABRASIVE JET FORCE VS. SAPPHIRE AREA
CARBIDE:30, DIST.12.7 mm, SIZE: 50
FORCE (N)
42
40
38
36
34
32
30
28
26
24
22
20
18
16
14
12
10
0.02
0.04
0.06
0.08
0.1
SAPPHIRE AREA (mm^2)
0
150
540.75
ABRASIVE FLOW RATE

FIGURE 6.67

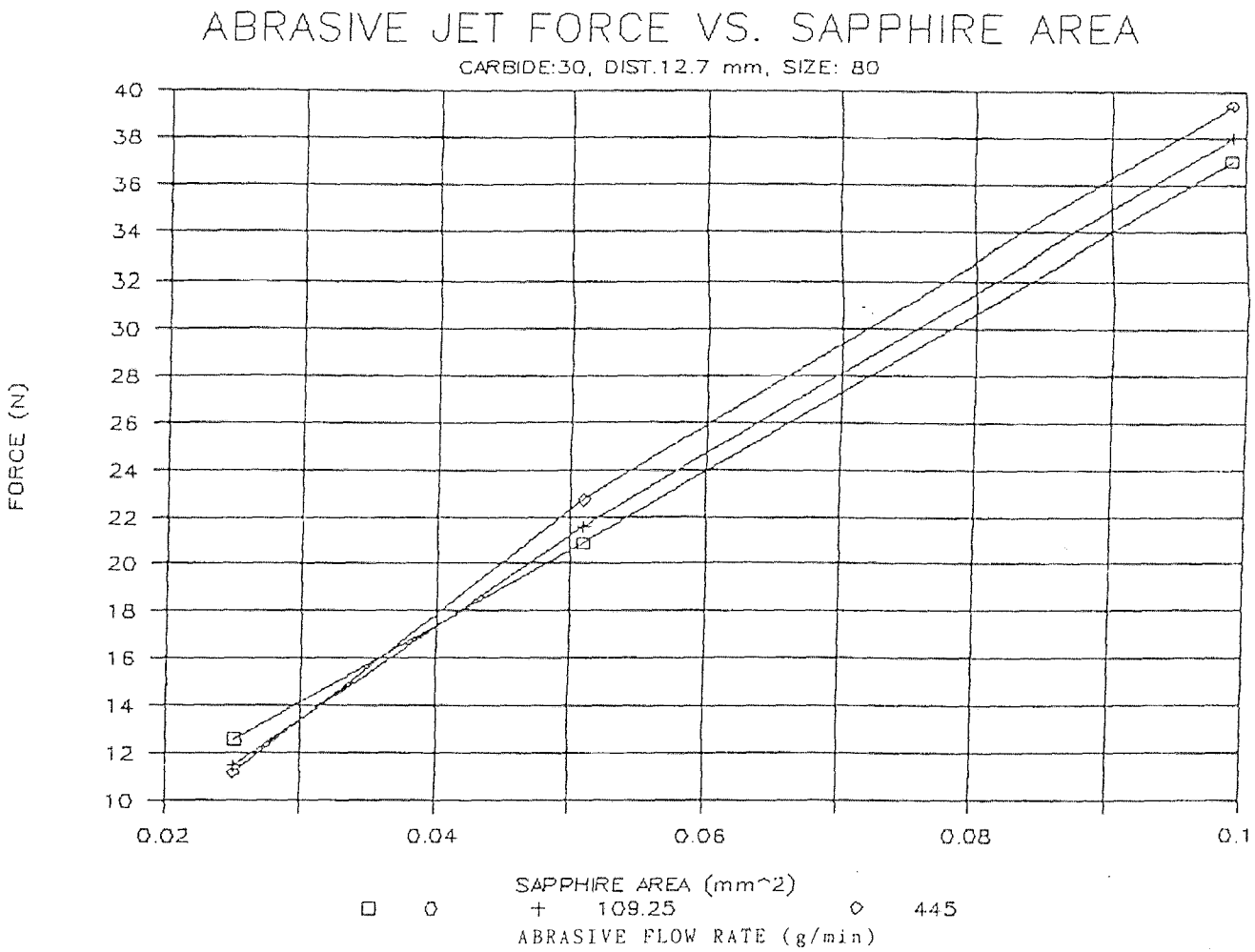
ABRASIVE JET FORCE VS. SAPPHIRE AREA
CARBIDE:30, DIST.12.7 mm, SIZE: 80
FORCE (N)
40
38
36
34
32
30
28
26
24
22
20
18
16
14
12
10
0.02
0.04
0.06
0.08
0.1
SAPPHIRE AREA (mm^2)
□ 0 + 109.25 ◇ 445
ABRASIVE FLOW RATE (g/min)

FIGURE 6.68

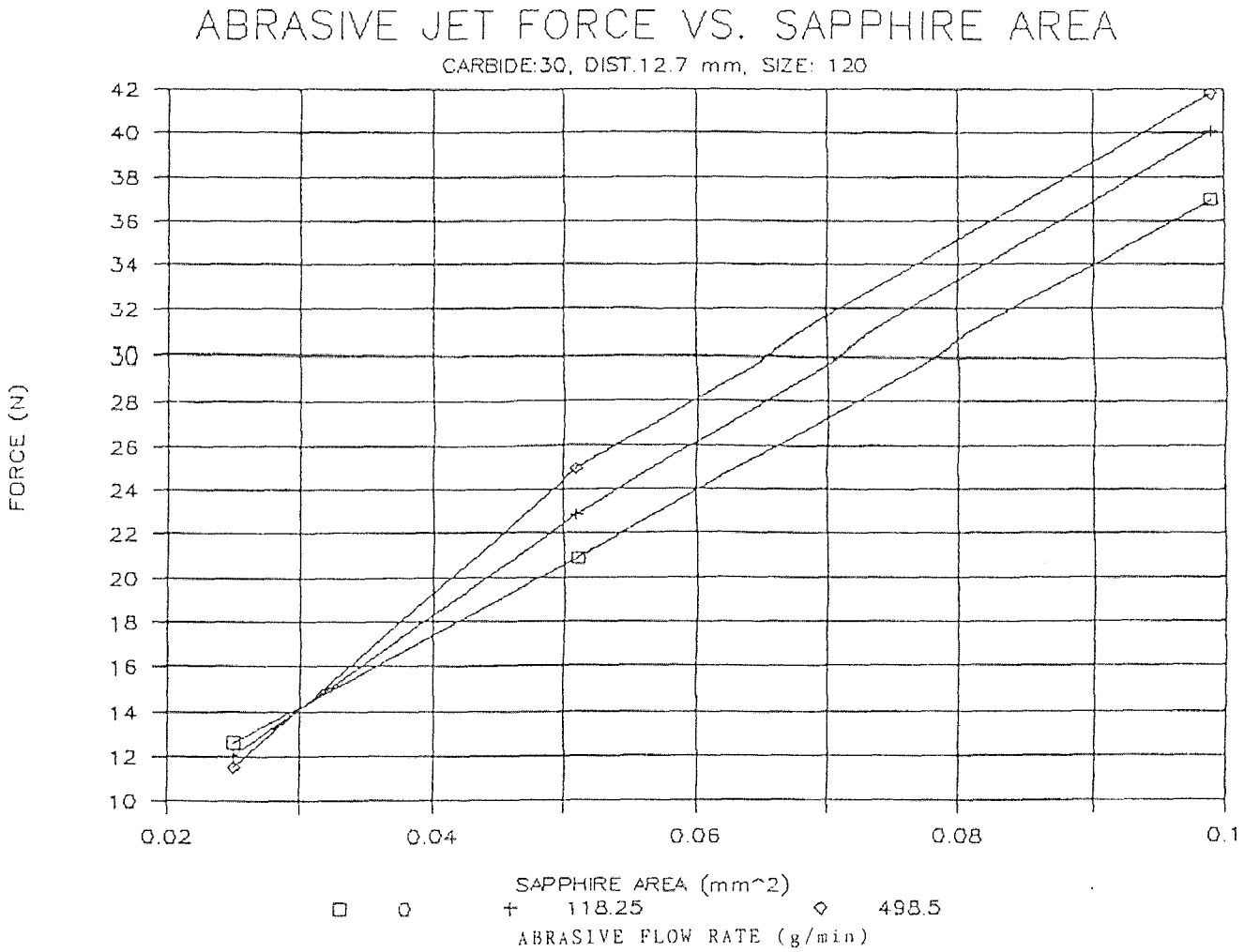
ABRASIVE JET FORCE VS. SAPPHIRE AREA
CARBIDE:30, DIST.12.7 mm, SIZE: 120
FORCE (N)
42
40
38
36
34
32
30
28
26
24
22
20
18
16
14
12
10
0.02
0.04
0.06
0.08
0.1
SAPPHIRE AREA (mm^2)
0
118.25
498.5
ABRASIVE FLOW RATE (g/min)

FIGURE 6.69

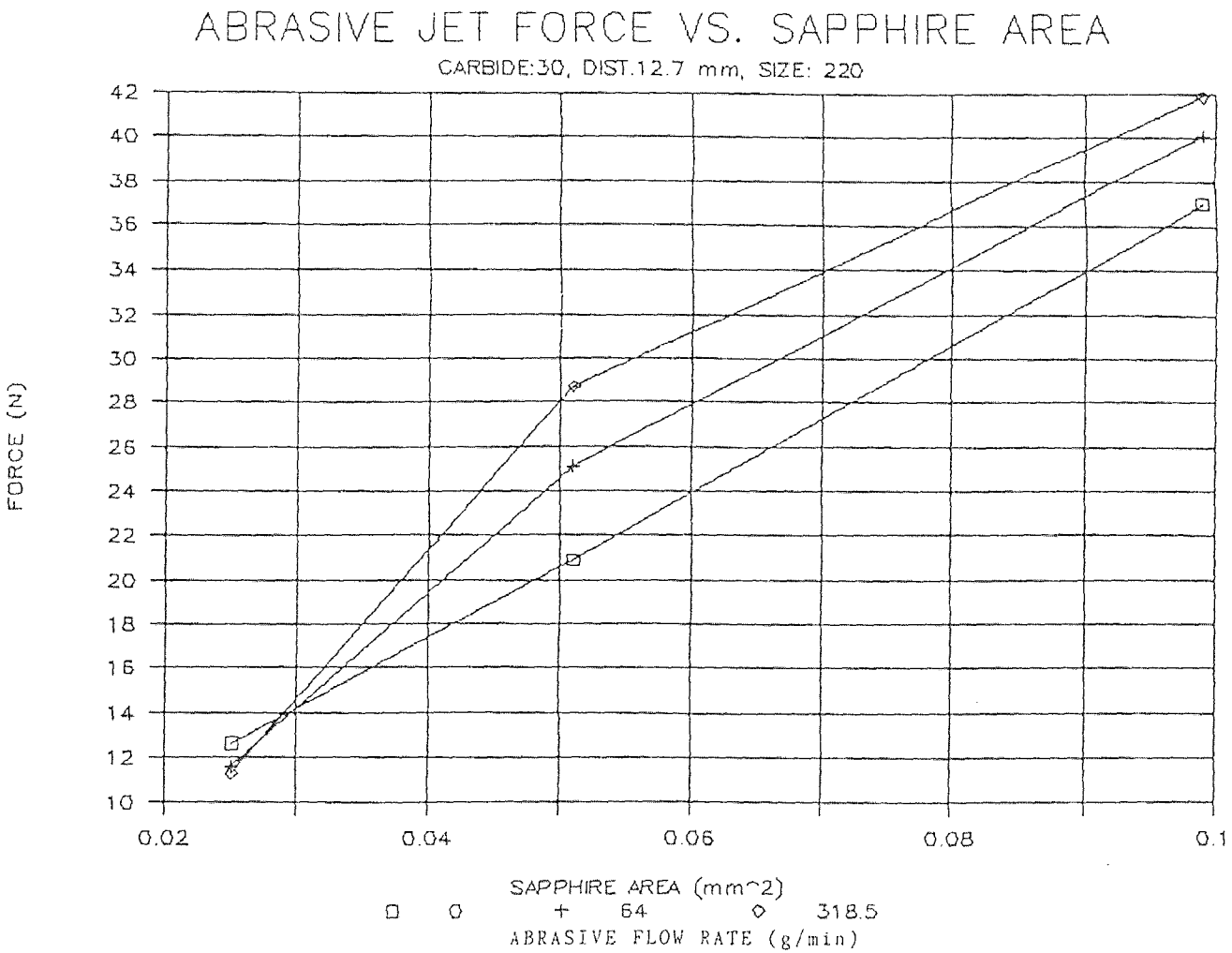
ABRASIVE JET FORCE VS. SAPPHIRE AREA
CARBIDE:30, DIST.12.7 mm, SIZE: 220
FORCE (N)
42
40
38
36
34
32
30
28
26
24
22
20
18
16
14
12
10
0.02
0.04
0.06
0.08
0.1
SAPPHIRE AREA (mm^2)
0
64
318.5
ABRASIVE FLOW RATE (g/min)

FIGURE 6.70

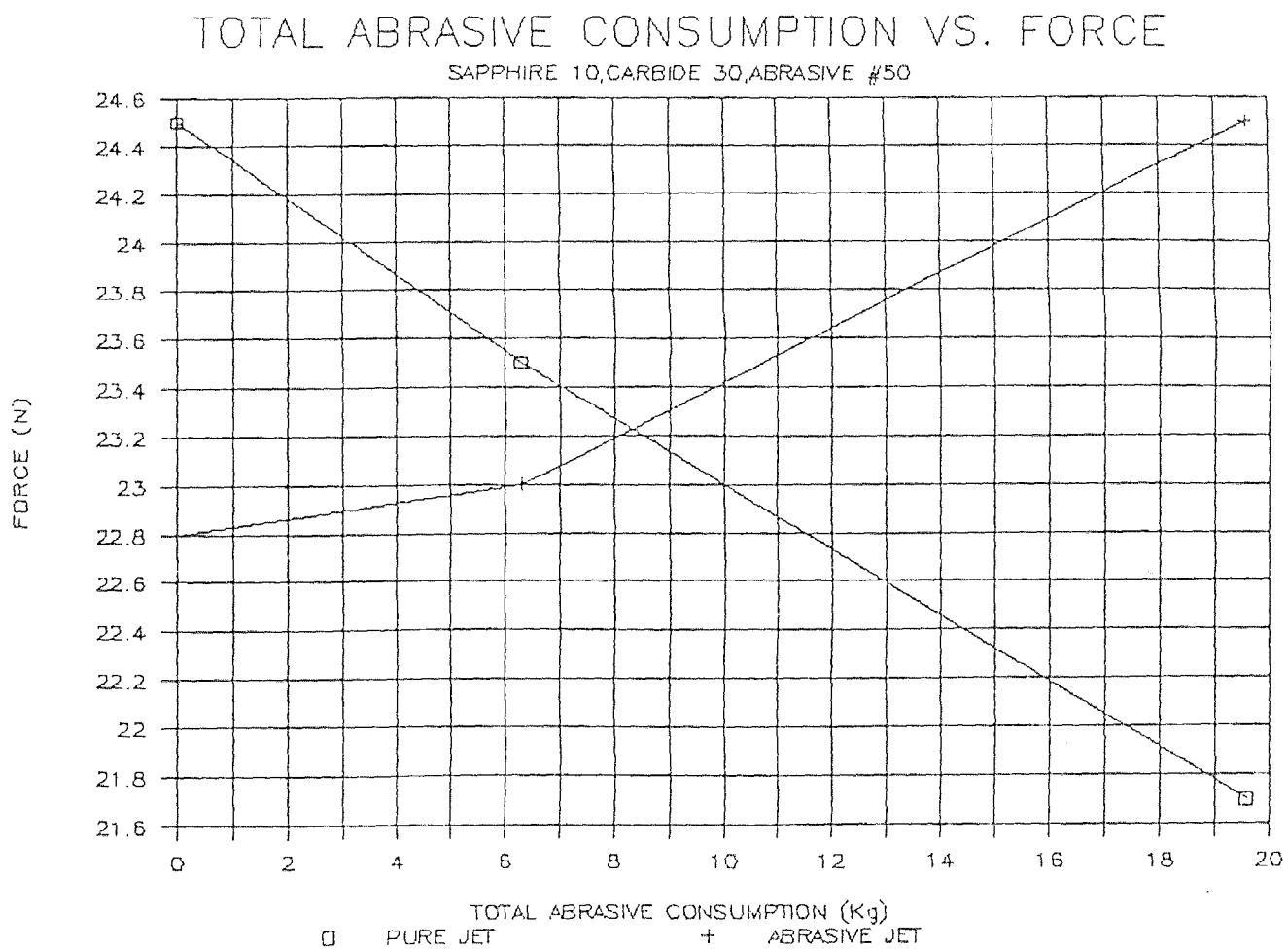
TOTAL ABRASIVE CONSUMPTION VS. FORCE
SAPPHIRE 10,CARBIDE 30,ABRASIVE #50
FORCE (N)
24.6
24.4
24.2
24
23.8
23.6
23.4
23.2
23
22.8
22.6
22.4
22.2
22
21.8
21.6
0
2
4
6
8
10
12
14
16
18
20
TOTAL ABRASIVE CONSUMPTION (Kg)
PURE JET
ABRASIVE JET

FIGURE 6.71

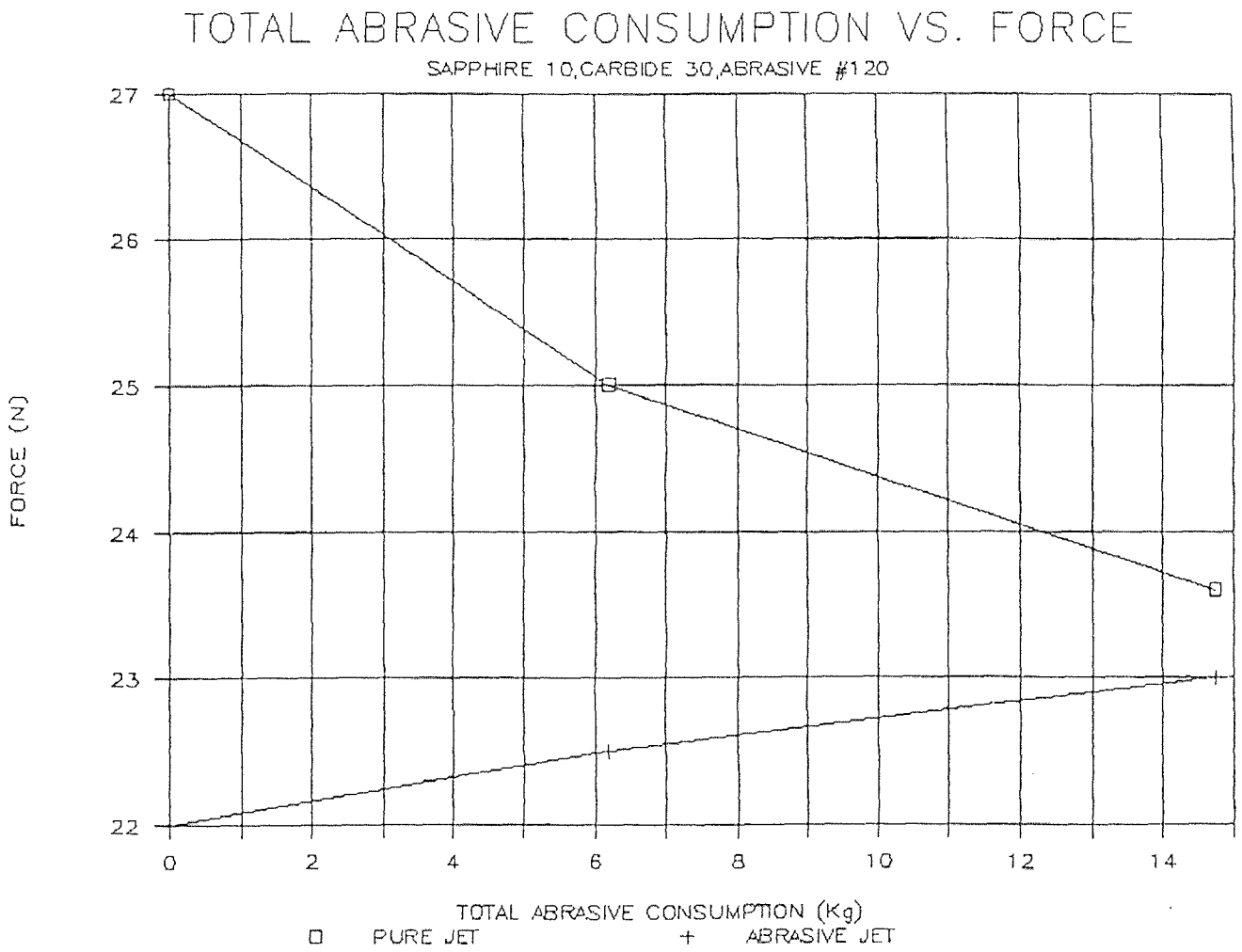
TOTAL ABRASIVE CONSUMPTION VS. FORCE
SAPPHIRE 10,CARBIDE 30,ABRASIVE #120
FORCE (N)
27
26
25
24
23
22
0
2
4
6
8
10
12
14
TOTAL ABRASIVE CONSUMPTION (Kg)
PURE JET
ABRASIVE JET

FIGURE 6.72

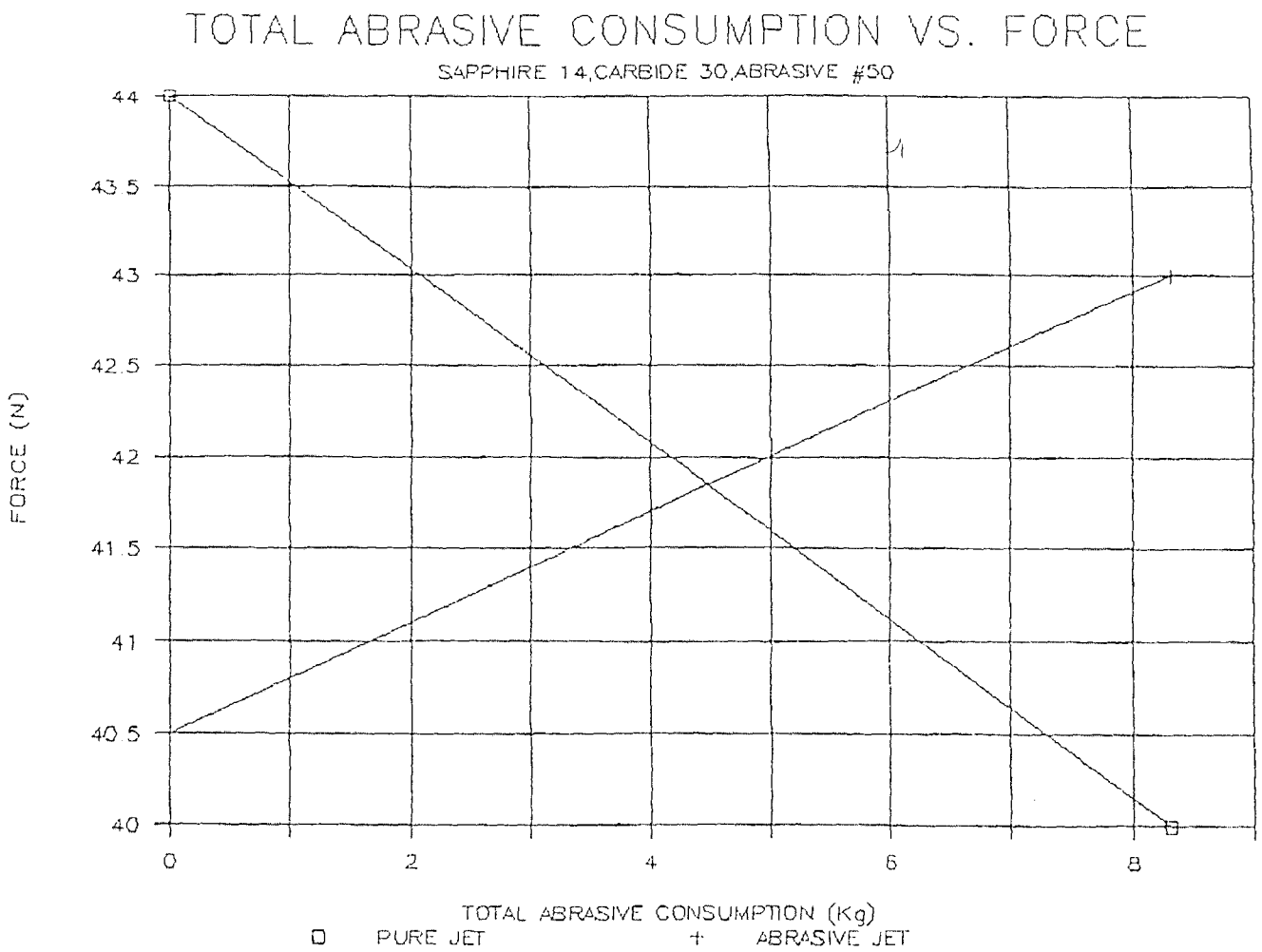
TOTAL ABRASIVE CONSUMPTION VS. FORCE
SAPPHIRE 14,CARBIDE 30,ABRASIVE #50
FORCE (N)
44
43.5
43
42.5
42
41.5
41
40.5
40
0
2
4
6
8
TOTAL ABRASIVE CONSUMPTION (Kg)
PURE JET
ABRASIVE JET

FIGURE 6.73

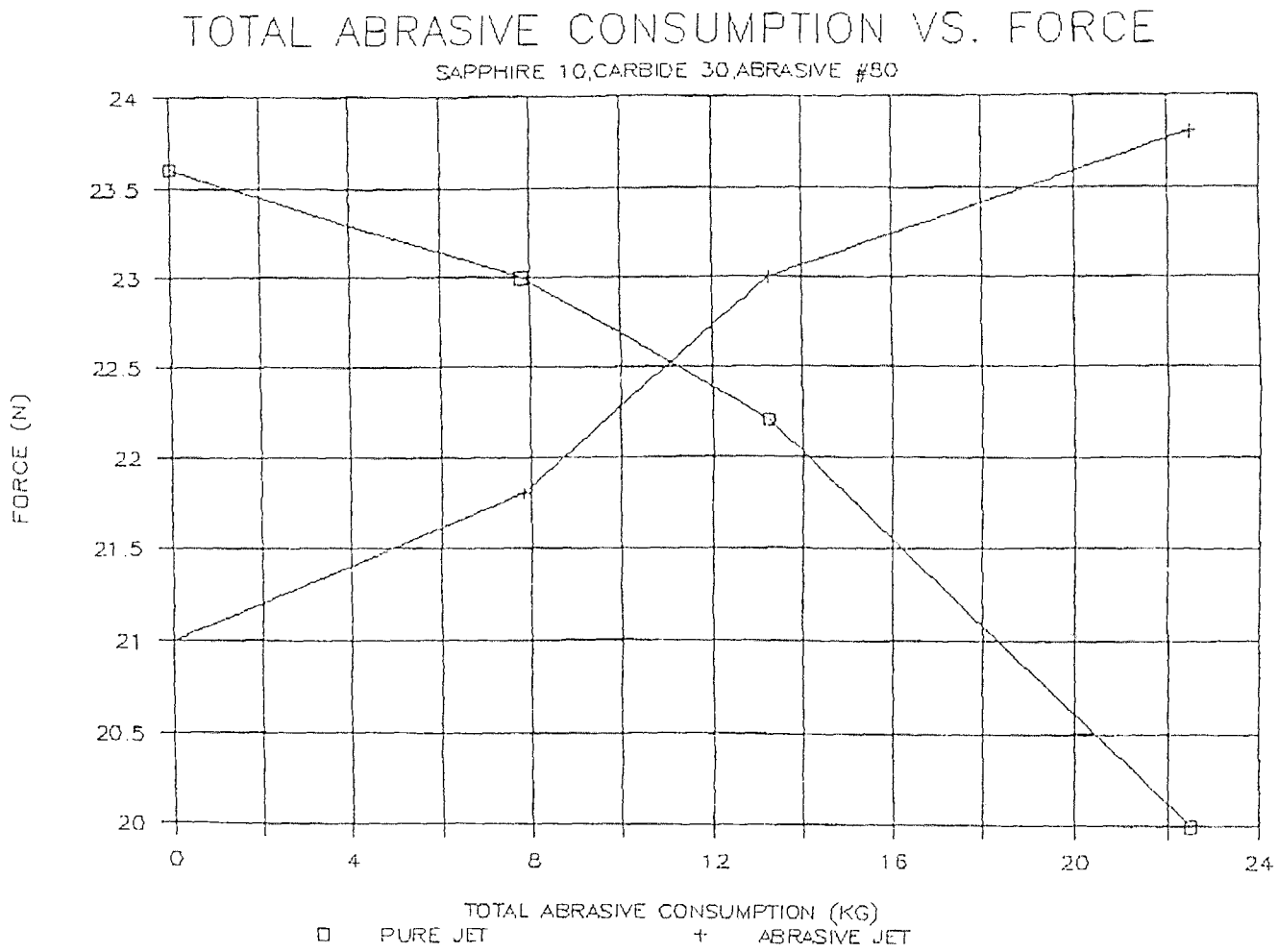
TOTAL ABRASIVE CONSUMPTION VS. FORCE
SAPPHIRE 10,CARBIDE 30,ABRASIVE #80
FORCE (N)
24
23.5
23
22.5
22
21.5
21
20.5
20
0
4
8
12
16
20
24
TOTAL ABRASIVE CONSUMPTION (KG)
PURE JET
ABRASIVE JET

FIGURE 6.74

REFRENCES

1. E.N. Leslie, "Automated Waterjet Cutting", Mechanical Engineering, Dec. 1976.

2. "Cutting with High-Pressure Waterjets", Plastics Machinery and Equipment, Mar. 1980.

3. E.J. Stefanides, "Flow Systems CAD/CAM For Total System Manufacturer", Design News, Apr. 1980.

4. J.M. Martin, "Using Waterjet as a Cutting Tool", American Mechinist, Apr. 1980.

5. M. Hashish, "The Application of Abrasive Jets to Concrete Cutting", Jet Cutting Technology, Apr. 1982.

6. M. Hashish, "Steel Cutting with Abrasive Waterjets", Jet Cutting Technology, Apr. 1982.

7. J.W. Twigg, "High-Pressure Water Jetting Techniques", Corrosion Prevention and Control, Apr. 1982.

8. C. Barker, "Evaluation of an Abrasive Cleaning System", Jet Cutting Technology, Apr. 1982.

9. G.G. Yie, "Cutting Hard Materials With Abrasive-

Entrained Waterjet", Jet Cutting Technology, June 1984.

10. K. Ostby, "Robotic Water jet Cutting", Proceeding of Robots 8 Conference, Jun. 1984, Detroit, Michigan.

11. H. Rob, "Waterjet Cutting", Proceeding of Automach Australia "85, Jul. 1985, Melbourne, Austrilia.

12. M. Hashish, "Application of Abrasive-Waterjets to Metal Cutting", Flow System, Jan. 1986.

13. L. Leonard, "WJC Article-Advanced Composites", Advanced Composite, Oct. 1986.

14. K.A. Godfrey, Jr., "Waterjets: Concrete Yes, Tunneling Maybe", Civil Engineering, May 1987.

15. W.C. Maurer, "Advanced Drilling Techniques", Houston, Texas, Maurer Engineering Inc., Techanical Report No. TR79-1, Jan. 1979.

16. G.H. Hurlburt, J.B. Cheung, "Submerged Waterjet Cutting of Concrete and Granite", In: Proc. Third Int. Symp. on jet Cutting Technolog, Chicago : May, 1976), Cranfield, U.K., BHRA Fluid Engineering, 1976.

17. J.G.A. Bitter, "A study of Erosion Phenomena-Part I", Wear, Vol.6, 1963, pp.5-21.

18. D.R. Oliver, "The Expansion/Contraction Behavior of Laminar Liquid Jets", Can. J. of Chem. Eng., Apr. 1966, pp.100-107.

19. A.G. Fredrickson, "Principles and Applications of Rheology", Prentice Hall, 1964, pp.214-221.

20. A.A. Semerchan, V.F. Vereshchagin, F.M. Filler, N.N. Kuzin, "Distribution of Momentum in a Continuous Liquid Jet of Supersonic Velocity", Feb. 1988.

21. S.K. Kesavan, N.P. Reddy, S. Yazdani-Ardakani, "Measurement of Dynamic Impact Thrust Exerted by High-Frequency Liquid Jet", Experimental Techanical, Sep. 1985.

22. W.N. Gill, R. Cole, J. Estrin, R.J. Nunge, H. Littman, "Fluid Dynamics-An Annual Review", I & EC, Dec. 1967.

23. W.G. Cady, "Piezoelectricity", Vol. 1&2, Dover Publication, 1964.

24. J. Curie, P. Curie, Acad. Science(Paris), 91, 294. (1880); 91, 383. (1880).

25. W.P. Mason, "Piezoelectricity, Its History and Applications", J. Acoust. Soc. Amer., 70(6), 1981, pp. 1561-1566.

26. H.U. Schwarzenbach, H. Lechner, B. Steinle, H.P. Baltes, P. Schwendamn, "Calculation of Vibrations of Thick Piezoceramic Disk Resenators", Appl. Phys. Lett., 38(11), 1981, pp.854-855.

27. P.I. Shnitser, "Analysis of Oscilliations in an open Acoustic Resonator with Reflective Piezoelectric Transducers", Sov. Phys. Acoust., 26(3), 1980.

28. M.B. Gitis, A.A. Shenker, "Pulsed Operation of a flat Piezoelectric Transducer", Sov. Phys. Acoust., 27(6). 1982.

29. H.S. Tzou, "Development of Polyvinylidene-Fluoride Transducers for Dynamic Measurements and control", Proceedings of Robotics and Design Automation Conference, May 1986.

30. G.M. Sessler, "Piezoelectricity in Polyvinylinded-Flouride", J. Acoust. Soc. Am., 70(6), Dec. 1981.

31. E. Fukada, "Piezoelectricity in Polymers and

Biological Substances", Ultrasonics, 6(4), 1968.

32. A.J. Schiff, "Identification of Large Structures Using Data from Ambinent and Low Lever Excitation.", System Identification of Vibrating Structure, ASME, 1973.

33. G.H. Gautschi, "Piezoelectric Multicomponent force Transducers and Measuring System", Proceedings Transducer '78 Conference, Wembley Conference Center, London, 1978.

34. G.H. Gautschi, "Cutting forces in Machining and their Routine Measurement with Multicomponent Piezoelectric Force Transducers", Proceedings of the Twelfth International Machine Tool Design and Research Conference, Manchester, Great Britian, 1971.

35. K. Langhammer, "Cutting Forces as Parameters for Determining Wear on Carbide Lathe Tools and as Machinability Criterion for Steel", The Carbide Journal, May 1976.

36. G. Bridel, H. Thomann, "Wind-Tunnel Balance based on Piezoelectric Quartz Force Transducers", J. of Aircraft, 17(5), 1980.

37. "Operation Manual for Three-Component Measuring

Plateform", Kistler Instrument Inc.

38. W. Mahr, "Measuring and Processing Charge Signals from Piezoelectric Transducer", Translated reprint from Technisches Messen, Vol. 49, 1982.

39. K.H. Martini, "Multicomponent Dynamometers using Quartz Crystals as Sensing Element", ISA Trans, Vol.22, 1982.

40. B.F. Langer, "Design and Application of a Magnetic Strain Gage", SESA Proc.,1,2:82, 1943.

41. J.W. Mark, W. Goldsmith, "Barium Titanate Strain Gage", SESA Proc., 13,1:139, 1955.

42. T.G. Beckwith, N.L. Buck, R.D. Marangoni, "Mechanical Measurements", 3rd. ed., Assison-Wesley Publication Co.,1981.